Discovery of novel therapeutic antibodies and targets using tumor-infiltrating B cells

Von der Fakultät für Lebenswissenschaften

der Technischen Universität Carolo-Wilhelmina zu Braunschweig

zur Erlangung des Grades

einer Doktorin der Naturwissenschaften

(Dr. rer. nat.)

genehmigte

D i s s e r t a t i o n

von Melanie Philippi
aus Wolfsburg

1. Referent: Professor Dr. Stefan Dübel
2. Referent: apl. Professor Dr. Andreas Gerstner
eingereicht am: 11.12.2019
mündliche Prüfung (Disputation) am 03.04.2020

Druckjahr 2020

Vorveröffentlichungen der Dissertation

Teilergebnisse aus dieser Arbeit wurden mit Genehmigung der Fakultät für Lebenswissenschaften, vertreten durch den Mentor der Arbeit, in folgenden Beiträgen vorab veröffentlicht:

Posterbeiträge

Zilkens, K., **Philippi, M.**, Kügler, J., Sellmann, C., Clarke, T., Toleikis, L., Dübel, S., Schirrmann, T.: Antibody and target discovery using tumor-infiltrating B lymphocytes. Poster 72. 12th PhD Symposium der HZI International Graduate School for Infection Research (GS-FIRE) am Helmholtz Zentrum für Infektionsforschung, Braunschweig (2019)

Table of content

Abbreviations

%	Percent
°C	Degree Celsius
Δ	Delta; deletion
µg	Microgram(s)
µL	Microliter(s)
µM	Micromolar
AJCC	American Joint Committee on Cancer
ANOVA	Analysis of variance
APC	Allophycocyanin or antigen-presenting cell
bp	Basepair(s)
BSA	Bovine serum albumin
Breg	Regulatory B cell
CD	Cluster of differentiation
cDNA	Complementary DNA
CDR	Complementary determining region
cfu	Colony forming unit(s)
CH	Constant heavy chain domain
CHO	Chinese hamster ovary
CIP	Calf intestine phosphatase
CL	Constant light chain domain
CO_2	Caron dioxide
CMV	Cytomegalovirus
DAB	3,3'-Diaminobenzidine
DC	Dendritic cell
DMSO	Dimethyl sulfoxide
DNA	Deoxyribonucleic acid
dNTP	Deoxyribonucleotide triphosphate
e.g.	*lat.: Exempli gratia* = for example
E. coli	*Escherichia coli*
EC50	Half maximal effective concentration
ECM	Extracellular matrix
EDTA	Ethylenediaminetetraacetic acid
EGFR	Epidermal growth factor receptor
ELISA	Enzyme-linked immunosorbent assay
et al.	*lat.: Et alii* = and others
Fab	Fragment antigen binding

FACS	Fluorescence-activated cell sorting
FBS	Fetal bovine serum
Fc	Fragment crystallisable
FC	Flow cytometry
FDA	Food and drug administration
FFPE	Formalin-fixed paraffin-embedded
FITC	Fluorescein isothiocyanate
Fv	Fragment variable
g	Gram(s); earth acceleration
GC	Germinal center
GFP	Green fluorescent protein
GI	Germline identity
gIII	gene of M13K07 minor coat protein III
h	Hour(s)
HC	Heavy chain
HEK	Human embryonic kidney
HPLC	High performance liquid chromatography
HIV	Human immunodeficiency virus
HNSCC	Head and neck squamous cell carcinoma
HPV	Human papilloma virus
HRP	Horseradish peroxidase
IL	Interleukin
Ig	Immunoglobulin
INF	Interferon
IPTG	Isopropyl-ß-D-thiogalactopyranosid
kDa	Kilodalton(s)
kV	Kilovolt(s)
LB	Lysogeny broth
LC	Light chain
LCD	Laser capture microdissection
M	Molar
MDSC	Myeloid-derived suppressor cell
min	Minute(s)
mL	Mililiter(s)
mM	Milimolar
MMP	Matrix metalloproteinase
mRNA	Messenger RNA

MS	Mass spectrometry
MTP	Microtiter plate
MW	Molecular weight
MWCO	Molecular weight cut-off
ng	Nanogram(s)
NGS	Next generation sequencing
NK	Natural killer cell
nm	Nanometer(s)
nt	Nucleotides
OD600	Optical density at wavelength 600 nm
ORF	Open reading frame
p53	Tumor suppressor protein 53
P	Probability value
PP	Polypropylene
PAGE	Polyacrylamide gel electrophoresis
PBMC	Peripheral blood mononuclear cells
PBS	Phosphate buffered saline
PCR	Polymerase chain reaction
PE	Phycoerythrin
pIII	M13K07 minor coat protein III
pRb	Retinoblastoma protein
PTGFRN	Prostaglandin F2 receptor negative regulator
PVDF	Polyvinylidene fluoride
RNA	Ribonucleic acid
rpm	Rounds per minute
s	Second(s)
scFv	single chain fragment variable
SDS	Sodium dodecyl sulfate
SLO	Secondary lymphoid organ
TAM	Tumor-associated macrophage
TEM	Tetraspanin-enriched microdomain
TIL	Tumor-infiltrating lymphocyte
TIL-B	Tumor-infiltrating B cells
TLS	Tertiary lymphoid structure
TME	Tumor microenvironment
TNF	Tumor necrosis factor
TNM	Tumor staging; T: tumor, N: lymph nodes, M: metastases

Treg	Regulatory T cell
U	Unit(s)
UV	Ultraviolet
V	Volt(s)
Vκ/Vλ	Variable light chain domain of kappa or lambda subtype
VEGF	Vascular endothelial growth factor
VH	Variable heavy chain domain
VL	Variable light chain domain
v/v	Volume per volume
WHO	World health organisation
YUHAN	patient number (Yumab head and neck)

List of figures

List of tables

1. Introduction

1.1 Antibodies

Antibodies or immunoglobulins are large proteins, which are part of the adaptive immune response in vertebrates. They were first described by van Behring and Kitasato who postulated the existence of blood agents neutralising diphtheria toxin, thus enabling the first successful therapy of this disease (von Behring and Kitasato 1890). Following decades of research revealed their structure and their essential role in the immune system. Biochemically, antibodies can be divided into five different isotypes – the monomeric IgA, IgD and IgG and the multimeric IgA (dimer) and IgM (pentamer). Herein, IgG is the most predominant isotype with the longest serum half-life (Schroeder and Cavacini 2010). Immunoglobulins are composed of two heavy (H) and two light chains (L) connected by disulfide bonds (Figure 1). Each chain consists of N-terminal variable (V) and C-terminal constant (C) domains. In case of IgG, the H-chain has a molecular weight of ~50 kDa and comprises one variable (VH) and three constant domains (CH). The hinge region between CH1 and CH2 harbours conserved cysteine residues facilitating disulfide bonding between the two H-chains. The L-chain only consists of one V- and C-domain (VL & CL) and has a molecular weight of ~25 kDa. Each L-chain is linked to one H-chain by disulfide bonds between CH1 and CL (Schroeder and Cavacini 2010). The constant domains CH2 and CH3 together form the Fc fragment (fragment crystallisable), which mediates effector functions through interaction with specific Fcγ-receptors expressed on several immune cells (Nimmerjahn and Ravetch 2008). The V-domains (VH & VL) in turn are summarised as the Fv fragment (fragment variable) and are essential for antigen binding. Each V-domain comprises three complementary determining regions (CDR) flanked by framework sequences (FRs). The hypervariable CDRs mainly determine the specificity of the antibody and form the paratope, which is a specific binding site for the epitope on the respective antigen. According to the lock-and-key-principle binding between paratope and epitope is highly specific. Hence, antibodies can distinguish between closely related antigens if they do not express the same epitope but also bind to different antigens if they share the same or a similar epitope, which is termed cross-reactivity (Schroeder and Cavacini 2010).

The vast diversity of the natural B cell repertoire is created by genetic recombination early in the development of the progenitor B cell. The V-domains are composed of different gene segments termed “variable” (V), “diversity” (D) and “joining” (J), which are assembled to the VH (VDJ-recombination) and the VL (VJ-recombination) (Tonegawa 1983). For the L-chain there are two sets of gene segments located on different chromosomes, thus resulting in the κ and λ light chain subtypes. Allelic exclusion herein ensures, that each B cell expresses antibodies of only one specificity (Rajewsky 1996). Initially, antibodies are expressed as

surface immunoglobulins as part of the B cell receptor on naïve B cells (IgM and IgD). Upon activation, B cells undergo class switch recombination (CSR) and somatic hypermutation (SHM) to shape antibody affinity and facilitate secretion of soluble antibodies (Rajewsky 1996). These can directly neutralise or block toxins or pathogens (Fühner et al. 2018) or activate effector cells by their Fc part leading to phagocytosis (Aderem and Underhill 1999) or cell lysis and apoptosis through perforins and granzymes secreted by NK cells (Seidel et al. 2013). Furthermore, through the interaction with C1q antibodies can activate the complement cascade mediating cell lysis (Ricklin et al. 2010).

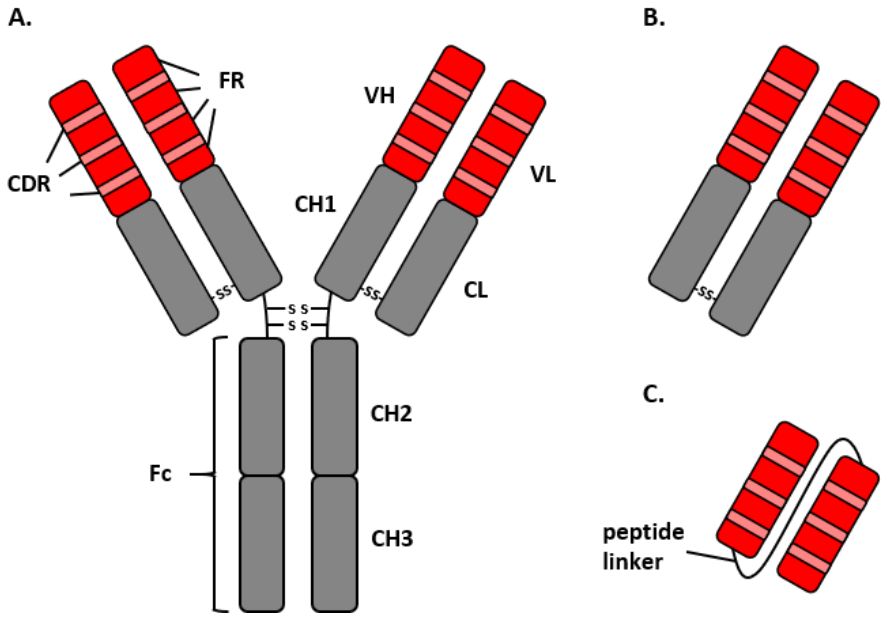

Figure 1: Antibody formats. A: Full-length IgG1. **B**: Fab fragment. **C**: scFv fragment with flexible peptide linker.

Apart from their natural function, antibodies find broad application in molecular biology, diagnostic and therapy. The production of monoclonal antibodies was revolutionised by the introduction of the hybridoma technology by Köhler and Milstein in 1975 (Köhler and Milstein 1975). Whereas previously antibodies were obtained from polyclonal sera of immunised animals, this technology was based on the fusion of antibody-producing B cells with immortal myeloma cells enabling infinite antibody production. In further investigations, antibodies were amplified from hybridoma clones and subcloned for recombinant production in different cellular systems (Jäger et al. 2013; Horwitz et al. 1988). Skerra and Plückthun firstly demonstrated the production of the Fv in bacteria (Skerra and Plückthun 1988), which was further improved by the introduction of a flexible peptide linker connecting VH and VL (Huston et al. 1988). The resulting single chain Fv (scFv) represents the smallest commonly used antibody format

facilitating antigen-binding. Due to its solubility and its easy and profitable production in bacterial systems, the scFv is widely used in different applications (Ahmad et al. 2012).

1.2 Phage display

The development of recombinant antibodies from hybridoma cells revolutionised antibody technology but still required immunisation of donor animals, thus involving a limitation for certain toxins. Furthermore, the isolated antibodies, which were mainly derived from mice were found to be immunogenic in humans, which complicated their clinical application (Schroff et al. 1985). Introduction of the phage display technology in the early 1990s enabled the *in vitro* isolation of monoclonal antibodies from fully human antibody libraries and was a breakthrough for modern antibody discovery (McCafferty et al. 1990; Barbas et al. 1991; Breitling et al. 1991). For generation of antibody libraries, V-genes are amplified directly from B cells obtained from human blood and subcloned into a special plasmid containing a phage packaging signal (phagemid). The phagemid system uncouples the phage production and thus facilitates improved antibody production and gene library amplification (Breitling et al. 1991). Within the phagemid, the resulting scFv fragments are fused to the gene gIII of the viral minor coating protein pIII of the filamentous phage M13K07 and cloned into *E. coli*. Thus, the scFv-pIII fusion is integrated during phage assembly resulting in phage particles, which both present the antibody on their surface and also contain its genetic information. Once the gene libraries are converted to phage libraries ("packaging"), specific antibodies can be selected in a process termed panning (Hust et al. 2014; Russo et al. 2018) (Figure 2). Antibody-phage are incubated on a desired antigen, which is immobilised on a defined surface. Whereas unbound phage are washed away, bound phage are eluted and amplified upon re-infection. This way, antigen-binding phage are enriched over typically three panning rounds. Thanks to the coupling of antibody phenotype and genotype within the phage, the selected antibodies can be easily produced in *E. coli*, screened and identified. This way, phage display facilitates the selection of fully human antibodies against any type of antigen under adjustable panning conditions.

Following the remarkable example of phage display, other display technologies have been developed including yeast (Boder et al. 2012) and mammalian cells (Bruun et al. 2017). Whereas in phage display, library sizes of 10^{10} can be easily covered, alternative technologies suffer from low transformation efficacies, which results in diversities of typically 10^{8} failing to represent the enormous diversity of many libraries. Depending on the application there are different library types divided into naïve, immune and synthetic libraries (Hust et al. 2014). For naïve and immune libraries, antibody genes are amplified form B cells isolated from human blood as described above. For naïve libraries, non-immunised healthy donors are used, from which the IgM genes are amplified. Thus, the naïve B cell repertoire is accessed resulting in large libraries (10^{9} to 10^{10}), which are particularly useful for universal antibody selection (Kügler

et al. 2015). Other universal libraries are synthetic libraries, which do not reflect a naturally accessible repertoire but are based on a defined framework, which is combined with random CDR sequences. These can be either mutated variants of natural CDRs (semi-synthetic) (Desiderio et al. 2001) or completely synthesised (fully synthetic) (Tiller et al. 2013). Immune libraries in contrast are based on the IgG repertoire of immunised donors such as vaccinated patients (Sadreddini et al. 2015), immunised animals (Miethe et al. 2014) or patients suffering from a certain disease such as HIV (Trott et al. 2014). Hence, in contrast to universal libraries, immune libraries need to be constructed *de novo* for each particular antigen. Due to the natural immune response, the resulting libraries are smaller (10^6 to 10^8) and biased towards the certain antigen, which increases the chance to select highly specific and already *in vivo* affinity matured antibodies.

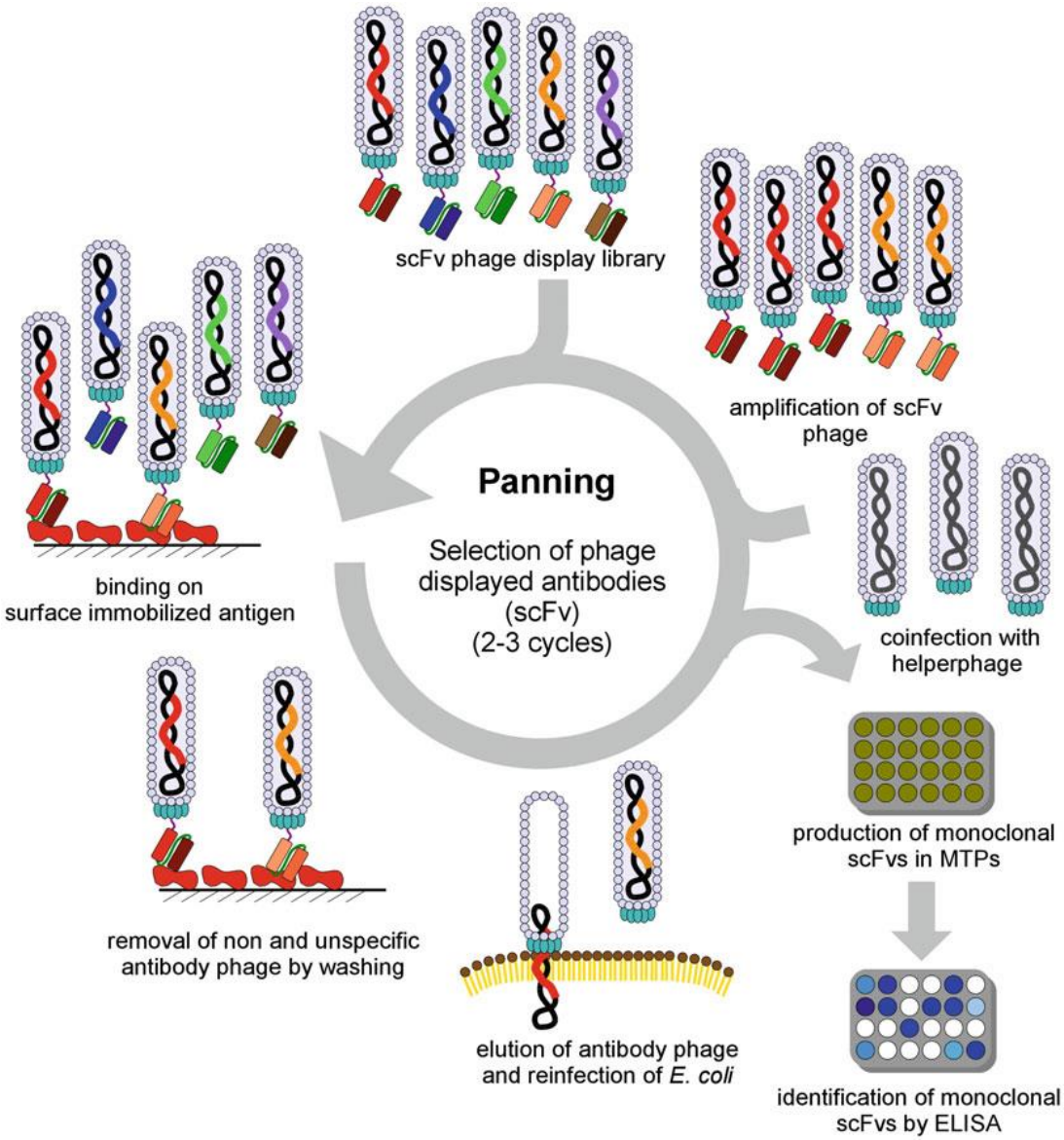

Figure 2: Panning for selection of scFv-phage (Russo et al. 2018)

1.3 Tumor-infiltrating lymphocytes and the tumor microenvironment

Referring to the observations of the world health organisation (WHO), cancer is still the leading cause of death worldwide accounting for the most or second most deaths before the age of 70 in 91 out of 172 countries (Bray et al. 2018). In order to facilitate successful tumor growth, cancer cells need to evolve specific capabilities, which have been comprehensively summarised by Hanahan and Weinberg as the major hallmarks of cancer (Hanahan and Weinberg 2011). According to these hallmarks, tumor cells need to ensure continuous proliferation, resistance to growth suppressors and cell death signals, immortalisation, regulation of angiogenesis and finally, the activation of invasion and metastasis formation. Tumors are complex tissues comprising various different cell subsets such as stromal cells, blood vessel endothelial cells and immune cells, which interact both with each other as well as the tumor cells, thus forming a complex network summarised as tumor microenvironment (TME) (Alsibai and Meseure 2018). In order to facilitate optimal tumor growth, cancer cells regulate their TME to accomplish tumor-beneficial conditions. Notably, stromal cells such as tumor-associated fibroblasts, adipocytes and mesenchymal stem cells massively contribute to tumor progression (Hanahan and Coussens 2012). They promote tumor growth, activate angiogenesis, suppress anti-tumor immunity and facilitate invasion through the secretion of various growth factors and cytokines such as IL-10 and VEGF and by modulating the extracellular matrix (ECM) (Alsibai and Meseure 2018; Hanahan and Coussens 2012). The TME additionally comprises lymphoid-derived cells such as T cells, B cells and plasmacytoid dendritic cells (pCD) as well as myeloid-derived cells like tumor-associated macrophages (TAM), conventional DCs, neutrophils, mast cells and platelets (Alsibai and Meseure 2018). Contrasting to the initial assumption, that all immune cells within the TME contribute to tumor suppression, controversial findings have been reported for the different subsets. Thus, TAMs of the immunosuppressive phenotype M2 and myeloid-derived suppressor cells (MDSC) secrete IL-10 and other cytokines to inhibit cytotoxic T cells (CTL), B cells and NK cells in the TME (Murdoch et al. 2008). Additionally, they induce the development of regulatory T cells (Treg), which themselves inhibit other immune cells (Ghiringhelli et al. 2005). Furthermore, they promote expression of the M2 phenotype in other macrophages through an upregulated expression of NFκB, thus retaining and spreading immunosuppression (Hagemann et al. 2008). Infiltration of tumors with CTLs and B cells in contrast, has been widely reported to correlate with improved prognosis and overall survival in different types of cancer (D.-Q. Zeng et al. 2016; Nazemalhosseini-Mojarad et al. 2019) strongly indicating, that these cells act anti-tumorigenic. Whereas TAMs and MDSCs are randomly spread within the tumor stroma, tumor-infiltrating lymphocytes (TIL) have been found to often form well-organised tertiary lymphoid structures (TLS) (Dieu-Nosjean et al. 2008; Germain et al. 2014). Majorly located at the invasive margin of the tumor, TLS show high similarity to conventional secondary lymphoid

organs (SLO) (Germain et al. 2015). They are composed of a B cell follicle, in which B cells are densely packed with follicular DCs and macrophages, a distinct T cell zone containing T cells accompanied by mature DCs and specialised high endothelial venules (HEV), which enable further immune cell infiltration from blood into the tissue (Colbeck et al. 2017; Germain et al. 2015). Surrounded by a ring of naïve B cells, a germinal center (GC) is formed, in which B cells expand and undergo class-switch recombination (CSR) and somatic hypermutation (SHM) (Germain et al. 2014). The T cells in turn are primed by DCs, which present tumor-associated antigens within their MHC class I and II molecules. CD4+ T helper cells in turn stimulate proliferation and survival of germinal center B cells (Gatto and Brink 2010). Formation of TLS has been observed in various diseases harbouring chronic inflammation such as in graft rejection, autoimmune disorders, infectious diseases and also in cancer (Koenig and Thaunat 2016; Humby et al. 2009; Houtkamp et al. 2001; Dieu-Nosjean et al. 2008). In contrast to the preceding cases, in which TLS usually reflect high activity of disease, occurrence and abundance of cancer-related TLS have been reported to correlate with prolonged survival and improved prognosis (Goc et al. 2013; Germain et al. 2014; Sautès-Fridman et al. 2016). These findings provide evidence, that TLS contribute to an anti-tumor immune response harbouring tumor-specific cytotoxic T cells (CTL) and antibody-secreting B cells thus representing a local immune machinery, which complements the conventional immune response initiated by APCs migrating to SLOs (Germain et al. 2014). Considering the pivotal impact of immune cells on cancer development, Pagès and co-workers suggested to quantify cytotoxic (CD8+) and memory (CD45RO+) T cells within the tumor core and the invasive margin to calculate an immunoscore, which correlated with the survival of colorectal cancer patients (Pagès et al. 2009). Although classification of cancer severity based on the universal TNM staging referring to the primary tumor burden (T) and the extension to draining lymph nodes (N) and metastases (M) established by the American Joint Committee on Cancer (AJCC) is widely accepted and provides information about tumor progression, this system fails to consider the immune microenvironment and its impact on prognosis. A recent comprehensive investigation comprising more than 2000 colon cancer patients indeed demonstrated the reliable prognostic value of the this novel system (Pagès et al. 2018). The immunoscore represents a promising complementation of the classical tumor staging model facilitating an improved prognostic estimation and outlines the great potential of the immune infiltrate for the development of novel diagnostic tools.

1.4 Immune surveillance and immune escape

Regarding the largely reported beneficial effects of some TILs, the prognostic impact of an immunoscore correlating with improved survival and the frequent occurrence of TLS in the tumor microenvironment, the question rises why tumors still develop, progress and even metastasise regardless of the ongoing immune response. To explain this controversial finding,

it has been suggested that the tumor is under immune control for an undefined period of time but manages to evade. This process is referred to as “immunoediting” and comprises three different states tumor-immune-interaction (Dunn et al. 2004). First, upon starting tumor development, an immune response is initiated keeping tumor growth under control. This process is termed immunosurveillance and has been initially described already 50 years ago by Burnet and Thomas (Burnet 1970). Within this state, neoepitopes on tumor cells are effectively recognised, immune cells are recruited to the tumor nest and TLS formation is induced to further drive an anti-tumor response (Dunn et al. 2004; Swann and Smyth 2007). Evidence for this theory has been provided by many studies reporting spontaneous tumor development in transplanted organs (Penn 1978), occurrence of paraneoplastic autoimmune syndromes (Graus et al. 1997) and an increased risk of tumorigenesis in immunosuppressed or immunodeficient patients (Gatti and Good 1971). Consistent with these findings it has been described, that the initial TME in lower staged tumors is mainly characterised by a high number of CTLs and pro-inflammatory macrophages (M1) as well as by high levels of IL-12 and INFγ (Fridman et al. 2014). However, if elimination of tumor cells is incomplete an equilibrium state is reached (Dunn et al. 2004), in which the cancer cells continue to undergo mutational cycles to overcome the immunogenic pressure for instance by losing or modifying their antigens or by downregulating their MHC complexes (Ferrone and Marincola 1995). Furthermore, as discussed before cancer cells interact with their TME to gain supportive cytokines and growth factors, to expand tumor vascularisation for an improved nutrient and oxygen supply and to promote an immunosuppressive environment. If these processes prevail and the immune system continues to fail in complete remission, immune-resistant and thus more aggressive tumor cells are selected over time finally evading the immune system (Swann and Smyth 2007). This last state is termed immune escape and is marked by tolerated tumor progression, further modulation of the TME and induction of metastasis formation. Consistently, the immune microenvironment in later tumor stages is altered and characterised by predominance of Tregs and immunosuppressive M2 macrophages as well as by low levels of IFNγ and increased levels of IL-6 and VEGF (Chimal-Ramírez et al. 2013; Fridman et al. 2014).

Immunoediting provides an explanation for the failing tumor regression in the presence of specialised immune cells. It is not surprising that this knowledge substantially drove the development of novel related therapeutic strategies. Various approaches have been described aiming to redirect the existing immune response and to invert immunoediting back to the state of immunosurveillance or even complete remission. To accomplish this, two major strategies have been described addressing the re-activation of exhausted or silenced immune cells on one hand and the enhancement of existing immune responses on the other (Velcheti and Schalper 2016). The first strategy majorly focusses on the blockade of immune checkpoints. These negative regulatory pathways exist in all immune cells to prevent tissue damage and

autoimmune reactions upon inflammations (Pardoll 2012). Ligand binding to surface checkpoint receptors such as CTLA-4, PD-1, TIGT or TIM-3, which are majorly expressed on T cells leads to their inactivation, thus mediating immunosuppression (Carter et al. 2002; Keir et al. 2005; Walunas et al. 1994; Yu et al. 2009; Zhu et al. 2005). Consequently, cancer cells upregulate expression of the respective ligands such as PD-L1 in order to promote inactivation of TILs, thus contributing to immune evasion (Blank et al. 2005; Hino et al. 2010; Mu et al. 2011). Indeed, therapeutic antibodies targeting CTLA-4 and PD-1 such as ipilimumab and nivolumab already have been FDA-approved and showed promising results in clinical trials (Garon et al. 2015; Larkin et al. 2015; Reck et al. 2016). However, low response rates represented considerable drawbacks. This could be explained by preceding immunoediting, the concomitant highly immunosuppressive TME and the reduced immunogenicity of the tumor, which massively affect successful treatment. The second therapeutic strategy aims to facilitate an enhanced immune response including the application of cancer vaccines, cytokines such as interferons and interleukins or the adoptive T cell therapy (Velcheti and Schalper 2016). The latter describes the isolation of autologous cytotoxic T cells from tumor tissue or blood, which are expanded and stimulated *in vitro* and re-administered to the patients (Ho et al. 2003). To improve affinity and to overcome limitation to MHC-dependent target recognition, T cells were further equipped with chimeric antigen receptors (CARs) composed of immunoglobulin fragments (Barrett et al. 2014). The resulting CAR-T cells indeed showed improved performance but again success was limited by the high plasticity of tumor cells and the immunosuppressive TME (Velcheti and Schalper 2016). In summary various therapeutic approaches targeting tumor-immunity are currently under investigation and many of them show promising results in clinical trials (Marin-Acevedo et al. 2018). Nevertheless, breakthrough success is crucially limited by the substantial plasticity of cancer cells, the pivotal impact of the immunosuppressive TME and the accessibility of cancer-specific targets outlining the importance to further investigate the complex network of tumor-infiltrating lymphocytes for future cancer therapy.

1.5 Tumor-infiltrating B lymphocytes and their controversial role in cancer

As described before, B cells account for a considerable amount of the TME and were shown to infiltrate most human cancers. However, the role of the tumor-infiltrating B cells (TIL-B) in anti-tumor immunity is highly controversial. Whereas a number of studies describes, that high frequencies of TIL-Bs correlate with tumor progression and worse prognosis, a contrasting beneficial function of TIL-Bs has been reported in various cases (Largeot et al. 2019; Yuen et al. 2016). Most notably it has to be considered, that many of these studies are difficult to compare as results may vary within different types of cancer and due to the highly complex composition of the TME as described before. As consequence, B cells may differ in their phenotype and function depending on their biological context defined by their localisation and

their surrounding interaction partners, thus resulting in different effects in anti-tumor immunity. Herein the special subpopulation of regulatory B cells (Breg) gained attention in the past few years. Initially described as a defined B cell type with immunosuppressive function in chronic inflammation, following studies revealed a number of different Breg phenotypes raising the suspicion, that they can originate from every subpopulation such as from memory, immature or plasma B cells (Sarvaria, Madrigal, and Saudemont 2017; M. Schwartz, Zhang, and Rosenblatt 2016; Mauri and Bosma 2012). As consequence, analogous to the well-described and previously mentioned Tregs, the term Breg now summarises all B cell subpopulations, which inhibit other immune cells und thus promote tumor progression in cancer (Largeot et al. 2019). Their immunosuppressive effect herein is mainly caused by the secretion of cytokines such as IL-10 (Mizoguchi et al. 2002; Bouaziz et al. 2010; Shalapour et al. 2015), which downregulates inflammatory cascades through the inhibition of T cell activation by induction of STAT3-signalling (Hutchins et al. 2013) as well as of TGF-ß, which transforms resting CD4+ T cells into immunosuppressive FoxP3+ Tregs (Olkhanud et al. 2011). Furthermore, Bregs can also express IL-35, which stimulates tumor growth directly (Pylayeva-Gupta et al. 2016) or suppressive ligands such as PD-L1, thus restricting T cell expansion and differentiation (Khan et al. 2015; Shalapour et al. 2015). Additionally, through stimulation of Fcγ-receptors expressed on myeloid cells, aggregated antibody complexes secreted by B regs can regulate MDSCs and TAMs, which in turn facilitate tumor angiogenesis and tumor cell survival (Andreu et al. 2010; Gunderson et al. 2016). Taken together, all these findings outline the pro-tumorigenic function of regulatory B cells and contribute to explain why depletion of TIL-Bs with an anti-CD20 antibody improved response to chemotherapy and suppressed tumor growth in mouse models (Affara et al. 2014; Maglioco et al. 2017).

In contrast to these findings, numerous studies outline an anti-tumorigenic effect of TIL-Bs mediated by different strategies. Thus, they can either opsonise tumor cells or inhibit tumor-associated proteins by secretion of autoantibodies, kill cancer cells directly or activate other immune cells through chemokine secretion (Nelson 2010; Tsou et al. 2016). A direct cytotoxic effect of B cells indeed has been observed on one hand by secretion of granzyme B upon anti-BCR and IL-21 stimulation (Hagn et al. 2009; Arabpour et al. 2019) and by expression of TRAIL/Apo-2L on the other, which has been shown to be IFN-α-dependently upregulated and induced tumor cell killing (Kemp et al. 2004). This effect could even be increased by B cell stimulation with an anti-CD40 agonist. Moreover, B cells can additionally function as antigen presenting cells (APC) to effectively prime T cells in order to complement absent, inactivated or dysfunctional DCs within the TME (Rubtsov et al. 2015). Consistent with these findings, the activation of B cells by CD40L to promote their antigen-presenting function has already been considered as therapeutic strategy and indeed positively correlated with reduced tumor growth by activation of T cells (Wennhold et al. 2017). Finally, B cells organised within TLS not only

have been found to correlate positively with improved survival but to secrete antigen-experienced antibodies, which were clonally enriched and somatically hypermutated, indicating that they actively contributed to an anti-tumor immunity (Coronella et al. 2002; Simsa et al. 2005; Nzula, Going and Stott 2003; Hansen et al. 2002; DeFalco et al. 2018). This data is also supported by the positive prognostic value of tumor-infiltrating plasma cells found in different solid tumor types (Gentles et al. 2015).

Although immunosuppressive Bregs naturally occur as part of homeostasis protecting tissue in chronic inflammation, B cells in cancer are not always initially pro-tumorigenic. Similarly, as previously described for Bregs, FoxP3-expressing Tregs in turn suppress the activation and proliferation of B cells as well as their antibody production (Kim 2006) and moreover can selectively kill antigen-presenting B cells through the secretion of perforins and granzymes (Zhao et al. 2006). This demonstrates that T and B cells mutually influence and render each other pro-tumorigenic when exposed to an immunosuppressive TME. Additionally, they are further influenced by MDSCs, TAMs and the tumor cells themselves. In conclusion, analogous to T cells, which are differentially investigated to function as predictive markers or therapeutic agents (Balermpas et al. 2014; Pagès et al. 2018), TIL-Bs need to be judged the same way. Whereas tumor-infiltrating T cells have been extensively studied in the past, the focus on B cells only raised recently. Thus, more comprehensive knowledge is crucially needed to better understand the different B cell subsets and their role in the TME. Although in some cases frequency of TIL-Bs correlated with decreased prognosis, TIL-B antibody repertoires have been shown to be a promising source of tumor-specific antibodies (Nzula et al. 2003; DeFalco et al. 2018). Thus, the TIL-B antibody repertoire could provide valuable knowledge about the humoral anti-tumor response in cancer patients and may lead to the discovery of novel cancer-specific target proteins.

1.6 TILs in head and neck cancer

Cancers of the head and neck are one of the most common cancer types worldwide with more than 800.000 new cases per year (Bray et al. 2018) and compromise malignancies of various anatomical structures within the sinonasal tract, oral cavity, pharynx and larynx. More than 90% of all cases are head and neck squamous cell carcinomas (HNSCC), whereas other types such as adenocarcinomas are rare (Pai and Westra 2009). The major risk factors for HNSCC are long and intense tobacco smoking as well as frequent consumption of alcohol (Pelucchi et al. 2008), which probably serves as solvent and thus synergistically increases the toxicity of carcinogenic substances within the tobacco smoke (Talamini et al. 2002). Despite smoking and alcohol consumption, infection with the human papilloma virus (HPV) is the second major risk factor. Indeed, HPV infection can be found in 26% of all HNSCC and herein is significantly more frequent in oropharyngeal carcinoma (36%) compared to oral (24%) or laryngeal

carcinoma (24%) (Kreimer 2005). The oncogenic HPV types HPV16 and HPV18 herein majorly mediate carcinogenesis by expressing the two viral proteins E6 and E7, which inactivate the tumor-suppressing transcription factor p53 and the retinoblastoma protein (pRb) (Münger and Howley 2002). Under normal cellular conditions, p53 is activated in response to different types of cellular stress and consequently promotes cell cycle arrest, senescence and apoptosis (Wang and El-Deiry 2007). Interestingly, its gene TP53 has been found to be highly mutated in different types of cancer as well as in tobacco-induced HNSCC, demonstrating its crucial role in tumor suppression (Smeby et al. 2019; Lukas, Niu, and Press 2000; Fagin et al. 1993; Brennan et al. 1995). The nuclear pRb in its dephosphorylated form inhibits entry of the S-phase mediating cell cycle arrest (Cobrinik et al. 1992). In HPV-infection, oncoproteins E6 and E7 directly interact with p53 and pRb to form complexes leading to their functional inactivation and ubiquitin-dependent degradation, thus facilitating tumor cell survival and increased proliferation (Werness et al. 1990; Scheffner et al. 1990; Boyer et al. 1996). As consequence of a feedback loop upon pRb inactivation, the cyclin-dependent kinase inhibitor p16, which prevents phosphorylation of pRb (Li et al. 1994) is overexpressed and thus widely used as reliable marker for HPV-infection in HNSCC (Klussmann et al. 2003; Smeets et al. 2007). Furthermore, high levels of p16 have been found to correlate with improved patient outcome (Weinberger 2004), whereas loss of p16 by deletion, mutation or promoter hypermethylation leads to worse prognosis (Reed et al. 1996; Namazie et al. 2002). Interestingly, although HPV-infection increases the risk for HNSCC development and in the course of disease metastases occur more frequently, patients suffering from HPV-induced HNSCC often show prolonged survival (Ang et al. 2010) and a better response to therapy compared to HPV-negative HNSCC (Lassen et al. 2011; Ang et al. 2010; Fakhry et al. 2008). Due to the close proximity to lymphatic tissue of the Waldeyer's ring and the frequent occurrence of related viral infection, HNSCC has been found to be one of the most highly infiltrated tumor types, which contributes to explain the observed improved survival (Mandal et al. 2016; Lei et al. 2016). Although infiltration rates are high in HNSCC, a large proportion of present immune cells fail to effectively suppress tumor growth due to immunoediting as discussed before. As consequence, dysfunctional T cells and abnormal T cell signalling have been widely observed in HNSCC and were often accompanied by reduced lymphocyte proliferation and frequent apoptosis (Reichert et al. 2002). Additionally, HNSCC patients show lower counts of T cells and mature DCs within the blood (Kuss 2004; Almand et al. 2000) but higher concentrations of immature MDSCs inhibiting T cells and supporting tumor progression (Chikamatsu et al. 2012). Notably, Tregs found within the immune infiltrate of HNSCC showed higher expression levels of PD-1, CTLA-4 and TIM-3 compared to Tregs found within the peripheral blood (Jie et al. 2013) and an increased expression of Fas-ligand on tumor cells has been reported to induce apoptosis in T cells (Gastman et al. 1999). In summary, the rich immune infiltrate in combination with the highly

immunosuppressive TME in HNSCC strongly indicate that HNSCC patients may particularly benefit from immunotherapy. Indeed, both prophylactic (Markowitz et al. 2014) and therapeutic cancer vaccines (Yang et al. 2017) as well as the anti-EGFR antibody cetuximab (M. H. Cohen et al. 2013) are already approved and widely used demonstrating their potential in HNSCC therapy. Nevertheless, most available therapeutic strategies still suffer from moderate to low response rates in some patient proportions. Adjunctions are believed to overcome this limitation and have already been shown to result in improved outcome compared to single strategies. Thus, targeting EGFR with cetuximab together with radiation (Bonner et al. 2006), application of therapeutic vaccines accompanied by PD-1 checkpoint blockade (Massarelli et al. 2019) and combination of the two checkpoint inhibitors nivolumab and ipilimumab (Schwab et al. 2018) for instance demonstrated that immunotherapies ideally complement each other as well as conventional therapies. HNSCC is a highly complex disease and its immunosuppressive TME, the broad variety of anatomical structures and the striking differences between HPV+ and HPV- HNSCC constitute many challenges for cancer therapy. Nevertheless, the high potential of immunotherapy in HNSCC outlines the urgent need of further investigations of the TME and related immune cells to improve therapeutic strategies and to discover novel therapeutic targets and antibodies.

1.7 Aim of this study

TIL-Bs have been shown to contribute to an anti-tumor immunity, deliver anti-tumor antibodies and to correlate with improved survival of patients suffering from different types of cancer. Since head and neck cancers belong to the most highly infiltrated cancer types, patients often benefit from immunotherapy aiming to redirect their own immune response. However, further development of these therapeutic strategies is decisively limited by the discovery of novel tumor-specific antibodies and targets. This study aimed to access the antibody repertoire of B cells infiltrating head and neck cancer. Antibody gene libraries are constructed based on TIL-Bs isolated from fresh tumor specimens and analysed to investigate their characteristics. Using the phage display technology, antibodies are selected on both a well-known tumor marker and a head and neck cancer cell line. The isolated antibodies are characterised, and the respective target proteins are identified by mass spectrometry to test if the TIL-B antibody repertoire can be used for the discovery of novel cancer-related antibodies and targets.

2. Material and methods

2.1 Material

2.1.1 Consumables

The consumables used in this study are listed in Table 1.

Table 1: List of consumables

Material	Manufacturer
Amicon Ultra 0.5 centrifugal filters 30K	Merck KGaA, Darmstadt, Germany
Anti-human IgG Fc capture (AHC) Biosensors	FortéBio, Fremont, USA
Anti-human Fab-CH1 2nd Generation (FAB2G) Biosensors	FortéBio, Fremont, USA
Blotting paper	Omnilab-Laborzentrum, Bremen Germany
Costar 96 well assay plate	Corning, Inc., New York, USA
Costar Stripette serological pipettes (2 mL, 5 mL, 10 mL, 25 mL)	Corning, Inc., New York, USA
Cryo tubes with 2D code	Greiner Bio-one, Frickenhausen, Germany
CytoFLEX cleaning agent	Beckman Coulter, Brea, USA
CytoFLEX Daily QC fluorospheres	Beckman Coulter, Brea, USA
CytoFLEX QC Sheath fluid	Beckman Coulter, Brea, USA
Disposable cuvettes	Sarsted, Nümbrecht, Germany
DT-20 eco tube with rotor-stator element	IKA, Staufen, Germany
Erlenmeyer flasks (baffled and non-baffled)	DWK Life Sciences, Wertheim, Germany
Falcon tubes (15 mL, 50 mL)	Corning, Inc., New York, USA
Filter tips (10 µL, 20 µL, 300 µL, 1000 µlL	Nerbe plus GmbH, Winsen, Germany
Fisherbrand cell strainers (40 µm)	Thermo Fisher Scientific, Dreieich, Germany
Freezing container	Thermo Fisher Scientific, Dreieich, Germany
GenePulser electroporation cuvettes	Bio-Rad Laboratories, Munich, Germany
Injekt-F syringes (1 mL, 10 mL, 20 mL)	B. Braun, Melsungen, Germany
Intellicyt Cleaning solution	Sartorius, Göttingen, Germany
Intellicyt Decontamination solution	Sartorius, Göttingen, Germany
Intellicyt Sheath Fluid	Sartorius, Göttingen, Germany
Intellicyt validation beads (6 peak, 8 peak)	Sartorius, Göttingen, Germany
LightSafe micro tubes (black, 0.5 mL)	Sigma-Aldrich, St. Louis, USA
Low binding tubes 1.5 mL	Sarstedt, Nümbrecht, Germany
Microtiter plate, 96 well, PP, f-bottom	Greiner Bio-one, Frickenhausen, Germany

Microtiter plate, 96 well, PP, u-shape	Greiner Bio-one, Frickenhausen, Germany
Microtiter plate, 384 well, PS	Greiner Bio-one, Frickenhausen, Germany
Microtiter plate, 96 well, PP, f-bottom, black	Greiner Bio-one, Frickenhausen, Germany
Microtiter plate, 96 well, barcoded	Microsynth Seqlab, Göttingen, Germany
Micro tubes (1.5 mL, 2 mL)	Sarstedt
Micro vials for autosampler	TECHLAB, Inc., Blacksburg, USA
Mini-Protean TGX stain-free gels (12%)	Bio-Rad Laboratories, Munich, Germany
Mini-Protean TGX stain-free gels (4 – 15%)	Bio-Rad Laboratories, Munich, Germany
Minisart sterile filters (0.2 µm, 0.45 µm)	Sartorius, Göttingen, Germany
Multiply Pro 8-strips	Sarstedt AG & Co. KG, Nümbrecht, Germany
Nalgene centrifuge bottles (50 mL, 500 mL, 1000 mL)	Sigma-Aldrich, St. Louis, USA
Neubauer counting chamber	BRAND GmbH & Co. KG, Wertheim, Germany
Nitril laboratory gloves	Starlab International GmbH, Hamburg, Germany
Nunc Bio Assay dish (pizza plate)	Merck KGaA. Darmstadt, Germany
Nunc cryo tubes (1.8 mL)	Thermo Fisher Scientific, Dreieich, Germany
Petri dish (10 cm)	Greiner Bio-one, Frickenhausen, Germany
Petri dish (60 mm)	Sigma-Aldrich, St. Louis, USA
Petri dish (glass)	BRAND GmbH & Co. KG, Wertheim, Germany
Pipette tips (10 µL, 300 µL, 1000 µL)	Starlab International GmbH, Hamburg, Germany
Pipette tips 125 µL 384 Tips	INTEGRA Biosciences GmbH. Biebertal, Germany
Pipette tips, 300 µL V96 Tips NS	INTEGRA Biosciences GmbH. Biebertal, Germany
Pipette tips, 300 µL V96 Tips SF	INTEGRA Biosciences GmbH. Biebertal, Germany
Plate sealer aluminium foil	HJ-Bioanalytik, Erkelenz, Germany
Plate sealer breathable foil	HJ-Bioanalytik, Erkelenz, Germany
PVDF membrane, 0.45 µm pore size	Carl Roth GmbH, Karlsruhe, Germany
Reservoir 300 mL sterile, bulk	INTEGRA Biosciences GmbH. Biebertal, Germany
Screw cap tubes (2 mL)	Sarstedt AG & Co. KG, Nümbrecht, Germany
Spatula, L-shape	VWR International, Radnor, USA
SureBeads Protein A magnetic beads	Bio-Rad Laboratories, Munich, Germany

TC flask T75, Stand., Bel. K.	Sarstedt AG & Co. KG, Nümbrecht, Germany
TC flask T175, Stand., Bel. K.	Sarstedt AG & Co. KG, Nümbrecht, Germany
Whatman Uniplate, 24 deepwell, PP	Sigma-Aldrich, St. Louis, USA
Whatman Uniplate, 96 deepwell, PP	Sigma-Aldrich, St. Louis, USA

2.1.2 Equipment

The equipment used in this study is listed in Table 2.

Table 2: List of equipment

Equipment	Model	Manufacturer
8-channel pipettes	Research plus (10 µL, 100 µL, 300 µL) VOYAGER	Eppendorf, Hamburg, Germany INTEGRA Biosciences GmbH, Biebertal, Germany
96-channel pipette	VIAFLO96	INTEGRA Biosciences GmbH, Biebertal, Germany
Blotting device	Trans-Blot SD	Bio-Rad Laboratories, Munich, Germany
Centrifuges	5810 R Heraeus Pico 17 Heraeus Biofuge Fresco Sovrall LYNX 4000 Allegra X-15R	Eppendorf, Hamburg, Germany Thermo Fisher Scientific, Dreieich, Germany Thermo Fisher Scientific, Dreieich, Germany Thermo Fisher Scientific, Dreieich, Germany Beckman Coulter, Krefeld, Germany
Colony picker	Qpix	Molecular devices, San José, USA
Disperser	Ultra-Turrax	IKA, Staufen, Germany
Electrophoresis chambers	Mini Protean Tetra cell PEQLAB	Bio-Rad Laboratories, Munich, Germany PEQLAB Biotechnologie GmbH, Erlangen, Germany
Electroporator	MikroPulser	Bio-Rad Laboratories, Munich, Germany
Flow cytometer	CytoFLEX Intellicyt iQue Screener	Beckman Coulter, Brea, USA Sartorius, Göttingen, Germany
HPLC system	Spark Mistral column oven L-4000 UV detector L-6200A intelligent pump Degasi Semi-Prep Plus KW-G 6B precolumn KW-803 Shodex column Autosampler 410	TECHLAB, Inc., Blacksburg, USA TECHLAB, Inc., Blacksburg, USA TECHLAB, Inc., Blacksburg, USA Biotech, Minneapolis, USA TECHLAB, Inc., Blacksburg, USA TECHLAB, Inc., Blacksburg, USA TECHLAB, Inc., Blacksburg, USA
Incubators	Axon IS-2-K SOK3190	Axon, Kaiserslautern, Germany Axon, Kaiserslautern, Germany

	VorTemp 56 ZWYC-290A UT 6200	Labnet International, Inc., Edison, USA LabWit Scientific, Burwood East, Australia Kendro Laboratory Products, Hanau, Germany
Magnetic rack	DynaMag-2 magnet	Thermo Fisher Scientific, Dreieich, Germany
Microplate stacker	Biostack	BioTek, Friedrichshall, Germany
Microplate washer	HydroFlex EL405 EL406	TECAN, Crailshaim, Germany BioTek, Friedrichshall, Germany BioTek, Friedrichshall, Germany
Microscope	IX70	Olympus K. K., Tokyo, Japan
Microwave	Inverter	Sharp K. K., Osaka, Japan
Octet	Octet QKe system	FortéBio, Fremont, USA
Photometer	ScanDrop²	Analytik Jena, Jena, Germany
Pipettes	Research plus (2.5 µL, 10 µL, 20 µL, 200 µL, 1000 µL)	Eppendorf, Hamburg, Germany
Pipetting aid	Accu-jet pro	BRAND GmbH & Co KG, Wertheim, Germany
Plate reader	Epoch	BioTek, Friedrichshall, Germany
Plate sealer	Quick-Combi Sealer Plus	HJ-Bioanalytik, Erkelenz, Germany
Power supply	PowerPac HC 200 & 300	Bio-Rad Laboratories, Munich, Germany
Rocker	Duomax 1030 & 2010	Heidolph Instruments, Schwabach, Germany
Rotator	Multi Bio RS-24	BioSan, Riga, Latvia
Scales	Entris	Sartorius, Göttingen, Germany
Sterile bench	Heraguard ECO	Thermo Fisher Scientific, Dreieich, Germany
Thermal cycler	T100 Thermal cycler	Bio-Rad Laboratories, Munich, Germany
Thermomixer	Comfort TS100-C	Eppendorf, Hamburg, Germany BioSan, Riga, Latvia
UV illuminator	ChemiDoc MP	Bio-Rad Laboratories, Munich, Germany
Vortexer	Reax top	Heidolph Instruments, Schwabach, Germany
Water system	Milli-Q UF plus	Merck KGaA, Darmstadt, Germany

2.1.3 Chemicals

The chemicals used in this study are listed in Table 3.

Table 3: List of chemicals

Chemical	Manufacturer
3,3',5,5'-Tetramethylbenzidine (TMB)	Carl Roth GmbH, Karlsruhe, Germany
3,3'-Diaminobenzidin (DAB)	Carl Roth GmbH, Karlsruhe, Germany
7-Aminoactinomycin D (7-AAD)	Thermo Fisher Scientific, Dreieich, Germany
Acetid acid	Carl Roth GmbH, Karlsruhe, Germany
Aceton	Carl Roth GmbH, Karlsruhe, Germany
Ampicillin sodium salt	AppliChem GmbH, Darmstadt, Germany
Bacto tryptone	BD Biosciences, Heidelberg, Germany
Bacto yeast extract	BD Biosciences, Heidelberg, Germany
Bovine serum albumin (BSA)	Pan Biotech GmbH, Aidenbach, Germany
Citric acid	Carl Roth GmbH, Karlsruhe, Germany
Cobalt chloride	Carl Roth GmbH, Karlsruhe, Germany
Coomassie brilliant blue	Carl Roth GmbH, Karlsruhe, Germany
D(+)-glucose-monohydrate	Carl Roth GmbH, Karlsruhe, Germany
Dimethyl sulfoxide (DMSO)	Merck KGaA, Darmstadt, Germany
Dipotassium hydrogen phosphate	Carl Roth GmbH, Karlsruhe, Germany
Disodium hydrogen phosphate dihydrate	Carl Roth GmbH, Karlsruhe, Germany
Dithiothreitol (DTT)	Carl Roth GmbH, Karlsruhe, Germany
Ethanol absolute	VWR International, Radnor, USA
Ethylenediaminetetraacetic acid	Carl Roth GmbH, Karlsruhe, Germany
Glycerol	Carl Roth GmbH, Karlsruhe, Germany
Glycine	Carl Roth GmbH, Karlsruhe, Germany
Hydrochloric acid	Carl Roth GmbH, Karlsruhe, Germany
Hydrogen peroxide	Carl Roth GmbH, Karlsruhe, Germany
Isopropyl-β-D-1-thiogalactopyranoside (IPTG)	Carl Roth GmbH, Karlsruhe, Germany
2-Propanol	Carl Roth GmbH, Karlsruhe, Germany

Kanamycin sulphate	Carl Roth GmbH, Karlsruhe, Germany
LE-Agarose	Biozym Scientific GmbH, Oldendorf, Germany
Lymphoprep	Stemcell Technologies, Vancouver, Canada
Phenylmethylsulfonylfluorid (PMSF)	Thermo Fisher Scientific, Dreieich, Germany
Potassium citrate	Carl Roth GmbH, Karlsruhe, Germany
Potassium chloride	Carl Roth GmbH, Karlsruhe, Germany
Potassium dihydrogen phosphate	Carl Roth GmbH, Karlsruhe, Germany
Propidium iodide	Carl Roth GmbH, Karlsruhe, Germany
Skim milk powder	SERVA Electrophoresis GmbH, Heidelberg, Germany
Sodium chloride	Carl Roth GmbH, Karlsruhe, Germany
Spam agar	WIECHERS & HELM GmbH & Co. KG, Hamburg, Germany
Sulfuric acid	Carl Roth GmbH, Karlsruhe, Germany
Tetracycline hypochloride	AppliChem GmbH, Darmstadt, Germany
Tris(hydroxymethyl)aminomethane	Carl Roth GmbH, Karlsruhe, Germany
TRIzol reagent	Thermo Fisher Scientific, Dreieich, Germany
Trypan blue	Merck KGaA, Darmstadt, Germany
Trypsin/EDTA	Biochrom GmbH, Berlin, Germany
Tween20	Thermo Fisher Scientific, Dreieich, Germany

2.1.4 Enzymes, markers and buffers

All commercial enzymes, markers and buffers used in this study are listed in Table 4.

Table 4: Enzymes, markers and buffers

Enzymes, markers and buffers	**Manufacturer**
Endonucleases	
AgeI-HF	New England Biolabs, Frankfurt am Main, Germany
BsiWI-HF	New England Biolabs, Frankfurt am Main, Germany

BsmBI	New England Biolabs, Frankfurt am Main, Germany
BssHII	New England Biolabs, Frankfurt am Main, Germany
Collagenase G	Sekisui Diagnostics GmbH, Burlington, USA
Collagenase H	Sekisui Diagnostics GmbH, Burlington, USA
Esp3I	New England Biolabs, Frankfurt am Main, Germany
DNase I	Merck KGaA, Darmstadt, Germany
DraIII-HF	New England Biolabs, Frankfurt am Main, Germany
HindIII-HF	New England Biolabs, Frankfurt am Main, Germany
MluI-HF	New England Biolabs, Frankfurt am Main, Germany
NcoI-HF	New England Biolabs, Frankfurt am Main, Germany
NheI-HF	New England Biolabs, Frankfurt am Main, Germany
NotI-HF	New England Biolabs, Frankfurt am Main, Germany
PacI	New England Biolabs, Frankfurt am Main, Germany
Ligases	
T4 DNA ligase	Promega GmbH, Mannheim, Germany
Polymerases	
GoTaq G2 DNA Polymerase	Promega GmbH, Mannheim, Germany
Q5 Hot Start High Fidelity DNA Polymerase	New England Biolabs, Frankfurt am Main, Germany
Buffers	
CutSmart Buffer (10x)	New England Biolabs, Frankfurt am Main, Germany

Gel Loading Dye Purple (6x)	New England Biolabs, Frankfurt am Main, Germany
Green GoTaq Flexi Reaction Buffer (5x)	Promega GmbH, Mannheim, Germany
Laemmli Sample Buffer (4x)	Bio-Rad Laboratories, Munich, Germany
NP40 Cell Lysis Buffer	Thermo Fisher Scientific, Dreieich, Germany
Q5 Reaction Buffer (5x)	New England Biolabs, Frankfurt am Main, Germany
T4 DNA Ligase Buffer (10x)	Promega GmbH, Mannheim, Germany
Tris/Glycine/SDS (TGS) running buffer (10x)	Bio-Rad Laboratories, Munich, Germany
Protein & DNA standards	
GeneRuler 1 kb DNA ladder	Thermo Fisher Scientific, Dreieich, Germany
Precision Plus Protein Standard all blue	Bio-Rad Laboratories, Munich, Germany
Precision Plus Protein Standard unstained	Bio-Rad Laboratories, Munich, Germany
Protein Standard Mix 15 – 600 kDa for SEC	Merck KGaA, Darmstadt, Germany
Others	
Alkaline phosphatase, calf intestinal (CIP)	New England Biolabs, Frankfurt am Main, Germany
Halt protease inhibitor cocktail (100x)	Thermo Fisher Scientific, Dreieich, Germany
HDGreen DNA Stain	INTAS Science Imaging Instruments GmbH, Göttingen, Germany

2.1.5 Commercial kit systems

All used commercial kit systems are listed in Table 5.

Table 5: Kit systems

Kit system	Manufacturer
CellTrace CFSE Cell Proliferation	Thermo Fisher Scientific, Dreieich, Germany
EasySep Release Human CD19 Positive Selection Kit	Stemcell Technologies, Vancouver, Canada

NucleoBond Xtra Midi	Macherey-Nagel, Düren, Germany
NucleoSpin Gel and PCR Clean up	Macherey-Nagel, Düren, Germany
NucleoSpin Plasmid Transfection-grade	Macherey-Nagel, Düren, Germany
Superscript IV First Strand Synthesis System	Thermo Fisher Scientific, Dreieich, Germany
Direct-zol RNA MiniPrep Plus	Zymo Research, Irvine, USA

2.1.6 Commercial antibodies and proteins

All used commercial antibodies are listed in Table 6. The myc-specific antibodies TUN219-2C1 (human-Fc) and TUN219-2C1 (mouse-Fc) were produced and purified in-house.

The used commercial proteins are listed in Table 7.

Table 6: Commercial antibodies

Antibody (clone)	Species	Conjugation	Manufacturer
Anti-human CD19 antibody (SJ25C1)	Mouse	FITC	BioLegend, San Diego, USA
Anti-human CD45 antibody (HI30)	Mouse	APC	BioLegend, San Diego, USA
Anti-mouse IgG HRP (polyclonal)	Goat	HRP	Merck KGaA, Darmstadt Germany
Anti-human IgG HRP (polyclonal)	Goat	HRP	Merck KGaA, Darmstadt Germany
Anti-pIII(g3p)-antibody (10C3)	Mouse	-	MoBiTec GmbH, Göttingen, Germany
Anti-human IgG (H+L) Cross-adsorbed Secondary antibody (polyclonal)	Goat	Alexa Fluor 647	Thermo Fisher Scientific, Dreieich, Germany
Anti-mouse IgG (H+L) Cross-adsorbed Secondary antibody (polyclonal)	Goat	Alexa Fluor 647	Thermo Fisher Scientific, Dreieich, Germany
CD9 antibody IHC-plus (MM2/57)	Mouse	-	LifeSpan BioSciences, Inc., Seattle, USA
Human Integrin α3/CD49c antibody (IA3)	Mouse	-	R&D Systems, Minneapolis, USA

Transferrin Receptor Antibody/CD71 (DF1513)	Mouse	-	NSJ Bioreagents, San Diego, USA
Human/Primate MMP-9 Antibody (36020)	Mouse	-	R&D Systems, Minneapolis, USA

Table 7: Commercial proteins

Protein	Manufacturer
Human MMP-9 / CLG4B Protein (His Tag)	Sino Biological, Inc., Peking, China
Human Transferrin Receptor / TFRC / CD71 Protein (His Tag)	Sino Biological, Inc., Peking, China
Recombinant Human CD9 protein (Tagged) ab152262	Abcam, Cambridge, UK
Recombinant Human Integrin α3β1/VLA-3	R&D Systems, Minneapolis, USA
Recombinant Human MMP-9	R&D Systems, Minneapolis, USA

2.1.7 Bacteria and bacteriophage

The used bacterial strains and bacteriophage are listed in Table 8.

Table 8: Bacteria and bacteriophage

Strain	Genotype	Manufacturer/Reference
E. coli ER2738	[F'*proA+B+ lacIq Δ(lacZ)M15 zzf::Tn10* (tetr)*] fhuA2 glnVΔ(lac-proAB) thi-1Δ(hsdS-mcrB)5*	Lucigen Corporation, Middleton, USA
E. coli XL1-Blue-MRF'	*∆(mcrA)183 ∆(mcrCB-hsdSMR-mrr)173 endA1 supE44 thi-1 recA1 gyrA96 relA1 lac [F´ proAB lacIqZ∆M15 Tn10 (Tetr)]*	Agilent, Santa Clara, USA
E. coli TG1	[F' *traD36 proAB lacIqZ ΔM15] supE thi-1 Δ(lac-proAB) Δ(mcrB-hsdSM)5(rK - mK -)*	Lucigen Corporation, Middleton, USA
M13K07	-	Vieira and Messing 1987
Hyperphage (M13K07ΔgIII)	-	Rondot et al. 200)

2.1.8 Mammalian cell lines

All cell lines used in this study are listed in Table 9.

Table 9: Mammalian cell lines

Cell line	Organism	Tissue	Disease	Reference
HEK293	Human	Kidney	-	ATCC, Manassas, USA
FaDu	Human	Pharynx	Squamous cell carcinoma	ATCC, Manassas, USA
Detroit-562	Human	Pharynx (pleural effusion)	Pharyngeal carcinoma	ATCC, Manassas, USA
CHO-K1	Hamster	Ovary	-	ATCC, Manassas, USA

2.1.9 Gene syntheses

All gene syntheses used in this work were provided by Integrated DNA Technologies (Coralville, USA). Sequences of human CD9, human CD71 and human MMP-9 were obtained from public database (https://www.uniprot.org/).

2.1.10 Plasmids and oligonucleotides

All plasmids and oligonucleotides used in this work are listed in Table 10. Oligonucleotides used for library construction were obtained from a previous publication (Kügler et al. 2018). Primers for cloning of IgG (2.2.2.7) were designed based on the respective antibody sequence containing the required restriction sites and provided by Biolegio (Nijmegen, Netherlands). Oligonucleotides used for standard colony PCR and gBlock amplification are listed in Table 11.

Table 10: Phagemid and plasmids

Plasmid	Description	Reference
pHAL30	Phagemid, coding for protein:pIII fusion, lacZ promoter, pelB leader sequence, Yol-linker	Kügler et al. 2015
pCSE2.6-mIgG2a-Fc-XP	Mammalian expression vector for scFv-Fc format, mouse2a-Fc, pCSE-backbone, CMV promoter	Based on pCSE2.5 (Jäger et al. 2013)
pCSEH1c	Mammalian expression vector for IgG-HC, human-CH1, -CH2 & -CH3, pCSE-backbone, CMV promoter	Based on pCSE2.5 (Jäger et al. 2013)

pCSL3k	Mammalian expression vector for IgG-LC (kappa), human-CL-lambda, pCSE-backbone, CMV promoter	Based on pCSE2.5 (Jäger et al. 2013)
pCSL3l	Mammalian expression vector for IgG-LC (lambda), human-CL-lambda, pCSE-backbone, CMV promoter	Based on pCSE2.5 (Jäger et al. 2013)
pCSE2.6-TM-GFP	Mammalian expression vector coding for a protein-GFP fusion with intermediate transmembrane domain, pCSE-backbone, CMV promoter	Based on pCSE2.5 (Jäger et al. 2013)
pCSE2.6-GFP	Mammalian expression vector coding for a protein-GFP fusion, pCSE-backbone, CMV promoter	Based on pCSE2.5 (Jäger et al. 2013)

Table 11: Oligonucleotides

ID	Description	Sequence (5'-3')
YP11	MHgIII_r	CTAAAGTTTTGTCGTCTTTCC
YP125	MHLacZ-Pro_f	GGCTCGTATGTTGTGTGG
YP411	Tor-pCMV-mIgG01_Fc-seq-r	CAGATGGCTGGCAACTAG
YP886	CM2_F	CGCAAATGGGCGGTAGGCGTG
YP1371	Gene_amp-fwd	GGGTAGGTAGGTAGGTAGGG
YP1461	Gene_amp-rev	CGCTATGCGTATCGCTATCGC

2.1.11 Buffers and solutions

The buffers and solutions used in this study are listed in Table 12.

Table 12: Buffers and solutions

Buffer/solution	Component	Concentration	Solvent
1 N sulfuric acid	Sulfuric acid	500 mM	Ultrapure water
2 M Glucose	Glucose	2 M	Ultrapure water
10x DTT	1,4'-Dithiothreitol	250 mM	Ultrapure water
10x GA	2 M Glucose 2xYT medium	49.5% (v/v) 49.5% (v/v)	-

	100 mg/mL Ampicillin	1% (v/v)	
10000x PI	Propidium iodide	1% (w/v)	Ultrapure water
0.1% Trypan blue	Trypan blue Sodium chloride	0.1% (w/v) 0.9% (v/v)	Ultrapure water
Agarose gel	Agarose HDGreen DNA Stain	1.5% (w/v) 0.0023% (v/v)	TAE buffer
Blotting buffer	TRIS Glycine	25 mM 192 mM	Ultrapure water
BSA-PBST	Bovine serum albumin	1% (w/v)	PBST
Coomassie staining solution	Coomassie brilliant blue 2-Propanol Acetic acid	0.05% (w/v) 25% (v/v) 10% (v/v)	Ultrapure water
DAB stock	3'-Diaminobenzidine	2.5% (w/v)	Ultrapure water
DAB reaction buffer	$CoCl_2$	0.02% (w/v)	PBS
DNase I reaction buffer	Tris $MgCl_2$ $CaCl_2$ BSA	50 mM 25 mM 25 mM 5% (w/v)	Ultrapure water
FACS buffer	EDTA Fetal bovine serum	2 mM 5% (v/v)	PBS
MilliQ-Tween	Tween20	0.05% (v/v)	Ultrapure water
MPBST	Skim milk powder	2% (w/v)	PBST
PBST	Tween20	0.05% (v/v)	PBS
PEG/NaCl	Polyethylene glycol NaCl	20% (w/v) 2.5 M	Ultrapure water
Phage dilution buffer	TRIS-HCl EDTA NaCl	10 mM 2 mM 20 mM	Ultrapure water

Phosphate buffered saline (PBS)	NaCl KCl Na_2HPO_4 x 2 H_2O KH_2PO_4	0.8% (w/v) 0.02% (w/v) 0.14% (w/v) 0.024% (w/v)	Ultrapure water
PMSF	PMSF	100 mM	2-Propanol
SDS running buffer	10x TGS running buffer	10% (v/v)	Ultrapure water
TAE buffer	TRIS EDTA Acetic acid	40 mM 2 mM 20 mM	Ultrapure water
TMBA	Potassium citrate Citric acid	30 mM 50 mM	Ultrapure water
TMBB	Acetone Ethanol Hydrogen peroxide Tetramethylbenzidine	10% (v/v) 90% (v/v) 0.3% (v/v) 1 mM	-
TMB reagent	TMBA TMBB	95% (v/v) 5% (v/v)	-
Trypsin (10 µg/mL)	Trypsin	0.003% (w/v)	PBS

2.1.12 Media and supplements

2.1.12.1 Media and supplements for bacterial culture

Recipes and composition of used media (Table 13 and Table 15) and the respective supplements (Table 14) are listed below.

Table 13: Recipes for basic media

Medium	Component	Concentration	Solvent
2xYT medium	Bacto tryptone Yeast extract NaCl	1.6% (w/v) 1.0% (w/v) 0.5% (w/v)	Ultrapure water

	optional: Spam agar	1.5% (w/v)	
LB medium	Bacto tryptone Yeast extract NaCl *optional:* Spam agar	1.0% (w/v) 0.5% (w/v) 1.0% (w/v) 1.5% (w/v)	Ultrapure water
SOB medium	Bacto tryptone Yeast extract NaCl KCl	2% (w/v) 0.5% (w/v) 0.5% (w/v) 0.02% (w/v)	Ultrapure water
SOC medium	$MgCl_2$ Glucose	20 mM 20 mM	SOB medium

Table 14: Concentration of media supplements

Supplement	Stock concentration	Final concentration
Ampicillin	100 mg/mL	100 µg/mL
Tetracycline	10 mg/mL	20 µg/mL
Kanamycin	50 mg/mL	50 µg/mL
Glucose	2 M	100 mM
IPTG	1 M	50 µM

Table 15: Composition of used media

Medium	Supplement	Final concentration
2xYT-A	Ampicillin	100 µg/mL
2xYT-AK	Ampicillin Kanamycin	100 µg/mL 50 µg/mL
2xYT-AT-IPTG	Ampicillin Tetracycline IPTG	100 µg/mL 20 µg/mL 50 µM

2xYT-GA	Glucose Ampicillin	100 mM 100 µg/mL
2xYT-GAT	Glucose Ampicillin Tetracycline	100 mM 100 µg/mL 20 µg/mL
2xYT-T	Tetracycline	20 µg/mL
LB-A	Ampicillin	100 µg/mL
LB-GA	Glucose Ampicillin	100 mM 100 µg/mL
LB-GAT	Glucose Ampicillin Tetracycline	100 mM 100 µg/mL 20 µg/mL

2.1.12.2 Media and solutions for mammalian cell culture

All media and supplements used in this study are listed in Table 16. FBS was heat-inactivated at 55°C for 1 h, aliquoted and stored at -20°C prior to use.

Table 16: Commercial media and solutions

Medium/solution	Manufacturer
FBS superior	Biochrom GmbH, Berlin, Germany
Penicillin/Streptomycin	Biochrom GmbH, Berlin, Germany
RPMI 1640	Biochrom GmbH, Berlin, Germany
Trypsin/EDTA	Biochrom GmbH, Berlin, Germany
Versene (EDTA)	Biozym Scientific GmbH, Oldendorf, Germany
VLE-DMEM	Biochrom GmbH, Berlin, Germany

2.1.13 Software

Software used in this study is in Table 17.

Table 17: Software

Software	Application	Source
Clarity	Data acquisition with HPLC system	DataApex, Prague, Czech Republik
CytExpert	Data acquisition with CytoFLEX	Beckman Coulter, Brea, USA
FlowLogic	Analysis of flow cytometric data	Miltenyi BioTec GmbH, Bergisch Gladbach, Germany
ForeCyt	Data acquisition and analysis with Intellicyt iQue Screener	Sartorius, Göttingen, Germany
Gen5	ELISA reader	BioTek Instruments, Vermont, USA
GraphPad Prism7	Data and statistical analysis	https://www.graphpad.com/
IMGT	Analysis of antibody sequences	http://www.imgt.org/
Liquid Handling Control	Microplate washer EL406	BioTek Instruments, Vermont, USA
Microsoft office	Data evaluation and writing	Microsoft Corporation, Washington USA
NCBI	Literature research	https://www.ncbi.nlm.nih.gov/
Octet DataAcquisition11	Operation and data acquisition with Octet System	FortéBio, Fremont, USA
Octet DataAnalysis11	Analysis of Octet System data	FortéBio, Fremont, USA
Protein atlas	Protein database	https://www.proteinatlas.org/
UGENE	Sequence analysis and alignment	Unipro LLC, Novosibirsk, Russia
UniProt	Protein database	https://www.uniprot.org/
Vortex	Data evaluation	Dotmatics, Bishop's Stortford, UK
Zotero	Literature management and citation	https://www.zotero.org/

2.1.14 Tumor material

Tumor specimens were obtained from head and neck cancer patients in the course of their curative surgery and kindly provided by Prof. Dr. Andreas Gerstner (Städtisches Klinikum Braunschweig, Germany). Regardless of their age, gender and previous therapy patients were included if they gave their free and informed consent. This study was examined and approved by the ethics committee of the faculty of life sciences (Technische Universität Braunschweig, Germany) (ID: FV-2016-10).

2.2 Methods

2.2.1 Microbiological methods

2.2.1.1 Cultivation of bacteria

Bacterial cultures were inoculated either from glycerol stocks of from single clones on agar plates and cultivated in 2xYT or LB medium supplemented with the appropriate antibiotics. If bacteria carried a pHAL-construct, 100 mM glucose was added to the medium. Cells were incubated overnight (16-18 h) at 37°C and 250 rpm.

2.2.1.2 Plating

Upon transformation or infection with phage, bacteria were plated on 2xYT or LB agar plates supplemented with 100 mM glucose and the respective antibiotics using disposable spatula. Plates were incubated overnight (16-18 h) at 37°C.

2.2.1.3 Storage of bacteria

Bacteria grown on agar plates were stored at 4°C for up to one week. For long-term storage of liquid cultures, glycerol stocks of 1 mL (tubes) or 180 µL (microtiter plate) were prepared by adding a final volume of 20% glycerol (v/v). Stocks were snap frozen in liquid nitrogen and stored at -80°C.

2.2.1.4 Preparation of plasmid DNA

Plasmid DNA was isolated and purified either in small (mini preparation) or in large scale (midi preparation). Plasmid-containing bacteria were cultivated overnight at 37°C and 250 rpm in 5 mL (mini) or 100 mL (midi) LB medium supplemented with the appropriate antibiotics (100 mM glucose for pHAL-constructs). Cultures were transferred into 1.5 mL tubes or 50 mL falcon tubes and centrifuged at 15.000xg for 30 s or at 3220xg for 10 min, respectively. Supernatants were discarded and cell pellets were used for plasmid preparation using the NucleoSpin Plasmid Mini Kit or the NuceloBond Plasmid Midi Kit (Macherey-Nagel, Düren, Germany) according to the manufacturer's protocol. DNA was eluted with ultrapure water and concentration was determined using a microvolume spectrophotometer. DNA was stored at 4°C for up to one week or at -20°C.

2.2.1.5 Transformation of bacteria

2.2.1.5.1 Heat-shock transformation

Within cloning of DNA constructs, chemically competent XL1-Blue-MRF' cells were transformed by the heat-shock method. 50 µL cells were slowly thawed on ice, mixed with the ligation and incubated on ice for 15 min. Heat shock was applied by incubating the cells at 42°C for 60 s followed by incubation on ice for 2 min. Cells were immediately resuspended in 150 µL pre-warmed SOC medium and incubated at 37°C and 650 rpm for 1 h. The whole cell suspension was plated on 2xYT-GA agar plates and incubated overnight at 37°C.

2.2.1.5.2 Electroporation

To increase transformation efficacies within antibody library cloning, electrocompetent bacteria were transformed by electroporation. To prevent arcing during electric pulsing ligation was desalted prior to electroporation. Reaction mix was transferred into Amicon Ultra Centrifugal Filters (30K) (Merck KGaA, Darmstadt, Germany), topped up with ice-cold ultrapure water and centrifuged at 14000xg for 10 min. Flow-through was discarded and procedure was repeated three times. Sample was eluted by centrifuging the inverted column into a fresh tube at 2000xg for 2 min. Electrocompetent cells (ER2738 or XL1-Blue-MRF') were slowly thawed on ice and mixed with the eluted ligation. Cells were incubated on ice for 2 min, transferred into an ice-cold electroporation cuvette and electric pulse was applied with 1.7 kV. Cells were immediately resuspended in 1 mL pre-warmed SOC medium, transferred into a 1.5 mL tube and incubated at 37°C and 650 rpm for 1 h. 10 µL of cell suspension was saved for titration (2.2.3.3). Remaining volume was plated on 2xYT-GAT pizza plates and incubated overnight at 37°C (XL1-Blue-MRF') or 30°C (ER2738).

2.2.2 Molecular biological methods

2.2.2.1 Polymerase-chain reaction

2.2.2.1.1 Colony-PCR

Amplification of inserts by colony-PCR was used to confirm correct insert size and to determine insert rates of antibody libraries upon transformation. GoTaq G2 DNA polymerase (Promega, Mannheim, Germany) was used according to the protocol provided by the manufacturer. Primer sets were selected respective to the vector backbone (Table 18) and added to the reaction mix. Single colonies were picked from agar plates and used as templates for PCR reaction, which was performed in a thermal cycler using the protocol suggested by the supplier. Amplified DNA was analysed in agarose gel electrophoresis (2.2.2.2).

Table 18: Primer sets for colony PCR

Vector backbone	Primer set
pHAL	YP11 / YP125
pCSE	YP411 / YP886

2.2.2.1.2 Amplification of genes

Within cloning of DNA, PCR was used to amplify genes. Plasmid DNA or DNA syntheses containing the desired sequence was used as template. For amplification of genes, Q5 Hotstart High Fidelity DNA Polymerase (New England Biolabs, Frankfurt am Main, Germany) was used. Reaction mix was prepared as suggested by the manufacturer. Oligonucleotide primers flanking the desired DNA fragment were selected respective to the given template and added to the reaction mix. PCR was performed according to the supplied protocol in a thermal cycler and amplification of correct DNA fragments was confirmed in agarose gel electrophoresis (2.2.2.2).

2.2.2.2 Agarose gel electrophoresis

DNA fragments were separated by size for analysis using agarose gel electrophoresis. DNA samples were mixed with DNA loading dye and loaded on a 1.5% agarose gel (w/v) supplemented with HD Green DNA Stain. The GeneRuler 1 kb Plus DNA ladder (Thermo Fisher Scientific, Dreieich, Germany) was used as reference for fragment size evaluation. Gel electrophoresis was run at 130 V for 30 min and gels were documented in a camera system under UV light.

2.2.2.3 Digestion and dephosphorylation of DNA

For cloning DNA fragments were digested with appropriate endonucleases. All endonucleases used in this study were provided by New England Biolabs (Frankfurt am Main, Germany) and digestions were performed according to the manufacturer's protocol. Digested plasmid DNA additionally was dephosphorylated to prevent undesired re-ligation using CIP (New England Biolabs, Frankfurt am Main, Germany) as suggested by the supplier. Upon digestion, DNA was purified (2.2.2.4), concentration was determined using a microvolume spectrophotometer and stored at -20°C.

2.2.2.4 Purification of amplified and digested DNA

Amplified DNA was purified upon amplification or digestion for further cloning. If DNA was separated by size in agarose gel electrophoresis first, the desired bands of expected size were excised from gel using a disposable scalpel and transferred into a 2 mL reaction tube. 200 µL NTI buffer per 100 mg gel were added and sample was incubated at 55°C for 20 min until gel fragments were dissolved completely. If DNA was purified directly from PCR or digestion

reaction mix, 200 µL NTI DNA binding buffer were added per 100 µL sample volume. DNA was purified using the NucleoSpin Gel and PCR Clean-up kit (Macherey-Nagel, Düren, Germany) according to the instruction given by the supplier. DNA was eluted with ultrapure water and concentration was determined using a microvolume spectrophotometer. DNA was stored at -20°C.

2.2.2.5 Cloning of GFP-fusion proteins

Genes of human MMP-9, CD9 and CD71 were obtained from public database (https://uniprot.org/) and synthesised (Integrated DNA Technologies, Coralville, USA). Genes were amplified by Q5-PCR (2.2.2.1.2), digested with PacI/NotI (CD9 and CD71) or BssHII/NotI (MMP-9) (2.2.2.3) and analysed in agarose gel electrophoresis (2.2.2.2). Desired bands were excised, purified (2.2.2.4) and ligated with the respective target vector, which was previously digested with the same enzymes and dephosphorylated. CD9 and CD71 were cloned into pCSE2.6-GFP, whereas MMP-9 was ligated with pCSE2.6-TM-GFP, which additionally adds a transmembrane domain between protein and GFP. Ligations were performed using the T4 DNA Ligase (Promega, Mannheim, Germany) according to the manufacturer's protocol adjusting a molar ratio of 3:1 (insert to vector), incubated at toom temperature for 3 h and used for heat-shock transformation of chemically competent bacteria (2.2.1.5.1). Successful cloning was confirmed by colony PCR (2.2.2.1.1) and sanger sequencing (2.2.2.8.1).

2.2.2.6 Cloning of scFv-Fc

For cloning of scFv-Fc fragments, whole scFv-sequences were amplified directly from phagemid and cloned into target vector pCSE2.6-mIgG2a-Fc-Xp. Purified plasmid DNA (1-10 ng) of the appropriate clone was used as template for Q5-PCR (2.2.2.1.2). Amplified DNA was digested with NcoI and NotI (2.2.2.3) and analysed in agarose gel electrophoresis (2.2.2.2). Desired band (~850 bp) was excised, purified from gel (2.2.2.4) and ligated with the previously NcoI/NotI-digested, CIP-treated target vector. Ligations were performed using the T4 DNA Ligase (Promega, Mannheim, Germany). Reactions were prepared according to the manufacturer's protocol adjusting a molar ratio of 3:1 (insert to vector), incubated at room temperature for 3 h and used for heat-shock transformation of chemically competent bacteria (2.2.1.5.1). Successful cloning was confirmed by colony PCR (2.2.2.1.1) and sanger sequencing (2.2.2.8.1).

2.2.2.7 Cloning of IgG

For cloning of IgG, variable domains of heavy and light chain were amplified separately and cloned into pCSEH1c (heavy chain) or pCSL3k/pCSL3l (light chain), respectively. Overnight culture (1 µL) of the appropriate clone was used as template for Q5-PCR (2.2.2.1.2). Two PCR reactions per clone were performed to amplify both the VH and VL of each antibody using the appropriate primers, which were designed based on the respective antibody sequence and

added the required restriction sites. Amplified insert DNA and target vectors were digested with the respective enzymes (Table 19) (2.2.2.3) and purified (2.2.2.4). Ligations were performed using the T4 DNA Ligase (Promega, Mannheim, Germany). Reactions were prepared according to the manufacturer's protocol adjusting a molar ratio of 3:1 (insert to vector), incubated at room temperature for 3 h and used for heat-shock transformation of chemically competent bacteria (2.2.1.5.1). Successful cloning was confirmed by colony PCR (2.2.2.1.1) and sanger sequencing (2.2.2.8.1).

Table 19: Combination of enzymes for IgG cloning

DNA	Target vector	Enzymes
VH	pCSEH1c	BssHII / NheI
VL (kappa)	pCSL3k	AgeI / BsiWI
VL (lambda)	pCSL3l	AgeI / DraIII

2.2.2.8 DNA sequencing

2.2.2.8.1 Single tube sequencing

Purified plasmid DNA containing the sequence of interest was diluted in ultrapure water (80 ng/µL) and sent to Microsynth SeqLab (Göttingen, Germany) for Sanger sequencing.

2.2.2.8.2 Plate sequencing

Sequencing plates (96-well) were prepared with 150 µL 2xYT medium supplemented with the appropriate antibiotics (100 mM glucose for pHAL constructs). Each well was inoculated with a clone carrying the DNA of interest and incubated at 37°C and 800 rpm for 3 h. Plate was sealed and sent to Microsynth SeqLab (Göttingen, Germany) for Sanger sequencing.

2.2.2.8.3 Next generation sequencing (NGS)

For next generation sequencing of scFv-libraries, plasmid DNA was purified from 1 mL glycerol stock upon library cloning (2.2.3.3). NGS sequencing, analysis and raw data processing was kindly performed by Dr. Thomas Clarke (EMD Serono, Billerica, USA). In detail, amplicon libraries were prepared via PCR and adapters for immobilisation and sequencing were annealed to both the 3' and the 5' ends. Libraries were then bridge-amplified for cluster formation and sequenced by synthesis in a MiSeq Illumina sequencer. Raw data was cleared from non-overlapping reads and short and non-productive sequences for further evaluation.

2.2.3 Construction of recombinant TIL-B antibody libraries

2.2.3.1 Processing of tumor samples

Specimens of primary tumors derived from head and neck cancer patients were obtained freshly upon curative surgery and kindly provided by Prof. Dr. Andreas Gerstner (Städtisches Klinikum Braunschweig, Germany). After determining the wet weight, tissue was manually minced using surgical scissors and digested with 30 U DNaseI, 3 U collagenase G and 10 U collagenase H in DNaseI reaction buffer for 1 h at 37°C. If sample weight was ≥250 mg, digested tissue was additionally homogenised in a disperser (IKA, Staufen, Germany). Samples <250 mg were directly passed through a 40 µm cell strainer in order to obtain a single cell suspension and 20 µL were used for counting the cells in a Neubauer chamber (2.2.6.3). In total 10^5 cells were aliquoted into a 1.5 mL tube, pelleted by centrifugation (500xg, 10 min) and resuspended in PBS. Cells were stained with fluorochrome-conjugated anti-CD19 (FITC) and anti-CD45 (APC) antibodies (BioLegend, San Diego, USA), which were diluted in 1:400 in FACS buffer. Upon 15 min of incubation on ice, cells were washed once, resuspended in FACS buffer and analysed in a flow cytometer (2.2.5.7). The amount of detected CD19+/CD45+ B cells in relation to the total number of counted cells was calculated to estimate the theoretical B cell count within the whole sample.

2.2.3.2 Isolation of B cells

CD19+ B cells were isolated from tumor tissue cell suspension using the EasySep Release Human CD19 Positive Selection Kit (Stemcell Technologies, Vancouver, Canada) according to the manufacturer's protocol. Upon isolation, eluted B cells were transferred into a 1.5 mL tube, pelleted by centrifugation at 500xg for 5 min, resuspended in 1 mL TRIzol reagent (Thermo Fisher Scientific, Dreieich, Germany) and stored at -80°C.

2.2.3.3 Construction of antibody gene libraries

B cells isolated from tumor samples (2.2.3.2) were thawed and total mRNA was isolated using the Direct-zol RNA MiniPrep Plus kit system (Zymo Research, Irvine, USA) according to the instructions provided by the manufacturer. Antibody gene libraries were constructed as described previously (Kügler et al. 2018). In detail, cDNA was synthesised from total RNA by reverse transcription and used as template for antibody gene amplification. Variable antibody domains were amplified and cloned successively into phagemid pHAL30. Transformed bacteria were titrated to determine the respective library size and colony PCR was conducted to calculate the insert rate. Library glycerol stocks were stored at -80°C or directly used for scFv-phage production (2.2.3.4).

2.2.3.4 Production of scFv-phage (packaging)

In this work, antibody gene libraries were packaged with Hyperphage, which lacks the gene gIII for the wild type minor coating protein pIII (Rondot et al. 2001) and therefore only integrates

scFv-pIII fusion proteins. This leads to a multivalent scFv-display on each phage, thus increasing the chance to select antigen-specific scFv fragments within the first panning round. Library packaging was performed as described before (Kügler et al. 2018). In short, culture was inoculated from library glycerol stock and infected with a 20-fold excess of Hyperphage. Upon incubation overnight, produced phage were precipitated with PEG/NaCl solution, purified and resuspended in phage dilution buffer. Phage libraries were titrated to determine the respective phage concentration and analysed in SDS-PAGE (2.2.5.1) and immunoblotting (2.2.5.3) to confirm the display of scFv-pIII fusion proteins. Phage libraries were aliquoted and stored at 4°C.

2.2.4 Selection of recombinant TIL-B-antibodies

2.2.4.1 Selection of scFv antibodies in microtiter plates

The selection of antibody fragments from phage libraries in microtiter plates was conducted as described previously (Hust et al. 2014; Russo et al. 2018). Briefly, scFv-phage libraries were incubated on the respective immobilised antigen. Whereas unbound phage were removed by stringent washing, bound phage were eluted and used for re-infection of bacteria. Upon co-infection with helper phage M13K07, scFv-phage were amplified overnight and used for the next panning round. In this work, antigen-binding phage were enriched over three panning rounds. Eluted phage of the last panning round were used for re-infection of bacteria. Single clones were picked for production of soluble scFv fragments, which were screened for antigen-binding in ELISA.

2.2.4.2 Selection of scFv antibodies on cells

The selection of scFv-phage libraries on whole cells was performed as described before (Fahr and Frenzel 2018). The pharyngeal carcinoma cell line FaDu was used target cell line for selection. Prior to selection, phage libraries were depleted on HEK293 and CHO-K1 cells, which served as negative cell lines. Upon washing, bound phage were eluted and used for re-infection of bacteria and phage production. FaDu-binding phage were enriched over three panning rounds. Eluted phage of the last panning round were used to re-infect bacteria. Single clones were picked for production of soluble scFv fragments, which were screened for FaDu-binding in flow cytometry. Enrichment of FaDu-binding antibodies was analysed by plotting the mean fluorescence intensity (MFI) of each clone on the respective cell line and by calculating the variance within the mean values by using the one-way ANOVA test (GraphPad Prism7 software). *P* values less than 0.05 were considered statistically significant (*$P < 0.05$; **$P < 0.01$; ***$P < 0.001$; ****$P < 0.0001$)

2.2.5 Biochemical and immunological methods

2.2.5.1 SDS-PAGE

For separation of proteins by their size, SDS-PAGE was performed. Mini-Protean TGX stain-free gels (Bio-Rad Laboratories, Munich, Germany) were used according to the instructions given by the supplier. For conventional protein samples 12% gels were used whereas eluate of immunoprecipitation was separated in 4-15% gradient gels. Protein samples were supplemented with 4x Laemmli buffer and 10x DTT and incubated at 95°C for 10 min. 14 µL of each sample and 5 µL of the respective protein standard were loaded and SDS-PAGE was run at 250 V for 25 min in running buffer. For conventional SDS-PAGE and Coomassie staining the Precision Plus Protein Standard unstained (Bio-Rad Laboratories, Munich, Germany) was used whereas for Western blotting the Precision Plus Protein Standard all blue (Bio-Rad Laboratories, Munich, Germany) was loaded additionally. Upon electrophoresis, gels were documented and analysed under UV light or used for Coomassie staining or immunoblotting.

2.2.5.2 Coomassie staining

Upon SDS-PAGE, gel was transferred into a glass petri dish and covered with Coomassie staining solution. Gel was heated in a microwave for 40 s and incubated at room temperature on a rocker for 20 min. Coomassie staining solution was removed and gel was covered with 10% acetic acid. Gel was heated in a microwave for 40 s and incubated at room temperature on a rocker for 1 h. Acetic acid was removed, gel was documented and used for mass spectrometric analysis.

2.2.5.3 Immunoblotting

Prior to immunoblotting, a PVDF membrane was incubated in 98% ethanol for 2 min whereas blotting paper was hydrated in blotting buffer. Blotting paper was placed in a blotting device and topped with membrane, the SDS-gel and another blotting paper. Blot was run at 20 V for 45 min. Upon incubation, blotting paper and gel were discarded and membrane was incubated in MPBST for 1 h on a rocker. Blocking solution was discarded and membrane was washed three times with PBST. Membrane was incubated in 5 mL primary antibody solution (1 mg/mL in MPBST) and incubated for 1 h at room temperature on a rocker. Solution was discarded, membrane was washed three times with PBST and incubated in 5 mL HRP-conjugated secondary antibody (Merck KGaA, Darmstadt, Germany) diluted 1:1000 in MPBST. Solution was discarded and membrane was washed three times in PBST. DAB reagent was prepared by adding 200 µL DAB stock and 1 µL 30% hydrogen peroxide to 10 mL DAB reaction buffer. Membrane was incubated in DAB reagent at room temperature for 20 min. Reagent was removed and collected in a special waste for heavy metals. Membrane was washed three times with water, dried between paper towels and documented.

2.2.5.4 Titration ELISA (enzyme-linked immunosorbent assay)

Titration ELISA was used in order to analyse dose-dependent binding of antibody candidates to desired antigens. A sufficient number of wells of a 96-well assay plate (Corning, Inc., New York, USA) were coated with the appropriate antigen diluted in PBS (2 ng/µL). In parallel, an identical number of wells was coated with BSA-PBST as negative control. Plate was incubated for 1 h at room temperature or overnight at 4°C. Solution was removed and wells were blocked with 300 µL BSA-PBST for 1 h at room temperature on a rocker. Upon incubation, all wells were washed 3 times with PBST in an ELISA washer. Starting from a concentration of 10 µg/mL, primary antibodies were diluted 1:$\sqrt{10}$ in BSA-PBST and added to the appropriate antigen and control wells. Upon incubated for 1 h at room temperature on a rocker wells were washed 3 times with PBST in an ELISA washer. HRP-conjugated secondary antibody (Merck KGaA, Darmstadt, Germany) was diluted 1:1000 in BSA-PBST and added to each well. Plate was incubated for 1 h at room temperature on a rocker and washed subsequently 3 times with PBST in an ELISA washer. TMB reagent was prepared freshly before use and added to each well. Upon 25 min of incubation at room temperature reaction was stopped by adding 1N sulfuric acid and plate was documented in an ELISA reader. Absorbance signals were normalised and plotted against a logarithmic scale of the respective antibody concentration to determine the EC50 value reflecting the half-maximal effective concentration.

2.2.5.5 Immunoprecipitation

In order to identify potential targets of antibody candidates, proteins were precipitated from whole cell lysate of FaDu or transfected antigen expressing HEK293 cells (2.2.6.9). Lysate prepared from non-transfected HEK293 cells was used as negative control. Immunoprecipitation was conducted using the SureBreads Protein A Magnetic Beads (Bio-Rad Laboratories, Munich, Germany) according to the manufacturer's protocol. Eluted proteins were analysed in SDS-PAGE (2.2.5.1) and Coomassie staining (2.2.5.2). Bands, which were exclusively present in the eluate of the target cell line but not or less intensely present in the control lysate were excised and identified in mass spectrometry. Protein purification from gel, mass spectrometric analysis and raw data evaluation were kindly performed by Dr. Roland Kellner (Merck KGaA, Darmstadt, Germany).

2.2.5.6 Immunostaining of mammalian cells

Cells, which were used for immunostaining were harvested using Versene (EDTA) to preserve surface antigens (2.2.6.4) whereas non-adherend HEK293 cells were always obtained freshly from current culture. For immunostaining, 2 x10^5 cells/well were aliquoted into a 96 well plate (u-shape, PP) and pelleted by centrifugation (300xg, 4°C, 5 min). Cells were washed once with FACS buffer and resuspended in the appropriate primary antibody diluted in FACS buffer. Upon 15 min of incubation on ice, cells were washed once with FACS buffer and resuspended

with an AlexaFluor647-conjugated secondary antibody (Thermo Fisher Scientific, Dreieich, Germany) diluted 1:2000 in FACS buffer. Upon 15 min of incubation of ice protected from light, cells were washed twice, resuspended in FACS buffer supplemented with propidium iodide (1:10000 of 1% PI) and analysed in a flow cytometer (2.2.5.7).

2.2.5.7 Flow cytometric analysis of cells

Forward scatter (FSC) plotted against sideward scatter (SSC) was used to remove cell debris and smaller highly granular cells by gating. Within the gated cell population, dead cells (PI+) were detected with a 585 ± 42 nm filter (PE-channel). Living cells were gated and plotted in forward scatter width (FSC-W) against sideward scatter area (SSC-A) to enable differentiation between single cells and doublets. Within the gated subpopulation, GFP and FITC signals were detected with a 525 ± 40 nm filter (FITC-channel) whereas APC and Alexa Fluor 647 signals were detected using a 660 ± 10 nm filter (APC-channel). Analysis and evaluation of flow cytometric data was performed using FlowLogic.

2.2.5.8 Size exclusion chromatography (SEC)

SEC was used to test if antibody solutions contained monomers, aggregates or degradation products. Antibodies were diluted in PBS (200 µg/mL) in a glass micro vial and placed into the autosampler of the HPLC system. The Protein Standard Mix 5 – 600 kDa (Merck KGaA, Darmstadt, Germany) was used as reference. Defined molecular weight of each component of the protein standard mix was plotted against the corresponding detected retention times to obtain a standard curve facilitating determination of the molecular weight of the appropriate analyte. Curve area represented the respective proportion of each component within the sample.

2.2.5.9 Measurement of antibody affinities

Kinetics measurement in this work were conducted using biolayer interferometry (BLI) in the Octet system (FortéBio, Fremont, USA) according to the manufacturer's protocol. Antibody candidates (human IgG format) were immobilised on anti-human IgG Fc capture (AHC) or on anti-human Fab-CH1 (FAB2G) biosensors and exposed to different concentrations of the desired antigen diluted in BSA-PBST. Upon loading, association of the respective antigen was detected followed by dissociation in BSA-PBST. Upon data acquisition, curves were fit using a mathematical model (1:1 interaction, global fit) facilitating calculation of the on-rate (k_{on}) and off-rate (k_{dis}) of the respective antibody. The resulting affinity constant K_d (k_{on}/k_{dis}) was determined to quantify the appropriate antibody affinity.

2.2.6 Cell culture methods

Each protocol described in this section was performed under sterile conditions using a laminar flow bench using sterile consumables, media and solutions.

2.2.6.1 Thawing of cells

Frozen cells were thawed in a water bath at 37°C until cells were not thawed completely. Cells were transferred into 13 mL of the appropriate culture medium in a 15 mL falcon tube. Cells were pelleted by centrifugation at 120xg and room temperature for 5 min. Supernatant was discarded, cells were resuspended in 5 mL medium and used for experiments or transferred into 15 mL medium in a T75 flask for further culturing. Cells were incubated at 37°C and 5% CO_2 for 48 h.

2.2.6.2 Subculturing of cells

FaDu, Detroit-562 and CHO-K1 cells were grown in T75 (or T175) cell culture flasks and subcultured every second or third day. Culture medium was removed, cell layer was rinsed with 5 mL (or 10 mL) PBS and 2 mL (or 5 mL) trypsin/EDTA were added. Cells were incubated at 37°C for 5 – 10 min until cells were detached completely. Trypsin/EDTA was inactivated by adding culture medium. An appropriate volume of cells was transferred into a fresh flask and topped up to 20 mL (or 40 mL) with medium. Cells were further incubated at 37°C and 5% CO_2 for 48 or 72 h. The respective culture media and splitting ratio is listed in the table below (Table 20). Culturing of HEK293 cells was performed by Marie Kastull (Yumab GmbH, Braunschweig, Germany).

Table 20: Culture media and splitting ratios of used cell lines

Cell line	Culture medium	Splitting ratio
FaDu	DMEM + 10% FBS + 1% Penicillin/Streptomycin	1:3 or 1:4
Detroit-562	DMEM + 10% FBS + 1% Penicillin/Streptomycin	1:3 or 1:4
CHO-K1	RPMI 1640 + 10% FBS + 1% Penicillin/Streptomycin	1:6 or 1:10

2.2.6.3 Counting of cells

Prior to counting, cells were stained with Trypan blue to facilitate differentiation of dead and living cells. Cells were mixed 1:1 with 0.1% Trypan blue, introduced into a Neubauer chamber and living cells were counted under a microscope. Number of counted cells in 4 larger squares was averaged for cell count calculation according to the manufacturer's protocol.

2.2.6.4 Harvesting cells for experiments

If needed for experiments, cells were detached using Versene (EDTA) instead of trypsin/EDTA in order to preserve surface proteins. Supernatant of a grown T75 (or T175) flask was discarded and cells were rinsed with 5 mL (or 10 mL) PBS. For detaching of cells, 2 mL (or 5 mL) Versene (EDTA) were added and incubated for 10 – 15 min at 37°C until cells were detached completely. Cells were rinsed with 8 mL (or 15 mL) culture medium, transferred into a falcon tube and counted in a Neubauer chamber (2.2.6.3). Cells were either frozen (2.2.6.5) or directly used for experiments.

2.2.6.5 Freezing of cells

Cells were harvested using Versene (EDTA) (2.2.6.4) for experiments or trypsin/EDTA (2.2.6.2) and counted in a Neubauer chamber (2.2.6.3). Cells were pelleted by centrifugation at 120xg and room temperature for 5 min. Supernatant was discarded, cells were resuspended in the appropriate volume of freezing medium (Table 21) (4 – 6 x10^6 cells/mL) and immediately aliquoted into 1.8 mL cryo tubes (1 mL/vial). Tubes were incubated in a freezing container filled with isopropanol at -80°C for 24 h and transferred into a liquid nitrogen tank for long term storage (cell bank) or kept at -80°C for experiments.

Table 21: Composition of freezing media

Cell line	Freezing medium
FaDu	DMEM + 20% FBS + 10% DMSO
Detroit-562	DMEM + 20% FBS + 10% DMSO
CHO-K1	RPMI 1640 + 20% FBS + 10% DMSO

2.2.6.6 Antibody production

Transient transfection of HEK293 cells for antibody production was performed as described before (Jäger et al. 2013). For production of human IgG, plasmid DNA of heavy and light chain were co-transfected in a ratio of 1:1. Antibodies were purified form culture supernatant using the MabSelect Sure Protein A purification system (Merck KGaA, Darmstadt, Germany) according to the manufacturer's protocol. Antibody production and protein purification were kindly performed by Marie Kastull and Chantal Lingner (Yumab GmbH, Braunschweig, Germany). Purified antibodies were aliquoted and stored at -20°C.

2.2.6.7 Transfection of cells for protein surface expression

In order to obtain target-expressing cells for antibody binding studies, HEK293 cells were transfected with plasmid DNA coding for the appropriate antigen-GFP fusion protein as described before (Jäger et al. 2013). Two days upon transfection cells were harvested and transfection efficacy was determined (2.2.6.8). Cells were counted (2.2.6.3) and either frozen (2.2.6.5) or directly used for experiments.

2.2.6.8 Determination of transfection efficacy

HEK293 cells were harvested two days upon transfection (2.2.6.7) and 500 µL of the collected cell suspension was transferred into a 1.5 mL reaction tube. Cells were pelleted by centrifugation (2000 rpm, 5 min, 4°C), washed and resuspended in PBS. Cells were diluted 1:2 in PBS and analysed in a flow cytometer (2.2.5.7). GFP-expressing cells were quantified to determine the transfection efficacy.

2.2.6.9 Preparation of whole cell lysate

For preparation of cell lysate, cells were harvested using Versene (EDTA) to preserve integrity of surface proteins (2.2.6.4). Non-adherend HEK293 cells were obtained freshly from current culture. In total 10^7 cells were aliquoted in a 15 mL falcon tube and centrifuged at 300xg and 4°C for 5 min. Supernatant was discarded and cells were washed twice in ice-cold PBS. NP40 cell lysis buffer was supplemented with 1 mM PMSF and Halt Protease Inhibitor Cocktail (Thermo Fisher Scientific, Dreieich, Germany) and cell lysate was prepared according to the manufacturer's protocol. Cell lysate was aliquoted and stored at -80°C or directly used for experiments.

3. Results

3.1 Antibody libraries from TIL-B cells

3.1.1 Processing of tumor samples and isolation of TIL-B cells

Tumor samples were obtained from head and neck cancer patients who had undergone curative surgery within their intended treatment and were kindly provided by Prof. Dr. Andreas Gerstner (Städtisches Klinikum Braunschweig, Germany). Tissue of 36 patients was processed to obtain a single cell suspension and B cells were quantified by CD19/CD45 co-staining and flow cytometric analysis. Samples were grouped into “high” (≥1.00%), “moderate” (≥0.10%), “low” (≥0.01%) or “not detectable” (<0.01%) according to the amount of detected B cells relative to all detected cells (Figure 3). In 69% (25 out of 36) of all considered samples CD19+/CD45+ cells were observed (Figure 4). Besides four samples, which were classified as “high” most samples showed “moderate” or “low” B cell amount. In 11 samples less than 0.01% B cells were found, which was considered as “not detectable”. Distribution of male and female patients was similar in each subgroup (75-91% male) and comparable to the complete sample collection (~82% male) (Figure 4). Thus, no obvious correlation of gender and detected B cell amount was seen.

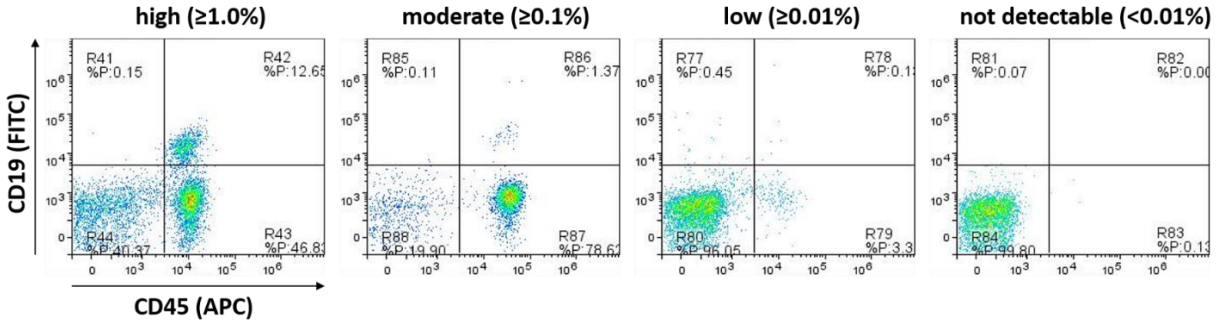

Figure 3: Division of tumor samples according to detected B cells. Cells from whole tissue single cell suspensions were co-stained with anti-CD19 FITC- and anti-CD45 APC-conjugated antibodies and analysed in flow cytometry. Amount of double-positive B cells (CD19+/CD45+) was calculated relative to all detected events. Samples were grouped into high (≥1.0%), moderate (≥0.1%), low (≥0.01%) and not detectable (<0.01%). Exemplary tumor samples (YUHANXXX = patient number) are shown in the following order: YUHAN012, YUHAN018, YUHAN025 and YUHAN006

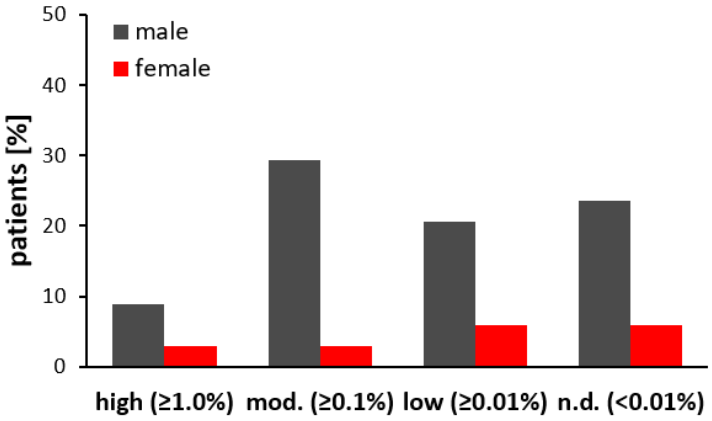

Figure 4: B cell amount detected in patient-derived tumor samples. Processed samples were grouped in "high" (≥1.0%), "moderate" (≥0.1%), "low" (≥0.01%) and "not detectable" (<0.01%) according to the B cell amount detected in flow cytometry. Bars indicate the sample count in each group relative to all considered samples.

If detectable in flow cytometry, B cells were isolated from whole tissue cell suspension using anti-CD19 magnetic beads. The CD19+ cells were lysed, and the lysate was stored in RNA preparation buffer for later antibody library construction.

3.1.2 Antibody library construction

TIL-B-derived scFv-libraries were constructed from seven different tumor samples. Total B cell RNA was isolated and used for cDNA synthesis by reverse transcription. Variable antibody domains were amplified (both IgG and IgM) and cloned into phagemid pHAL30. The final library sizes ranged from $1x10^7$ to $2x10^8$ with insert rates of scFv gene fragments varying between 79% and 100% (Table 22). No correlation was observed when comparing the library size to the appropriate B cell amount within each sample. Samples with higher B cell numbers (e.g. YUHAN028) did not result in larger libraries compared to samples with lower B cell numbers (e.g. YUHAN007). On the other hand, although B cell counts were below detection level in YUHAN009, amplification of antibody genes was still successful (Table 22).

Within this work, several batches of phage libraries were prepared freshly before use. Here, titers were batch-dependent, but they always ranged between $7x10^{10}$ – $2x10^{12}$ cfu/mL. In Western blotting two prominent bands at approximately 90 kDa and 100 kDa were observed for all libraries corresponding to the expected size of pIII-scFv-fusion proteins (Figure 5). Given the well-known aberrant electromobility shift of pIII and its fusion proteins in SDS-PAGE (Goldsmith and Konigsberg 1977), this indicated a sufficient display of scFv-fragments on phage particles confirming that all libraries were suitable for phage display selection.

Table 22: Antibody library and sample characteristics

Library	Origin*	Gender	B cells	B cell count**	Library size	Insert rate
YUHAN007-κ YUHAN007-λ	hpx	m	0.35%	2.4 x10^4	8.3 x10^7 7.3 x10^7	95% 88%
YUHAN008-κ YUHAN008-λ	hpx	m	0.39%	3.2 x10^5	2.7 x10^7 8.6 x10^7	79% 87%
YUHAN009-κ YUHAN009-λ	opx	m	n.d.	0	1.7 x10^8 1.7 x10^8	100% 100%
YUHAN011-κ YUHAN011-λ	lrx	m	0.29%	5.6 x10^4	1.7 x10^7 1.2 x10^7	96% 100%
YUHAN012-κ YUHAN012-λ	opx	f	2.34%	1.8 x10^5	3.4 x10^7 4.6 x10^7	91% 91%
YUHAN022-κ YUHAN022-λ	opx	m	3.59%	4.9 x10^5	5.5 x10^7 4.1 x10^7	96% 96%
YUHAN028-κ YUHAN028-λ	opx	m	8.58%	2.5 x10^6	3.6 x10^7 9.4 x10^7	88% 88%

* hpx: hypopharynx; opx: oropharynx; lrx: larynx ** theoretical count (from FC data)

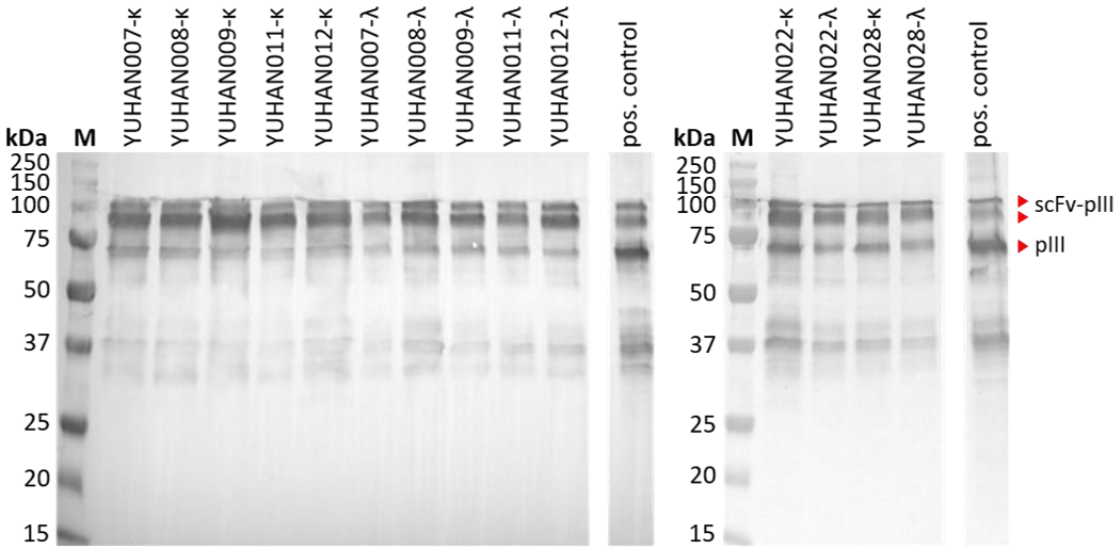

Figure 5: Packaging of TIL-B libraries. After packaging with Hyperphage, 10^{10} phage were analysed by immunoblotting. pIII-particles were detected using a pIII-specific antibody as primary antibody and an HRP-conjugated secondary antibody. M: Precision Plus Protein Standard (all blue).

3.1.3 NGS analysis of antibody libraries and patient data

In order to obtain an insight into the characteristics of the TIL-B-derived antibody libraries, next generation sequencing (NGS) was conducted. Sequencing reactions and raw data processing were kindly performed by Dr. Thomas Clarke (EMD Serono, Billerica, USA). Libraries were

sequenced in a multiplexed MiSeq run resulting in approximately $2x10^4 – 8x10^4$ sequences each of VH and Vκ/Vλ. Data was cleared form non-overlapping reads and short sequences (<375 bp). To address library diversities (NGS), unique antibody domains (VH and Vκ/Vλ) were identified based on their combination of CDR3 and V-gene and counted. The unique light and heavy chain variable regions (10^2 to 10^4 each) were multiplied to estimate the maximal possible library diversity (NGS) assuming, that all possible combinations were represented. The resulting library diversities ranged from $1.2x10^5$ to $7.8x10^7$ and, thus were covered by the library size determined upon transformation (Figure 6). Corresponding to the detected B cell amount, the highest library diversities were observed for YUHAN012, YUHAN022 and YUHAN028. Both YUHAN009-derived libraries showed the lowest diversity in NGS analysis, which correlated with the lowest B cell count but was not consistent with the highest library size. Diversity and size of all libraries were lower than the maximal theoretical B cell diversity, which was calculated by potentiating the theoretical B cell count derived from the B cell amount detected in flow cytometry in relation to the total cell count of the tissue cell suspension.

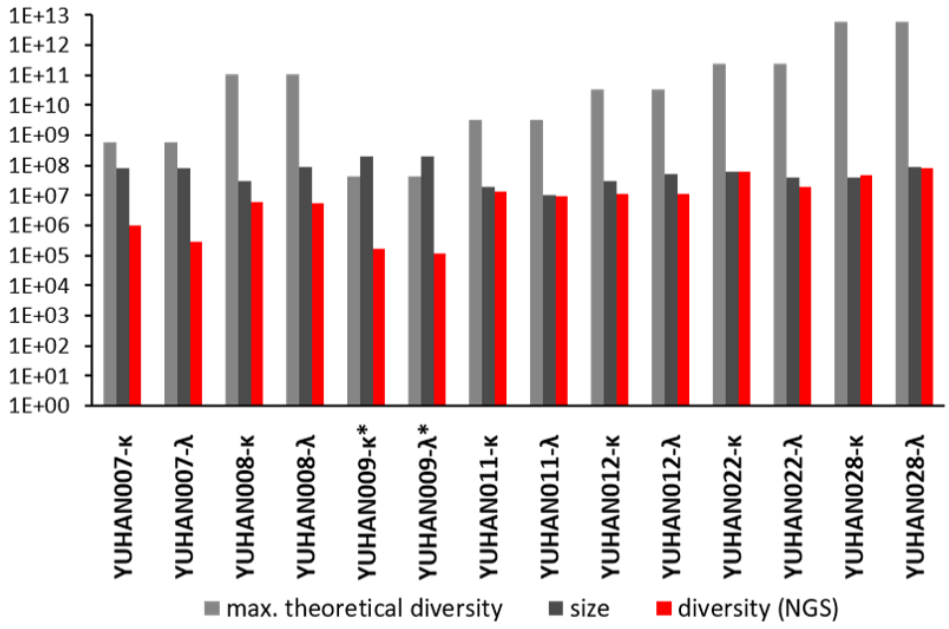

Figure 6: TIL-B library sizes and diversities. Maximal theoretical diversity was calculated based on the B cell amount detected in flow cytometry in relation to the total cell count within the tissue cell suspension and the random pairing of VH and VL during cloning (B cell count ²). *: For YUHAN009, the maximal possible B cell amount below detection level of 0.009% was assumed for calculation. Real library size was determined by counting single colonies after transfection in library cloning. Maximal possible diversity (NGS) was estimated by multiplication of unique VH and VK/VL observed in NGS analysis.

Quantification of antibody sequences according to their origin revealed that all considered libraries were dominated by IgG with a proportion of 60.5% to 95.5% (Figure 7). YUHAN009

and YUHAN022 showed a comparable distribution of IgG and IgM but differed considerably in B cell number. The same was observed for YUHAN011 and YUHAN028 (Figure 7). Thus, no correlation of the IgG proportion with the appropriate B cell numbers detected in the corresponding sample was observed.

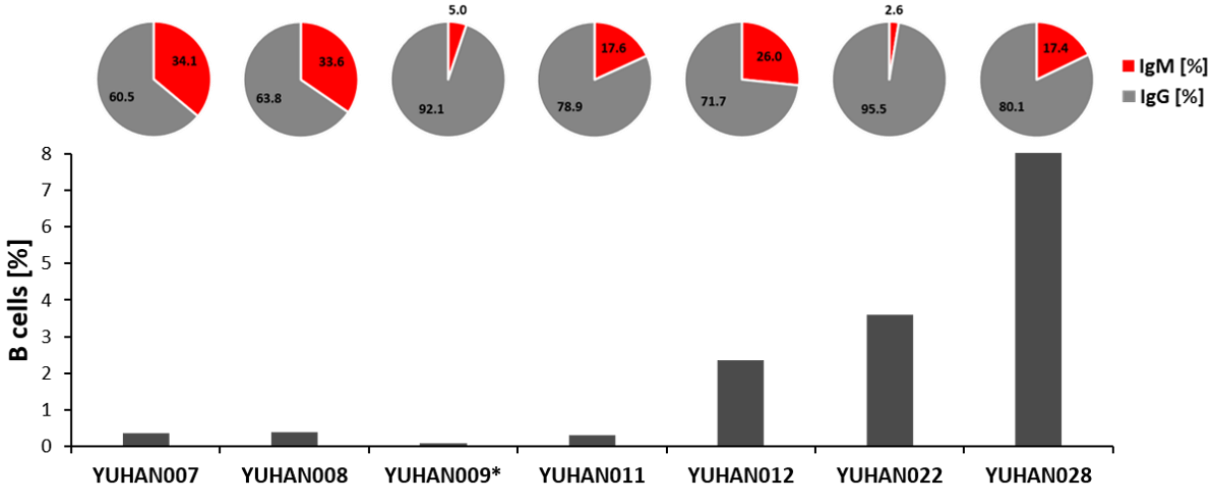

Figure 7: Abundance of IgG genes versus B cell count. Bars indicate the amount of B cells detected in flow cytometry. *: For YUHAN009, the maximal B cell amount below detection limit of 0.009% was assumed. Proportion of IgM and IgG genes in the respective library is shown in the pie charts above.

To analyse the antibody repertoire of the TIL-B cell populations used for the library construction, the abundance of all V-gene subfamilies of variable heavy and light chain domains were determined based on the NGS data (Figure 8). Comparing the heavy chains of both kappa and lambda libraries, a highly similar V-gene abundance was observed within each sample as expected regarding the same TIL-B cell source. The overall distribution was similar between the considered libraries except for YUHAN007 and YUHAN009, which differed in many cases. In average IGHV3 and IGHV4 were the most abundant subfamilies (25-30%) followed by IGHV1 representing the third leading group. For YUHAN007 in contrast, a higher abundance of IGHV5 and IGHV7 was observed whereas in YUHAN009 the IGHV3 subfamily dominated with ~60%. Within the kappa light chains IGKV1 and IGKV4 were the most abundant V-genes followed by IGKV4 (Figure 8). As exception, in YUHAN009 the subfamily IGKV6 accounted for ~35% of the clones, whereas in the other libraries this subfamily was negligibly represented. Except of YUHAN007 and YUHAN009, the V-gene distribution within the lambda light chains was mainly dominated by IGLV3 (~40%) followed by IGLV2 and IGLV3, which were both represented in similar abundance (Figure 8). Consistently, IGLV3 was most abundant in YUHAN009 and accounted for ~70% of all V-genes resulting in an under-

representation of IGLV1 and IGLV2 compared to the other libraries. In YUHAN007 in contrast, IGLV1 was the most abundant subfamily accounting for ~70% of all observed v-genes whereas IGLV2 and IGLV3 were evenly distributed (~10%).

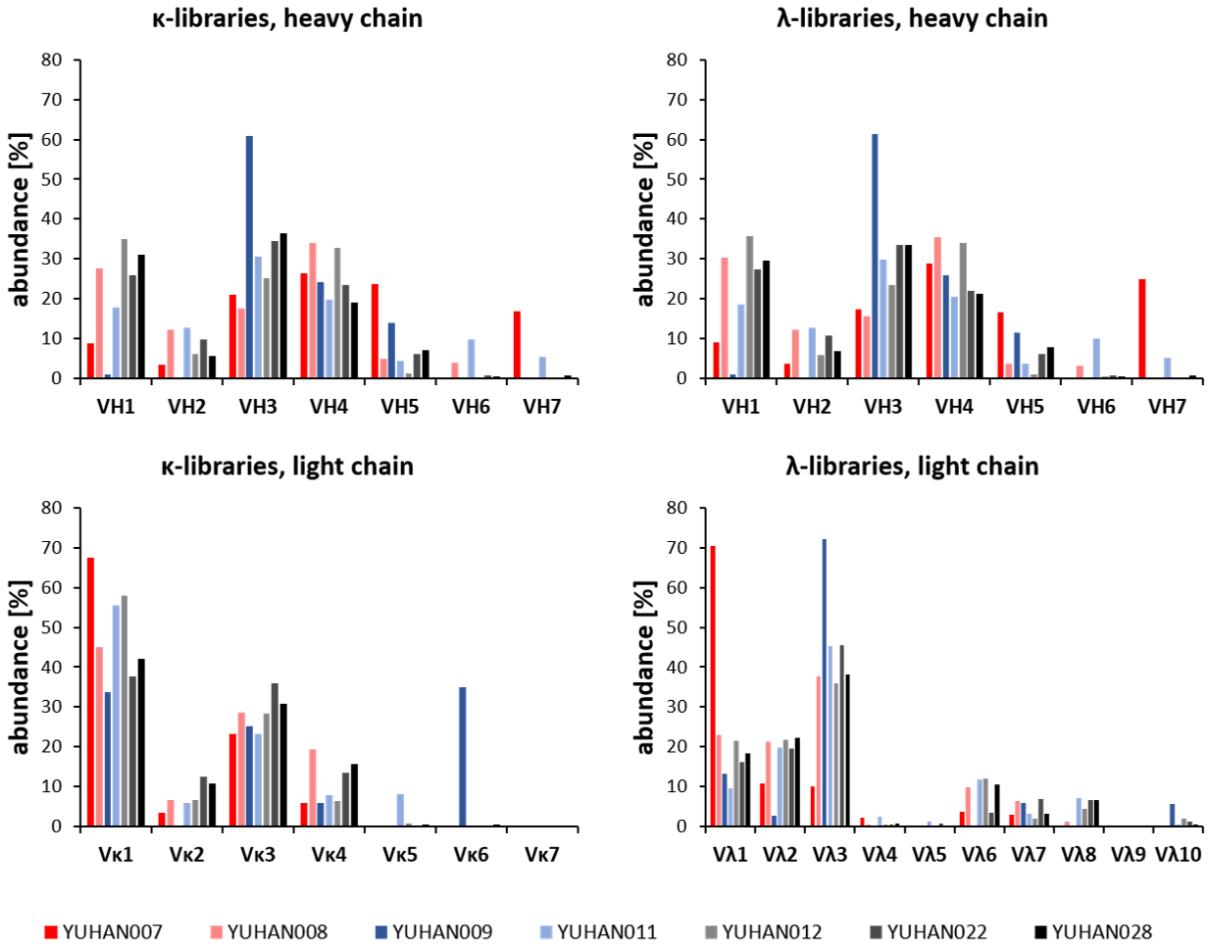

Figure 8: Distribution of V-genes within TIL-B libraries. Abundance of V-genes within the TIL-B libraries was calculated based on NGS data

In summary, NGS analysis revealed good quality of all considered libraries with high diversities representing a diverse V-gene repertoire. Thus, libraries were considered as suitable for phage display selection.

3.2 Selection of TIL-B-antibodies on cancer-related targets

To analyse the presence of cancer-related antibodies within the TIL-B-derived libraries, selection on a known cancer target was conducted. The matrix metalloproteinase 9 (MMP-9) was chosen as model protein since a correlation of MMP-9 with tumor progression, metastasis

formation and patient survival has been widely described making it a potential prognostic marker for various cancer types (Shao et al. 2011; Cho et al. 2003). Investigation of antibody responses performed in our laboratory with the patient samples used in this study also detected response against MMP-9 (Kilian Zilkens, personal communication)

3.2.1 Panning and screening on MMP-9

In order to select MMP-9-specific antibodies, phage libraries of all seven donors were pooled (kappa and lambda kept separately) and used for panning on immobilised recombinant human MMP-9 in microtiter scale. After third panning round, bacteria were re-infected with eluted phage for production of soluble scFv fragments. A total of 644 clones were screened (276x kappa, 368x lambda) for binding to MMP-9. BSA and skim milk powder served as control antigens (Figure 9).

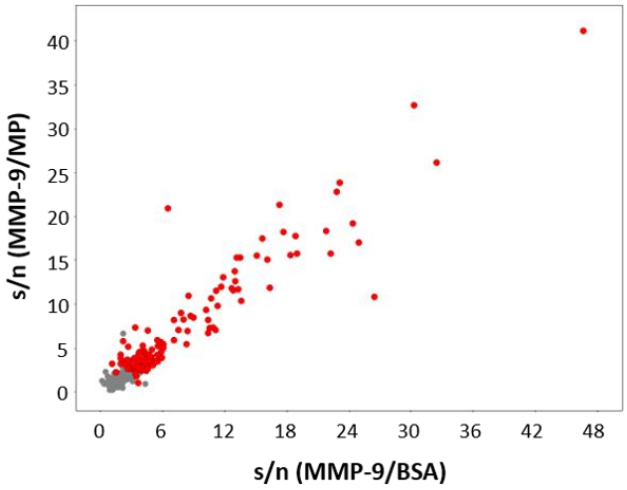

Figure 9: Screening for MMP-9-specific antibodies. Soluble scFv-fragments were produced after three panning rounds and tested for MMP-9-specific binding in screening-ELISA. scFv-containing production supernatants were incubated on immobilised antigen and detected by a myc-tag-specific antibody and an HRP-conjugated antibody. Skim milk powder (MP) and BSA were used as control antigens. Clones were considered as hits (red dots) if signal to noise ratio (s/n) on both MP and BSA were >2 and the absorbance on MMP-9 was >0.1. If clones, which did not meet these thresholds are depicted as grey dots.

In total, 148 hits were detected (23% hit rate), which showed binding to MMP-9 but no cross-reactivity to the two control antigens (Figure 9). From 95 sequenced clones, 19 were identified as unique upon sequencing. Analysing the NGS data, these 19 antibodies could be assigned to four different patients out of seven (>50%), revealing that MMP-9-specific antibodies occurred in several independent patients suffering from head and neck cancer.

3.2.2 Characterisation of anti-MMP-9 antibodies

3.2.2.1 Binding to MMP-9 in ELISA and immunoblotting

Based on the signals observed in screening, three anti-MMP-9 antibodies were chosen for further characterisation and converted to human IgG format. To confirm that binding abilities remained unaffected upon format conversion, reactivity was analysed in ELISA (Figure 10).

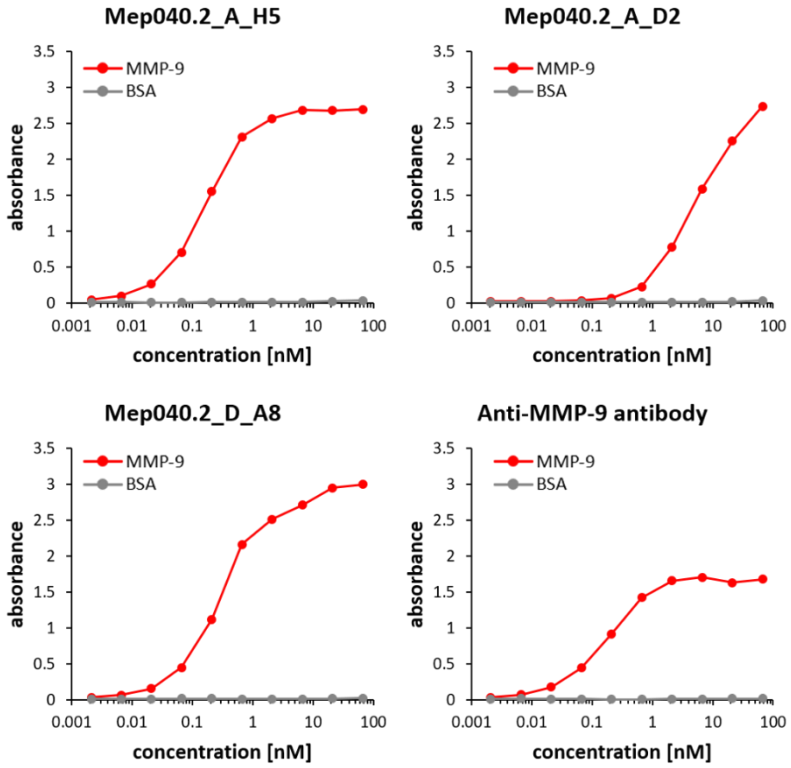

Figure 10: Titration-ELISA on recombinant human MMP-9. Dilution series of the antibodies (human IgG) were incubated on immobilised MMP-9 or BSA as control antigen and detected by an HRP-conjugated secondary antibody. EC50 values were determined upon signal normalisation and amounted 0.16 nM for Mep040.2_A_H5, 5.03 nM for Mep040.2_A_D2, 0.34 nM for Mep040.2_D_A8 and 0.18 nM for the anti-MMP-9 antibody used as positive control.

All antibodies showed a sigmoidal dose-dependent binding curve on human MMP-9 without background signals on BSA (Figure 10). The calculated EC50 values varied from 0.16 nM to 5.03 nM. In immunoblotting, MMP-9 (80 – 90 kDa) was detected using Mep040.2_A_H5 and Mep040.2_D_A8 as primary antibodies, whereas no signal was obtained using Mep040.2_A_D2 (Figure 11). In case of Mep040.2_A_H5 additional bands (50 – 75 kDa) were detected probably representing impurities or degradation products of MMP-9.

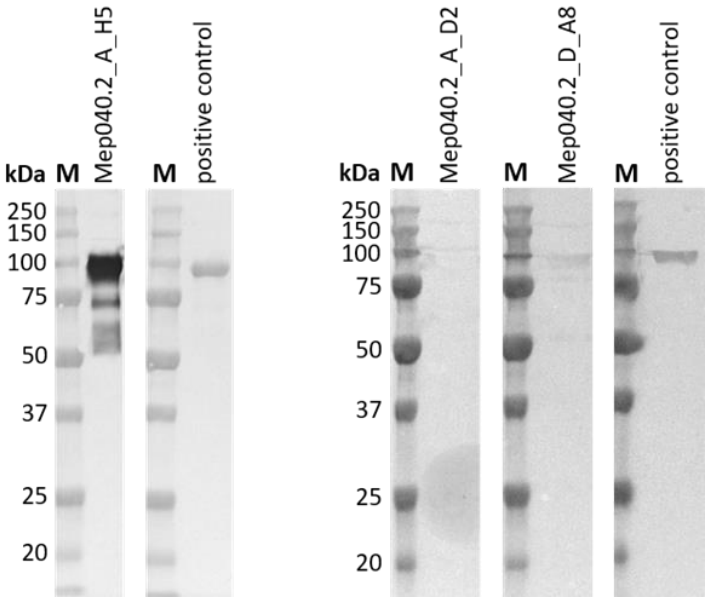

Figure 11: Immunoblot of MMP-9. Antibodies (human IgG) were used as primary antibodies for staining of recombinant human MMP-9 and were detected by an HRP-conjugated secondary antibody. M: Precision Plus Protein standard (all blue).

3.2.2.2 Binding to MMP-9-expressing cells

The selected MMP-9- antibodies were tested in flow cytometry and in immunoprecipitation assays. HEK293 cells were transfected with an MMP-9-GFP fusion protein comprising a transmembrane domain to ensure surface expression of the target. Two days upon transfection cells were harvested and transfection efficacy was determined (52.8% GFP+ cells). Cells were stained with MMP-9-specific antibodies, which were detected using a fluorochrome-conjugated secondary antibody (APC+). Non-transfected population (GFP-), cells transfected with a control antigen or empty vector as well as non-transfected cells were used as negative controls (Figure 12).

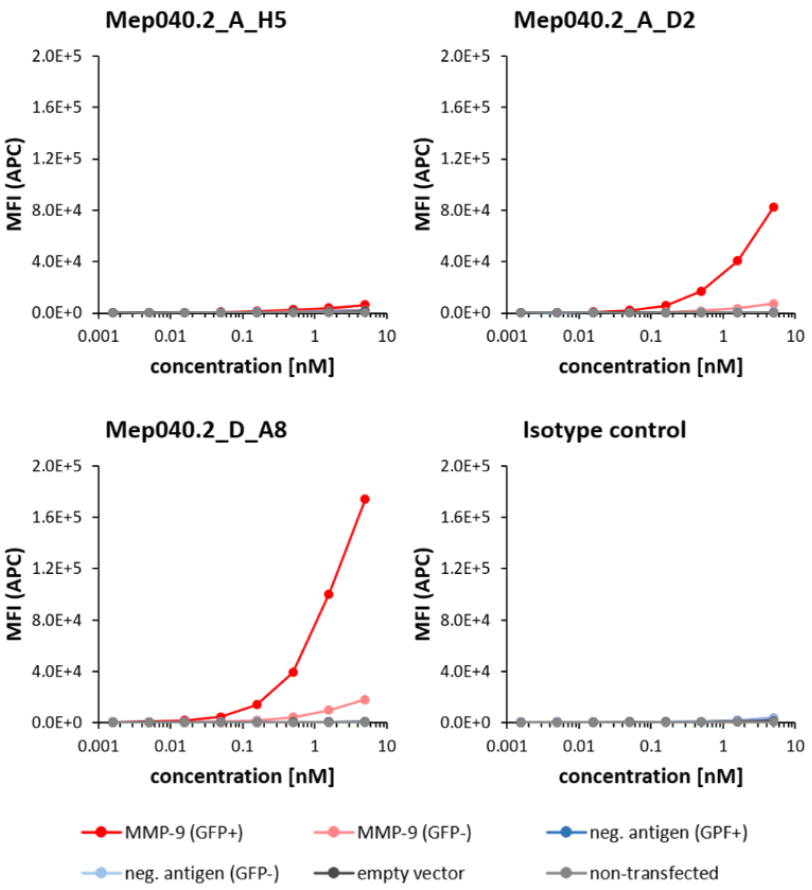

Figure 12: Binding to MMP-9-expressing cells in flow cytometry. Antibodies (human IgG) were titrated and tested for binding to MMP-9-expressing cells. Bound antibodies were detected by an AlexaFluor647-conjugated secondary antibody. Binding to non-transfected cells and to cells transfected with a control antigen or empty vector was tested as negative controls. Non-specific human IgG served as isotype control.

In flow cytometry only weak binding to MMP-9-expressing cells could be observed for Mep040.2_A_H5 (Figure 12). For Mep040.2_A_D2 and Mep040.2_D_A8 strong binding was detected on MMP-9-expressing cells (Figure 12). Reaction to all control cell lines was not detectable or negligible indicating MMP-9-selective binding.

3.2.2.3 Immunoprecipitation of MMP-9

To further evaluate target-selectivity of the considered antibodies, immunoprecipitation from cell lysate was conducted. Antibodies were bound to magnetic beads and incubated with lysate derived either from MMP-9-transfected cells or from non-transfected cells as reference. Bound proteins were analysed in SDS-PAGE and selected bands were identified by mass spectrometry, which was kindly performed by Dr. Roland Kellner (Merck KGaA, Darmstadt, Germany).

Mep040.2_A_H5 precipitated many proteins from both tested lysates indicating a high cross-reactivity of this antibody if exposed to whole cell lysate (Figure 13). In contrast, three proteins were precipitated in high abundance by Mep040.2_A_D2 and Mep040.2_D_A8 from lysate of transfected cells but not from the control lysate. These proteins were identified as MMP-9-GFP fusion and single MMP-9 by mass spectrometry (Figure 13). Both antibodies co-precipitated only few proteins from control lysate indicating low cross-reactivity to tested whole cell lysates and thus highly selective binding to MMP-9.

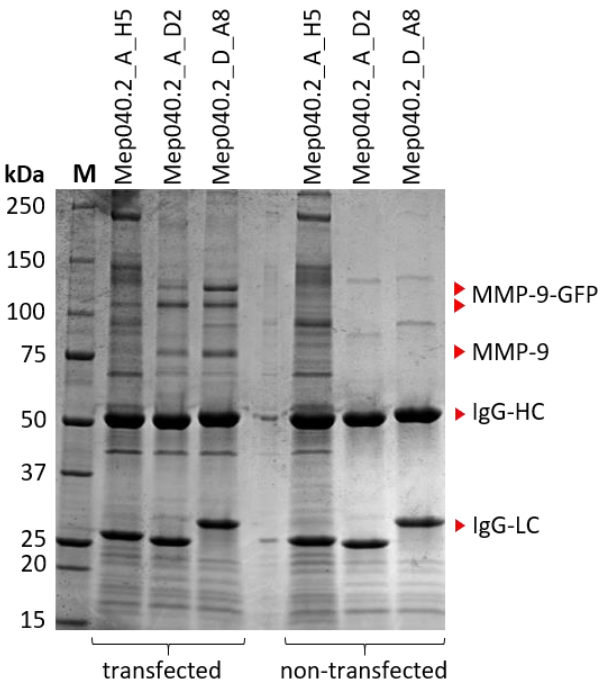

Figure 13: Immunoprecipitation from MMP-9-expressing cells. Antibodies (human IgG) were used for immunoprecipitation form lysate of MMP-9-trasnfected cells or non-transfected cells as negative control. Eluted proteins were analysed in SDS-PAGE and Coomassie staining. Bands were excised for mass spectrometric analysis. Red arrows indicate identified proteins. M: Precision Plus Protein Standard (unstained).

3.2.2.4 Kinetics assay

The previous experiments addressed functionality and MMP-9-selectivity of the new antibodies using ELISA, flow cytometry and immunoprecipitation. As expected, performance of each antibody varied depending on the given assay. To assess the binding characteristics of each antibody in more depth, antigen binding kinetics were analysed using biolayer interferometry (BLI).

Antibodies were captured on human-Fab-CH1-specific sensor tips and exposed to different concentrations of diluted antigen in solution. Association and dissociation curves were

obtained for each antibody (Figure 14). After applying a global fit (1:1 interaction model), association (k_{on}) and dissociation constants (k_{dis}) were determined allowing the calculation of the equilibrium constant K_d (Table 23). High affinities were observed for Mep040.2_A_D2 and Mep040.2_D_A8 with binding constants of K_d = 3.66 nM and K_d = 3.02 nM, respectively. For Mep040.2_A_H5 the affinity observed in BLI was 10 times lower compared to the other considered antibodies (Table 23).

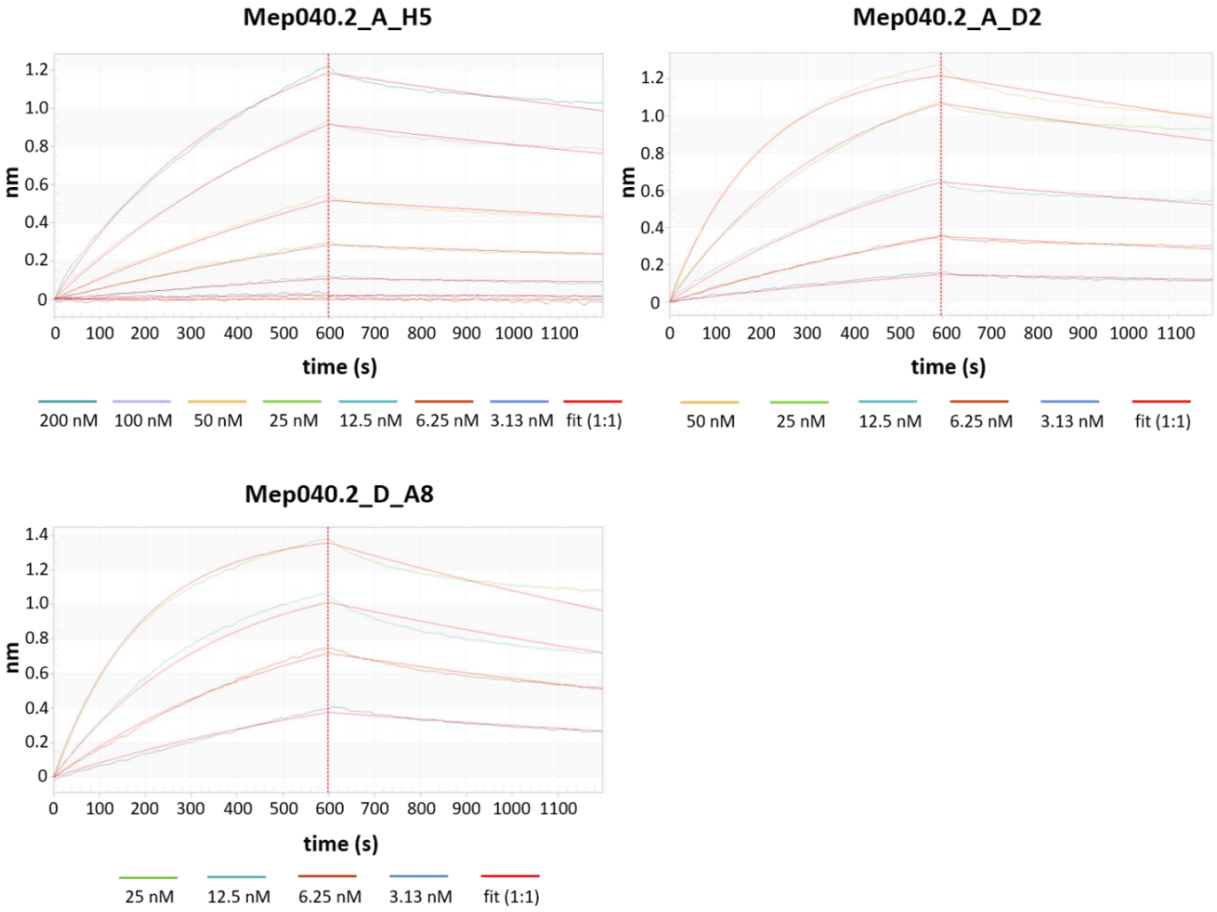

Figure 14: Kinetics assay with MMP-9. Antibodies (human IgG) were immobilised on anti-human Fab-CH1 biosensors and exposed to different concentrations of diluted MMP-9. Association and dissociated curves were detected and a mathematical model (1:1 interaction) was applied for calculation of binding parameters.

Table 23: Summary of MMP-9-binding parameters

Antibody	Antigen	k_{on} [1/Ms]	k_{dis} [1/s]	K_d [nM]
Mep040.2_A_H5	MMP-9	1.13×10^{4}	3.06×10^{-4}	27.1
Mep040.2_A_D2	MMP-9	9.55×10^{4}	3.50×10^{-4}	3.66
Mep040.2_D_A8	MMP-9	1.89×10^{5}	5.70×10^{-4}	3.02

In summary, three MMP-9-specific antibodies were isolated from TIL-B libraries. Two of these antibodies showed highly affine binding to MMP-9 with low cross-reactivity and were functional in different assays comprising ELISA, immunoprecipitation and flow cytometry. Furthermore, the discovery of antibodies against a well-described cancer-related protein confirmed the presence of cancer-relevant antibodies within the TIL-B libraries.

3.3 Selection of TIL-B-antibodies on cancer cells

3.3.1 Cell panning and screening on FaDu

To overcome the limitation to known cancer targets, TIL-B-derived phage libraries were used for selection on whole cancer cells to discover cancer-relevant antibodies independent of their appropriate target proteins. FaDu is an epithelial cell line, which originates from human pharyngeal squamous cell carcinoma (Rangan 1972). Since it is a well-studied model cell line for head and neck cancer (Schmidt et al. 2016; J. T. Cohen et al. 2015; Young et al. 2018) it was chosen for antibody discovery in this study.

For panning on cancer cells, TIL-B-derived phage libraries of five donors were pooled, while keeping kappa and lambda libraries separately, and panned on FaDu cells. Upon three panning rounds, eluted phage were used for re-infection of bacteria and production of soluble scFv-fragments. In total, 736 clones were screened (368x kappa and lambda each) by flow cytometry for specific cell binding. Antibodies selectively binding to FaDu without showing reactivity with CHO-K1 or HEK293 were considered as specific hits. Of 736 screened clones, 74 hits were isolated (10% hit rate) (Figure 15 A), of which 26 clones (35%) were found to be unique in respect of their sequence. The total number of FaDu-binding antibodies upon selection was significantly higher compared to the number of CHO-K1- or HEK293-reactive antibodies (Figure 15 B). This confirms a successful enrichment of antibodies by FaDu cell panning.

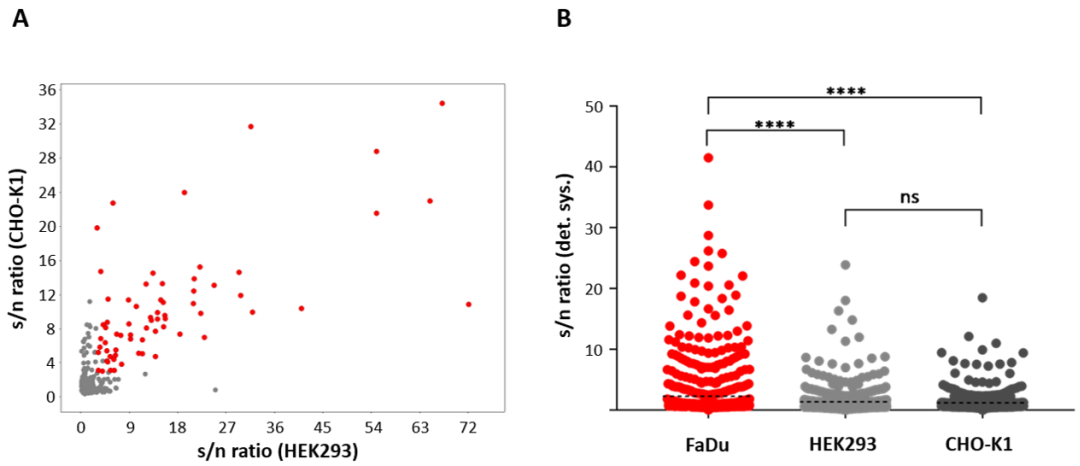

Figure 15: Screening for FaDu-specific antibodies. Soluble scFv-fragments were produced after three cell panning rounds and tested for FaDu-specific binding in flow cytometry. ScFv-containing supernatants were incubated with the respective cells and detected by a myc-tag-specific antibody and an AlexaFluor647-conjugated secondary antibody. Binding to HEK293 and CHO-K1 cells was tested for negative control. Mean fluorescence intensity (MFI) of each clone was divided by the MFI of the detection system (det. sys.) control to obtain signal to noise (s/n) ratios relative to the background signal. (**A**) s/n ratios on negative control cells were calculated by dividing s/n ratios (det. sys.) of FaDu-signals by control signals. Clones were considered as hits if s/n ratio on HEK293 and CHO-K1 < 3 (red dots). (**B**) s/n ratios (det. sys.) of each clone on all three cell lines. Mean is indicated by a dotted line and variations were calculated using the one-way ANOVA test. Signals on FaDu were significantly increased compared to HEK293 and CHO-K1 (****P < 0.0001).

For further investigation, all 26 unique antibodies were converted into the IgG-like scFv-Fc format and re-tested for binding to FaDu and the metastatic site derived Detroit-562 cell line (Peterson et al. 1971) in flow cytometry (Figure 16).

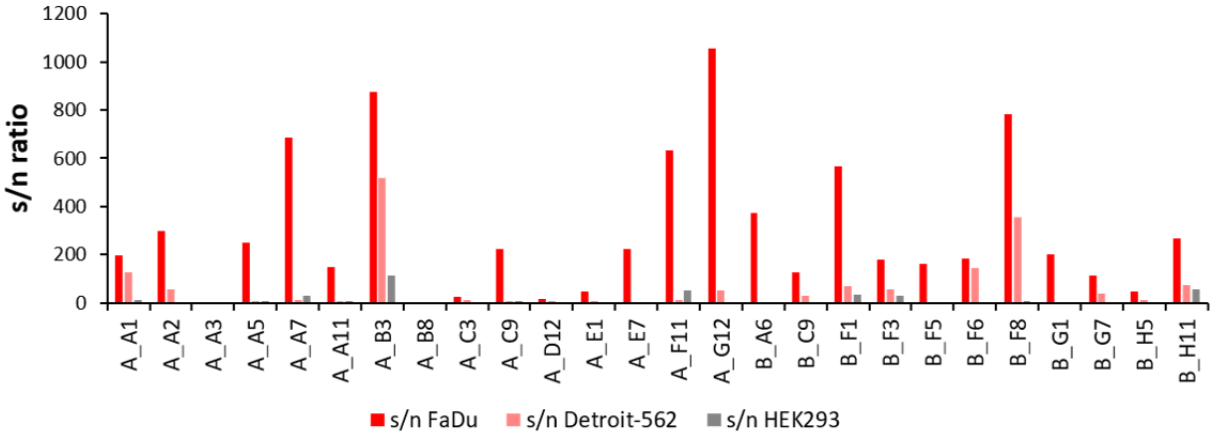

Figure 16: Cell binding in flow cytometry. Purified scFv-Fc fragments (50 nM) were tested for binding to FaDu, Detroit-562 and HEK293 cells. Clone names are shown as abbreviations (Mep038.1_MPX_XX). Bound antibodies were detected by an AlexaFluor647-conjugated secondary antibody. Median fluorescence intensity (MFI) of each clone relative to the MFI of the detection system was calculated to obtain signal to noise (s/n) ratios.

After format conversion from scFv to scFv-Fc, four candidates showed no (Mep038.1_MPA_A3 & Mep038.1_MPA_B8) or no sufficient binding (Mep038.1_MPA_C3 & Mep038.1_MPA_D12) to FaDu cells (Figure 16). These clones were excluded from further analysis. The remaining 22 antibodies all showed binding to FaDu cells. A total of 12 antibodies also bound to Detroit-562 cells, indicating that the appropriate targets were expressed on both head and neck cancer cell lines. Binding intensities on Detroit-562 were generally lower compared to the signals obtained on FaDu but still well detectable.

3.2.2 Target identification via immunoprecipitation and mass spectrometry

Selection of FaDu-specific antibodies from TIL-B-derived scFv-phage libraries resulted in 22 unique candidates binding to FaDu cells but the identity of the recognised antigen was still unknown. To identify the respective targets, antibodies were bound to protein-A-coated magnetic beads and exposed to cell lysate derived from FaDu or HEK293 as reference. Precipitated proteins were eluted and analysed in SDS-PAGE. Bands, which exclusively or more intensely occurred within the FaDu-lanes were considered as potential targets and were furhter analysed by mass spectrometry (Figure 17). Protein purification from gel, mass spectrometric analysis and raw data evaluation were kindly performed by Dr. Roland Kellner (Merck KGaA, Darmstadt, Germany).

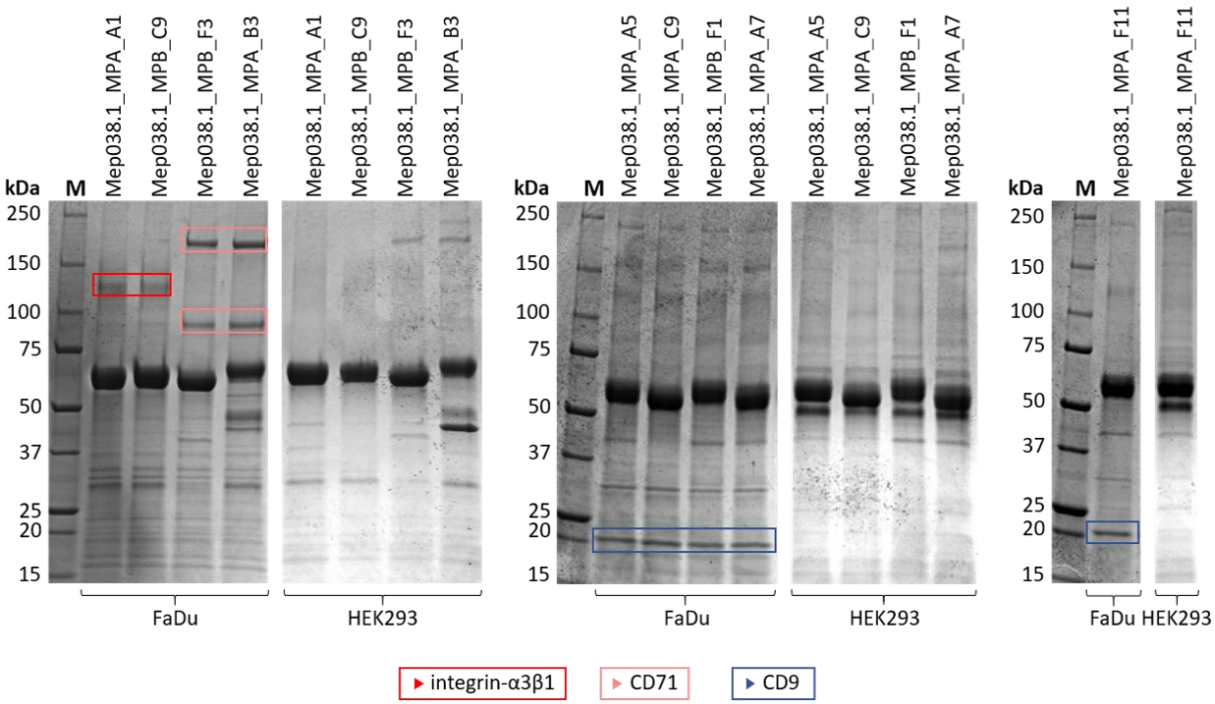

Figure 17: Immunoprecipitation for target identification. FaDu-binding antibodies (scFv-Fc; mouse Fc) were used for immunoprecipitation form FaDu cell lysate or HEK293 cell lysate as reference. Eluted proteins were analysed in SDS-PAGE and Coomassie staining. Bands were excised for mass spectrometric analysis. Coloured frames indicate the proteins identified by mass spectrometry of the respective bands. M: Precision Plus Protein Standard (unstained).

FaDu-selective bands were observed for nine antibodies, which were identified as three different proteins by mass spectrometry. This correlated with the highly similar precipitation patterns of the appropriate antibodies observed in SDS-PAGE (Figure 17). According to their proposed target (integrin-α3β1, CD71 or CD9) antibodies were grouped and compared. Sequence analysis revealed that within the integrin-α3β1- and CD9-binding fraction the antibodies shared the same V-gene subfamilies and patient origin (Table 24). Sequence alignment revealed that although the same V-genes were used the antibodies were still unique due to several silent and non-silent point mutations (Figure 18). In total, 16 differing amino acids were found within the integrin-α3β1-binders, which were evenly distributed over the whole sequence. For the CD9-binders, 21 different amino acids occurred, which were majorly located within the variable light chain domain. Some mutations were shared by all antibodies (see CDR2 in VL) whereas other differed in the same position indicating that the considered antibodies were clonally related.

Table 24: Sequence analysis of FaDu-binding antibodies

Antibody	Target	V-gene VH (identity [%])	V-gene VL (identity [%])	Patient (NGS)
Mep038.1_MPA_A1	Integrin-α3β1	IGHV3-30*18 (96.3)	IGLV3-19*01 (90.7)	YUHAN012
Mep038.1_MPB_C9	Integrin-α3β1	IGHV3-30*18 (95.4)	IGLV3-19*01 (91.8)	YUHAN012
Mep038.1_MPA_A5	CD9	IGHV4-34*01 (97.2)	IGLV3-21*01 (91.8)	YUHAN008
Mep038.1_MPB_F1	CD9	IGHV4-34*01 (97.2)	IGLV3-21*01 (86.6)	YUHAN008
Mep038.1_MPA_A7	CD9	IGHV4-34*01 (97.2)	IGLV3-21*01 (86.6)	YUHAN008
Mep038.1_MPA_C9	CD9	IGHV4-34*01 (98.1)	IGLV3-21*01 (91.8)	YUHAN008
Mep038.1_MPA_F11	CD9	IGHV4-34*01 (97.2)	IGLV3-21*01 (90.7)	YUHAN008
Mep038.1_MPB_F3	CD71	IGHV3-21*03 (96.3)	IGLV6-57*02 (91.1)	YUHAN012
Mep038.1_MPA_B3	CD71	IGHV1-18*04 (89.9)	IGLV1-51*01 (94.9)	YUHAN012

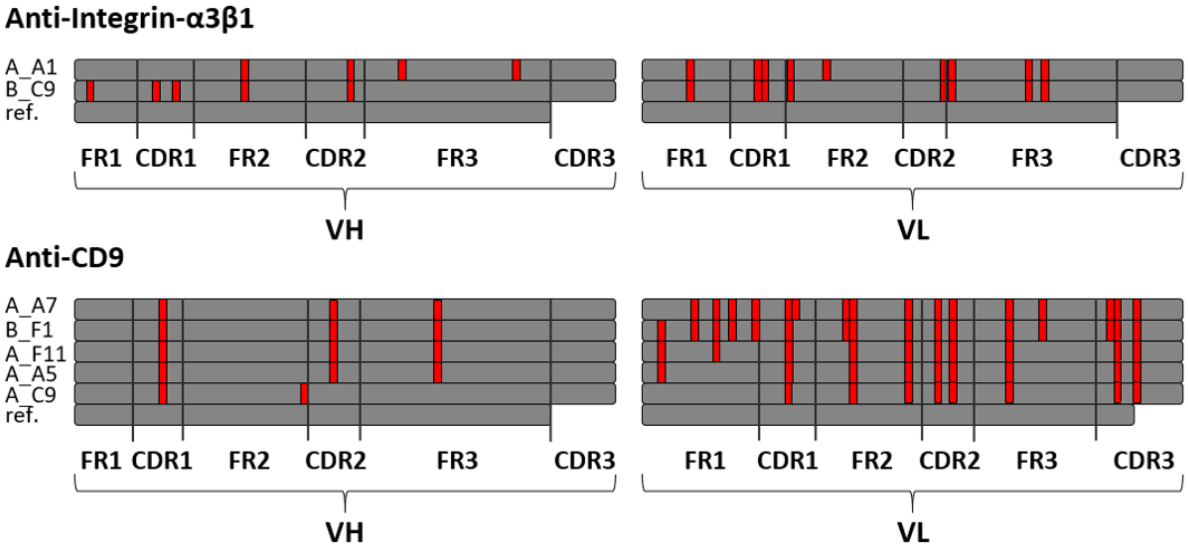

Figure 18: Non-silent mutations in FaDu-binding antibodies. Alignments of anti-integrin-α3β1 and anti-CD9 antibodies. Non-silent mutations in the respective sequence region (FR: framework; CDR: complementary determining region) are depicted in red. Sequences were compared to germline (ref.) derived from public database (IMGT).

3.2.3 Antibody characterisation

For further characterisation, antibodies were converted to human IgG format. In order to exclude potential protein aggregation, antibodies were analysed by size exclusion chromatography (SEC). All antibodies showed a prominent peak at a retention time of ~9 min (Figure 19), which corresponded to monomeric IgG and amounted 94 – 99% of the samples

(Table 25). Only small amounts of degradation products (~9 kDa at ~12 min) and dimers (~300 kDa at ~8 min) were detected in some samples indicating sufficient quality of the tested antibodies.

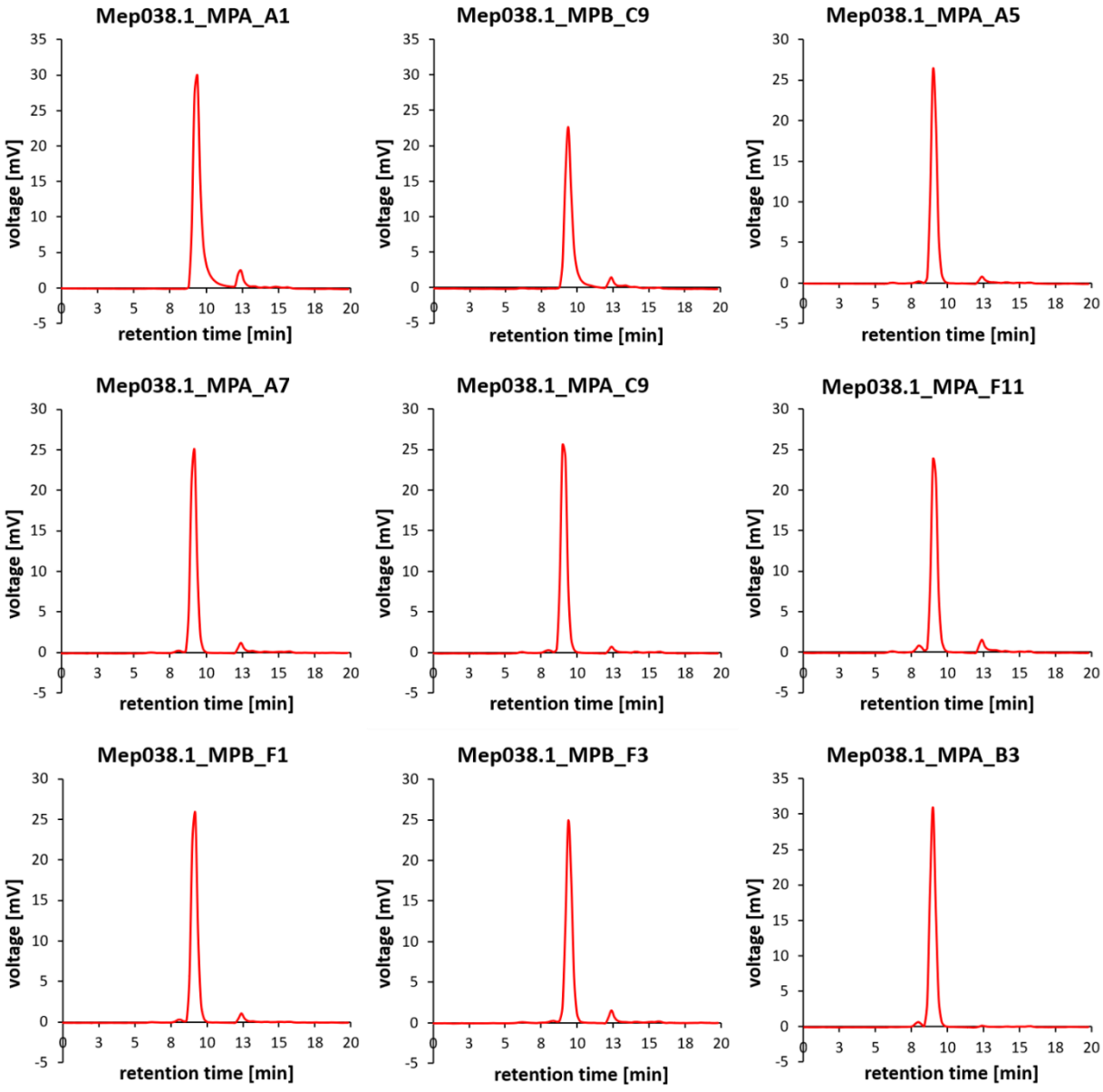

Figure 19: SEC of FaDu-binding antibodies. Antibodies (human IgG) were analysed in SEC and detected voltage was plotted against the retention time. A defined protein standard was measured as well to allow the calculation of the appropriate molecular mass by a regression curve.

Table 25: Summary of SEC analysis

Antibody	Retention time [min]	Percentage area	Molecular mass
Mep038.1_MPA_A1	9.38	95.8%	122.5 kDa
Mep038.1_MPB_C9	9.45	97.3%	114.3 kDa
Mep038.1_MPA_A5	9.14	98.4%	148.0 kDa
Mep038.1_MPA_A7	9.22	97.1%	139.2 kDa
Mep038.1_MPA_C9	9.18	98.9%	143.7 kDa
Mep038.1_MPA_F11	9.17	94.6%	145.0 kDa
Mep038.1_MPB_F1	9.22	97.9%	139.2 kDa
Mep038.1_MPA_B3	9.07	98.4%	157.6 kDa
Mep038.1_MPB_F3	9.53	97.1%	107.1 kDa

3.2.3.1 Integrin-α3β1-specific antibodies

3.2.3.1.1 Binding of integrin-α3β1

Human integrin-α3β1 was identified as target of Mep038.1_MPA_A1 and Mep038.1_MPB_C9 by immunoprecipitation and mass spectrometry. To confirm these results, binding to recombinant human integrin-α3β1 was analysed in ELISA (Figure 20). For both antibodies a concentration dependent sigmoidal binding curve was observed on the antigen without showing cross-reactivity to BSA. EC50 values were 0.21 nM and 0.31 nM, respectively.

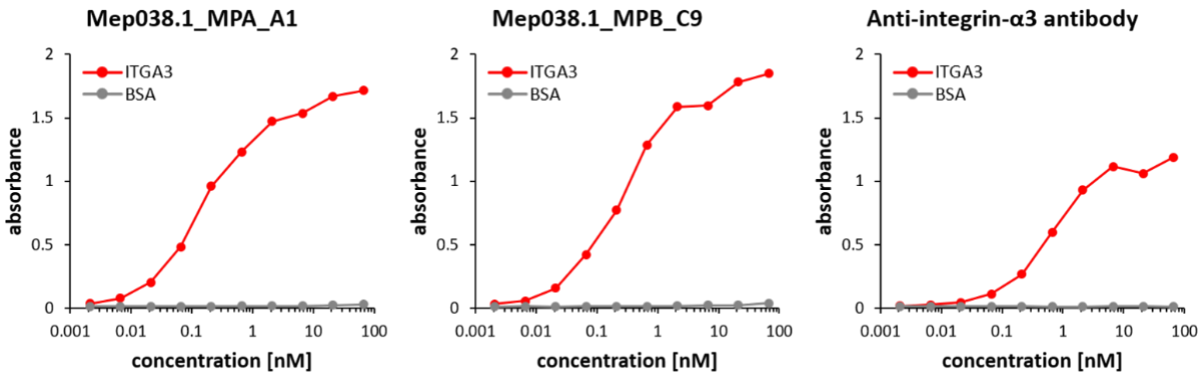

Figure 20: Titration-ELISA on recombinant human integrin-α3β1. Dilution series of the antibodies (human IgG) were incubated on immobilised integrin-α3β1 or BSA as control antigen and detected by an HRP-conjugated secondary antibody. EC50 values were determined to be 0.68 nM for the anti-integrin-α3 antibody used as positive control.

Binding of Mep038.1_MPA_A1 and Mep038.1_MPB_C9 was observed to both pharyngeal carcinoma cell lines FaDu and Detroit-562 (Figure 16), which indicated relevance of integrin-α3β1 in head and neck cancer. This assumption is supported by literature describing integrin-α3β1 to be expressed in various types of cancer (Thul et al. 2017). Therefore, binding of Mep038.1_MPA_A1 to different cancer cell lines was analysed (Figure 21). The selected cell line panel comprised NCI-H1975 (non-small cell lung cancer), MKN-45 (gastric cancer), A549 (lung cancer), NCI-H358 (non-small cell lung cancer, metastatic site), U-87-MG (glioblastoma), A431 (epidermoid carcinoma) as well as FaDu, Detroit-562 and HEK293 as references. Cultivation of cells, immunostaining and flow cytometry were kindly performed by Laura Unmuth (Merck KGaA, Darmstadt, Germany).

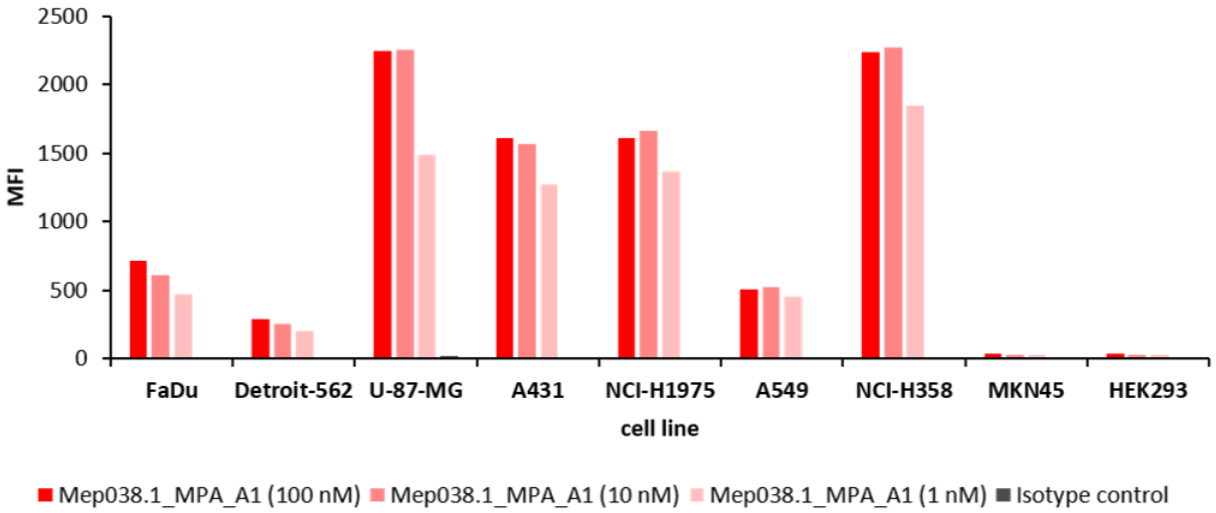

Figure 21: Binding of Mep038.1_MPA_A1 to cancer cell line panel. Different concentrations (100 nM, 10 nM, 1 nM) of Mep038.1_MPA_A1 (human IgG) were used as primary antibody for staining of different cancer cells. Bound antibodies were detected by an AlexaFluor647-conjugated secondary antibody. A non-specific human IgG was used as isotype control.

As observed before Mep038.1_MPA_A1 showed reactivity to FaDu and Detroit-562 and no binding to HEK293, which was expected since for the latter no expression of integrin-α3β1 has been reported (Thul et al. 2017). Highest signals were observed on U-87-MG and NCI-H358, which was consistent with the high expression level of integrin-α3β1 expected for U-87-MG (Thul et al. 2017). For A431 and A549 a moderate expression of integrin-α3β1 has been described (Thul et al. 2017) correlating with the signals obtained with Mep038.1_MPA_A1. NCI-H358 and NCI-H1975 both originated from lung cancer and were bound by the tested antibody. Herein, signal intensity on the metastasis-derived cell line NCI-358 was higher. No binding was observed on MKN45 cell originating from gastric cancer, however, no information about the expression of integrin-α3β1 in this cell line was available. Apart from that,

Mep038.1_MPA_A1 showed reaction to all tested cancer cell lines derived from lung cancer, glioblastoma, epidermoid carcinoma and pharyngeal carcinoma.

3.2.3.1.2 Kinetics measurement

To further evaluate the binding profile of both integrin-α3β1-binding antibodies, kinetics analysis was conducted using BLI. Antibodies were immobilised on anti-human-Fc (AHC) sensor tips and exposed to different dilutions of recombinant human integrin-α3β1. Binding profiles obtained in BLI were similar to each other (Figure 22). For both antibodies a very high on-rate (kon = 10^5 1/Ms) and off-rate (kdis = 10^{-2} 1/s) were observed (Table 26) resulting in overall dissociation constants of 370 nM and 214 nM, respectively.

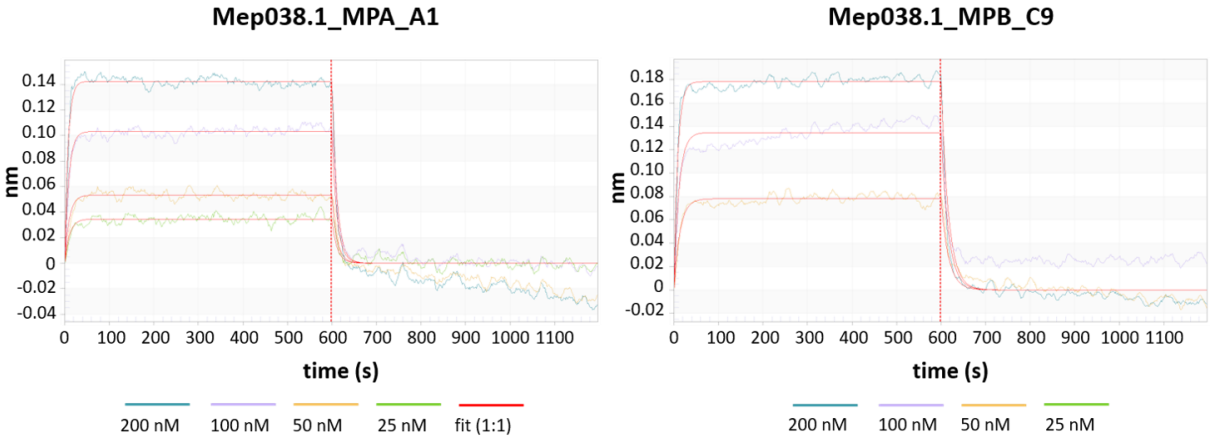

Figure 22: Kinetics assay with integrin-α3β1. Antibodies (human IgG) were immobilised on anti-human IgG-Fc biosensors and exposed to different concentrations of diluted integrin-α3β1. Association and dissociated curves were detected and the mathematical model "1:1 interaction" was applied for the calculation of binding parameters.

Table 26: Summary of integrin-α3β1-binding parameters

Antibody	Antigen	kon [1/Ms]	kdis [1/s]	K_d [nM]
Mep038.1_MPA_A1	Integrin-α3β1	$2.38x10^5$	$8.79x10^{-2}$	370
Mep038.1_MPA_A1	Integrin-α3β1	$2.82x10^5$	$6.03x10^{-2}$	214

In summary of the results described above, two integrin-α3β1-binding antibodies were successfully isolated by cell panning, demonstrating the presence of cancer-related antibodies within the TIL-B libraries. Both antibodies showed binding to integrin-α3β1 in ELISA, flow

cytometry and immunoprecipitation and low cross-reactivity to other components of the tested cell lysates.

3.2.3.2 CD9-specific antibodies

In order to confirm the specificity for CD9 of some of the patient-derived antibodies selected by cell panning as identified by immunoprecipitation and mass spectrometry, binding to recombinant human CD9 was analysed in ELISA (Figure 23). Except for Mep038.1_MPA_C9, which showed binding at the highest concentration, none of the tested antibodies showed reactivity (Figure 23). Thus, binding to human CD9 could not be confirmed in ELISA.

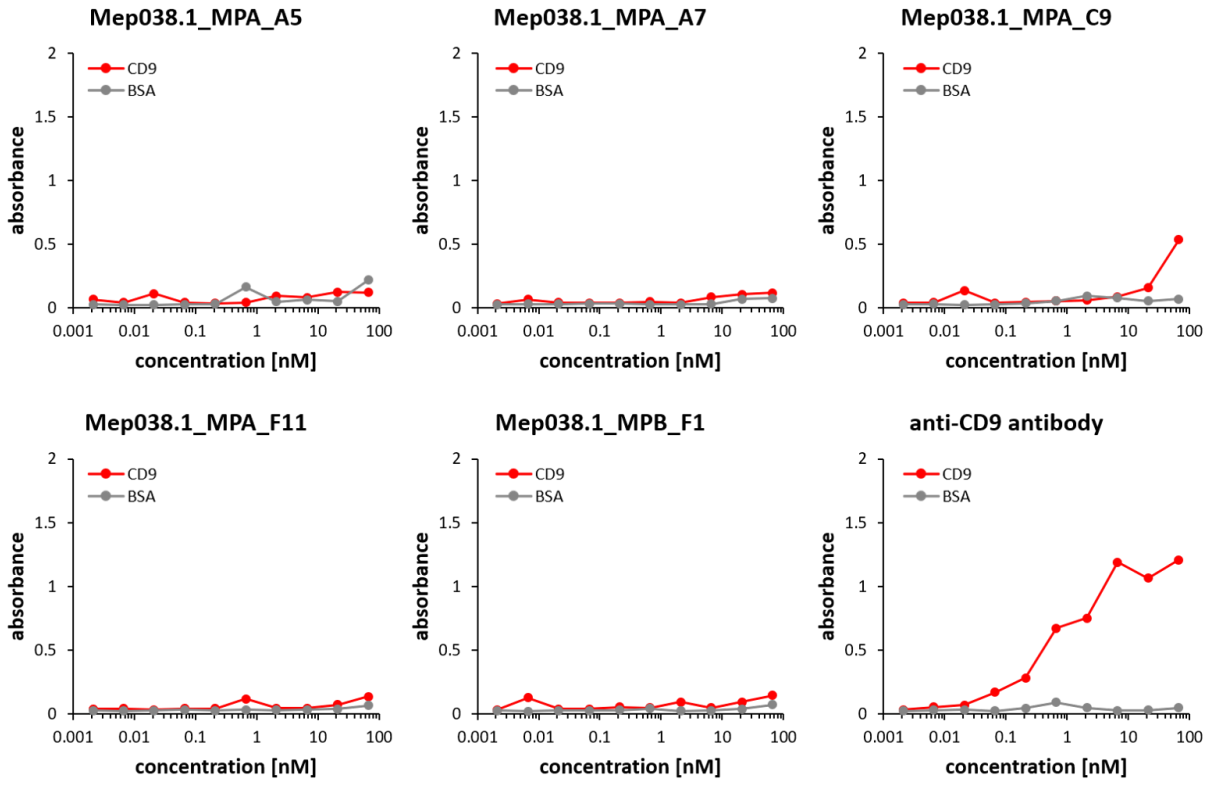

Figure 23: Titration-ELISA on recombinant human CD9. Dilution series of the antibodies (human IgG) were incubated on immobilised CD9 or BSA as control antigen and detected by an HRP-conjugated secondary antibody. EC50 values were not determined since no signals were observed.

In order to exclude complications caused by partial denaturation of CD9 upon immobilisation in the ELISA setup, CD9-specificity was tested in flow cytometry. HEK293 cells were transfected with a CD9-GFP fusion protein and harvested after two days of cultivation. Transfection efficacy of ~68% was determined by quantification of GFP-positive cells. Cells transfected with a control antigen (GFP-fusion) or empty vector and non-transfected cells were

used as negative controls. Staining of the different cells revealed reaction of all tested antibodies to the GFP-positive population of CD9-transfected cells (Figure 24). In contrast to the CD9-specific positive control antibody, no cross-reactivity to the negative controls was observed indicating CD9-selective binding.

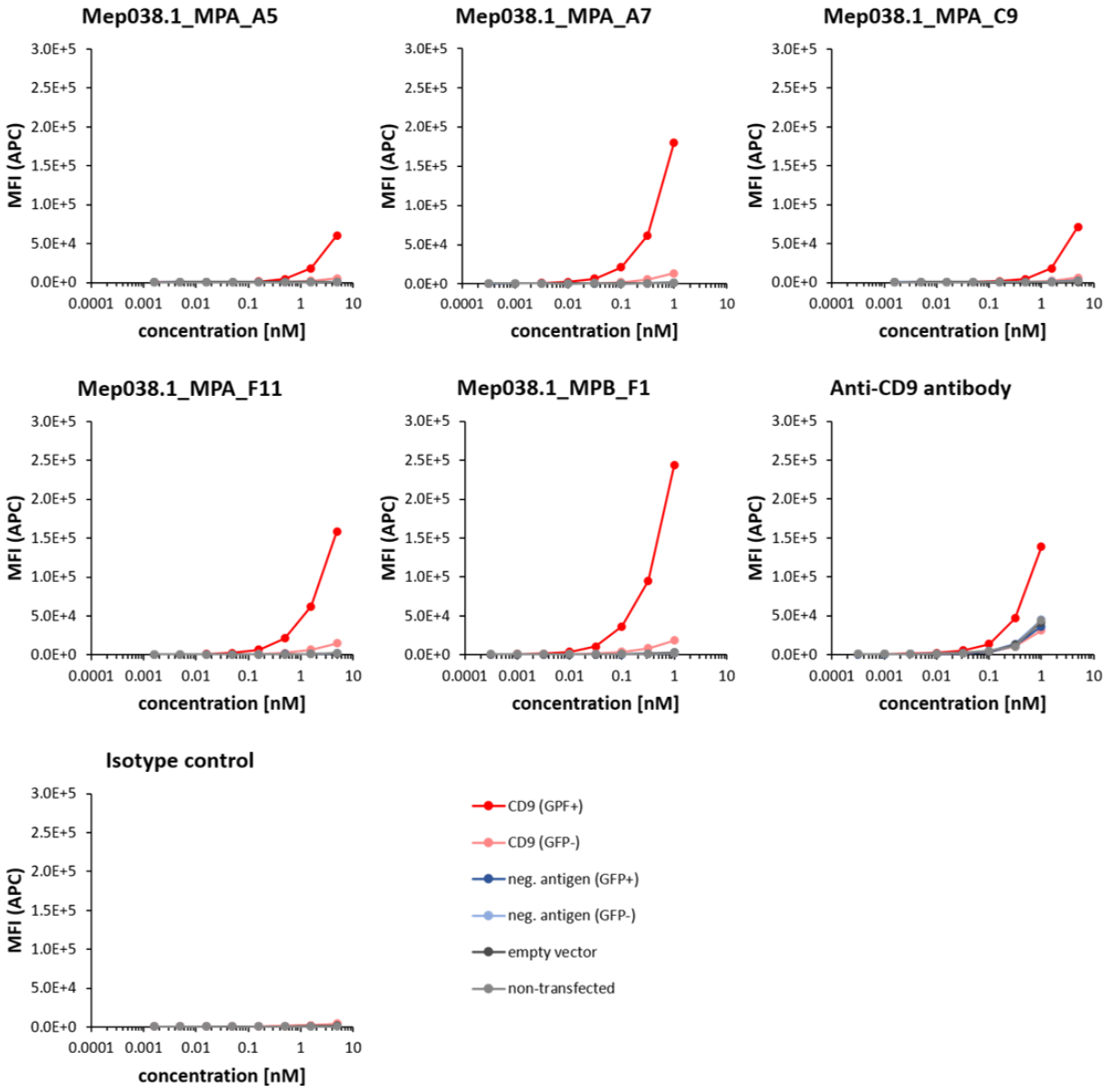

Figure 24: Binding to CD9-expressing cells in flow-cytometry. Antibodies (human IgG) were titrated and tested for binding to CD9-expressing cells. It has to be noted that due to high signal intensities titration of Mep038.1_MPA_A7, Mep038.1_MPB_F1 and the anti-CD9 antibody started at 1 nM whereas for the other antibodies a higher concentration of 5 nM was used. Bound antibodies were detected by an AlexaFluor647-conjugated secondary antibody. Binding to non-transfected cells and to cells transfected with control antigen or empty vector was tested as negative controls. Non-CD9-specific human IgG served as isotype control.

In conclusion, five antibodies isolated from TIL-B libraries were shown to bind CD9-expressing cells and to precipitate CD9 from whole cell lysate of the pharyngeal carcinoma cell line FaDu. Although binding to CD9 in ELISA was not detected for unknown reason, flow cytometric analysis confirmed CD9 as their target.

3.2.3.3 CD71-specific antibodies

Mass spectrometric analysis identified CD71 as target of the remaining two FaDu-binding antibodies. In ELISA, binding to recombinant human CD71 protein was confirmed for both tested candidates (Figure 25). Mep038.1_MPB_F3 only showed low signals compared to Mep038.1_MPA_B3 and the positive control antibody, but still resulted in a comparable EC50 of 2.66 nM. For Mep038.1_MPA_B3 intense signals developed faster resulting in an expected sigmoidal binding curve and an EC50 of 2.11 nM. In Western blotting no staining was observed for both tested antibodies (data not shown).

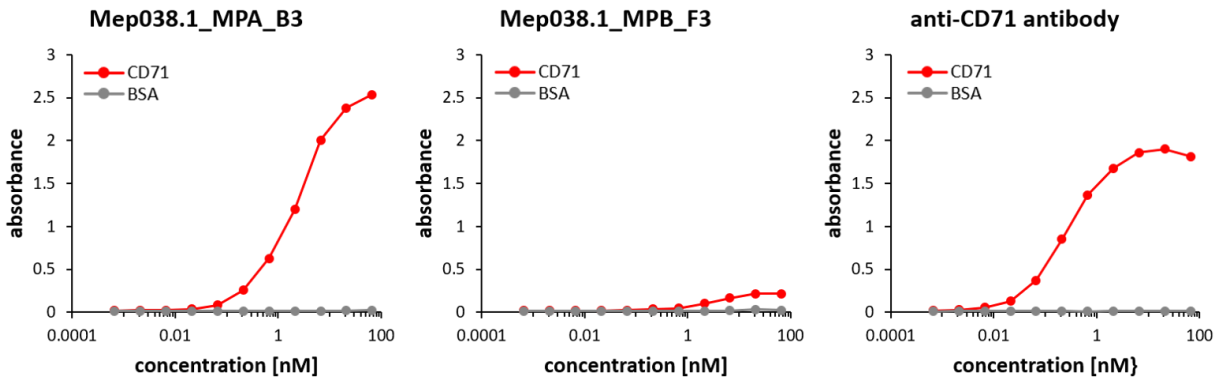

Figure 25: Titration-ELISA on recombinant human CD71. Dilution series of the antibodies (human IgG) were incubated on immobilised CD71 or BSA as control antigen and detected by an HRP-conjugated secondary antibody. EC50 values were determined upon signal normalisation and amounted 2.11 nM for Mep038.1_MPA_B3, 2.66 nM for Mep038.1_MPB_F3 and 0.27 nM for the anti-CD71 antibody used as positive control.

Binding to CD71-expressing cells was further analysed in flow cytometry. HEK293 cells were transfected with a CD71-GFP fusion protein and tested for GFP-expression. After two days, 42% GFP-positive cells were detected indicating successful transfection and target-expression on the cell surface. Cells transfected with a control antigen (GFP-fusion) or empty vector and non-transfected cells were used as negative controls. Both tested antibodies bound to the GFP-positive population of CD71-transfected cells (Figure 26). Binding to negative controls was negligible regarding the signals obtained with the positive control antibody. Consistent

with the ELISA results, signals observed for Mep038.1_MPB_F3 were lower when compared to Mep038.1_MPA_B3.

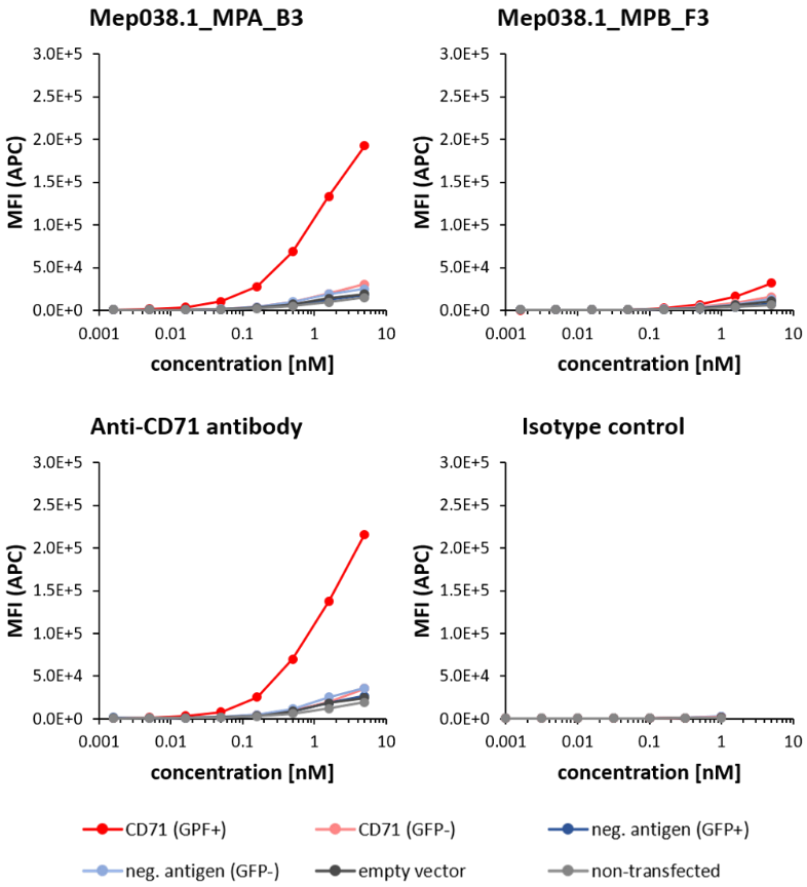

Figure 26: Binding to CD71-expressing cells in flow cytometry. Antibodies (human IgG) were titrated and tested for binding to CD71-expressing cells. Bound antibodies were detected by an AlexaFluor647-conjugated secondary antibody. Binding to non-transfected cells and to cells transfected with control antigen or empty vector was tested as negative controls. Non-CD71-specific human IgG served as isotype control.

In order to investigate the binding profile of the CD71-specific antibodies, kinetics was analysed using BLI. Antibodies were bound to human-Fab-CH1-specific sensor tips and exposed to different concentrations of CD71 (Figure 27). For both antibodies, calculated affinity constants were very low (Table 27) indicating highly affine binding. Consistent with the results obtained in ELISA and flow cytometry, Mep038.1_MPA_B3 again performed better showing a K_d of 0.37 nM.

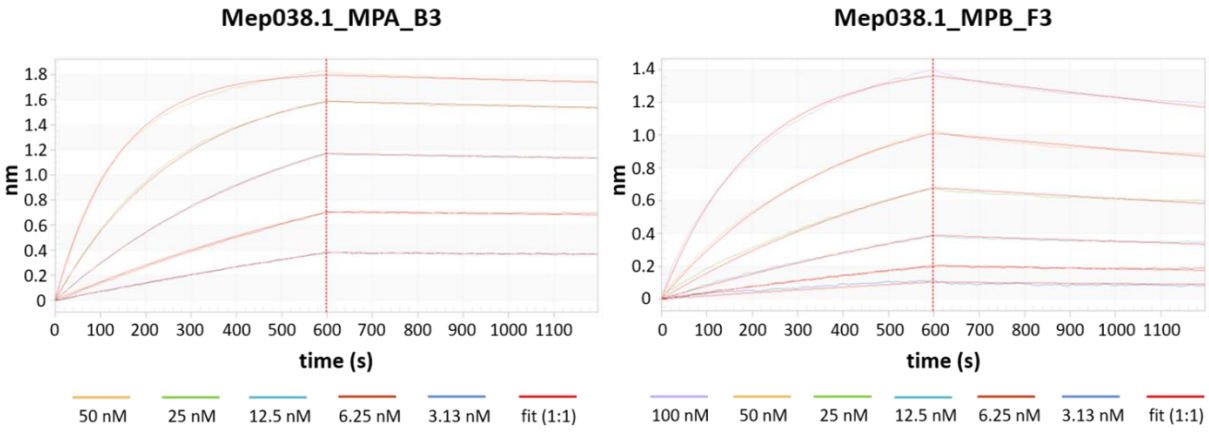

Figure 27: Kinetics assay with CD71. Antibodies (human IgG) were immobilised on anti-human Fab-CH1 biosensors and exposed to different concentrations of diluted CD71. Association and dissociated curves were detected and mathematical model (1:1 interaction) was applied for calculation of binding parameters.

Table 27: Summary of CD71-binding parameters

Antibody	Antigen	kon [1/Ms]	kdis [1/s]	K_d [nM]
Mep038.1_MPA_B3	CD71	$1.45x10^{5}$	$5.38x10^{-5}$	0.37
Mep038.1_MPB_F3	CD71	$4.75x10^{4}$	$2.54x10^{-4}$	5.35

In summary two CD71-specific antibodies were identified, which were shown to be functional in ELISA and flow cytometry. Immunoprecipitation revealed CD71-selective binding with low cross-reactivity to other proteins present in whole cell lysates. BLI revealed high affinities in the nanomolar and even sub-nanomolar range. The data confirmed the successful selection of highly affine, cancer-selective antibodies from TIL-B libraries.

4. Discussion

4.1 Antibody libraries from TIL-B cells

The present study describes the identification of novel cancer-related antibodies from patient-derived antibody libraries. The antibody repertoire of tumor-infiltrating B lymphocytes (TIL-B) was used, which were isolated directly from fresh tumor specimens. The construction of these libraries for selection of cancer-specific autoantibodies has already been investigated before for various types of cancer. In most of these studies, B cells were obtained from whole blood, tumor draining lymph nodes or the tumor itself (Punt et al. 1994; Pavoni et al. 2007; Campa et al. 2016; Novinger et al. 2015). Herein, the isolation of B cells from the tumor core or its microenvironment was mainly done by laser capture microdissection (LCD) (P. M. O'Brien et al. 2005; Simsa et al. 2005), whereas in the present study B cells were isolated from freshly prepared tumor tissue cell suspensions. This procedure facilitated the isolation of larger numbers of cancer-associated B cells including a broad variety of B cell subsets. In contrast, LCD only allows the isolation of small cell populations from frozen or formalin-fixed paraffin embedded (FFPE) tissue sections, which may not reflect the complexity of the complete tumor immune environment (Almeida et al. 2015; Espina et al. 2007). Furthermore, LCD suffers from low yields of cells, poor cell viability and potential DNA- and RNA-damage caused by tissue preparation and the applied laser (Hu et al. 2016). Moreover, the isolation of B cells from freshly prepared single cell suspensions enabled the usage of the tumor cells as by-product for additional investigations and thus, a more efficient usage of the valuable patient-derived material.

For first proof-of-concept studies, B cells isolated from tumor tissue of seven donors were selected for the construction of antibody libraries. Besides three samples with the highest and three samples with a moderate B cell amount, one sample was also included with a B cell count below detection level (YUHAN009, <0.01%), but which still allowed the amplification of antibody genes with PCR. Interestingly, the resulting library size of YUHAN009 was 10 times larger compared to e.g. YUHAN011, in which a moderate B cell count was found. This observation demonstrates, that probably due to PCR amplification, there was no obvious correlation between library size and underlying B cell count. The maximal theoretical library diversity including all combinations of VH and Vκ/Vλ of all isolated B cells can be calculated based on the theoretical B cell count to the second power and was much higher (10^7 to 10^{12}) than the size of the generated antibody libraries. Besides experimental limitations due to tissue processing, RNA isolation, cDNA reverse transcription and PCR amplification, the generation of libraries with a diversity of 10^{12} is extremely time consuming and therefore not feasible for patient-derived libraries. Nevertheless, it can be assumed that cancer-associated B cell clones, which actively infiltrated the tumor and proliferated there are covered in their paired combination in the generated antibody libraries. To access the actual library diversity, NGS

analysis was conducted. Analysing the real diversity of a scFv antibody library by deep sequencing requires long reads covering the complete scFv (up to 750 bp) and a read depth of more than one complete MiSeq run (10^8 reads) for each library (Glanville et al. 2015), which was not possible in the present study. Instead, all TIL-B libraries were analysed in a multiplexed MiSeq run, which resulted in 10^4 to 10^5 reads each for the VH and the Vκ/Vλ, from which 10^2 to 10^4 sequences were found to be unique (suppl. Table 1). To estimate the maximal possible diversity, the unique VH and Vκ/Vλ sequences found in the respective library were multiplied. The resulting diversities (NGS) correlated with the underlying B cell count in lower infiltrated samples but did not further improve in libraries derived from patient samples with a higher B cell count reaching a plateau at a combinatory antibody diversity of ~10^7. This diversity plateau actually meets the typical size of immune libraries (Kramer et al. 2005) caused by clonal enrichment within the patient. On the other hand, the obtained read depth of ~10^4 sequences per sample only allowed a maximal detectable diversity of 10^8 to 10^{10}. This means, that libraries from samples with low B cell infiltrate are completely covered by NGS, whereas for libraries from samples with high B cell count, such as YUHAN022 and YUHAN028 the risk of unseen clones is increased (suppl. Table 1). Nevertheless, the diversities calculated from the multiplexed MiSeq data represent a good estimation, which probably is very accurate for most of the generated TIL-B libraries with low or moderate B cell infiltration and reveals that they are covered by library size. In turn, the YUHAN022- and YUHAN028-derived libraries with high B cell infiltration may not contain every possible heavy and light chain combination.

Analysing the relation of IgG and IgM genes within the TIL-B libraries, no obvious correlation with the B cell infiltration was observed. If clonality increases due to clonal expansion in samples with higher B cell count as suggested for YUHAN022 and YUHAN028, IgG class switch should be expected more often, which should result in a higher amount of IgG genes. However, this effect was not observed for all TIL-B libraries. In non-small cell lung cancer (NSCLC), the B cell distribution has been reported to be similar between distant non-tumoral and tumor tissue but different to peripheral blood, in which the proportion of naïve B cells (IgM) was significantly increased (~30% in blood and ~10% in NSCLC) (Germain et al. 2014). Consistent with these findings, all TIL-B libraries generated in this study were clearly dominated by IgG genes. However, the amount of IgM genes in some libraries was more similar to that observed in blood (Germain et al. 2014) indicating, that the higher amount of IgM genes may derive from naïve B cells passing through tumor-related blood vessels. Due to the isolation of B cells from whole tissue cell suspensions, the B cell subpopulations and their localisation in the tumor were unknown, which does not allow comparison of different libraries and may distort the correlation of IgG amount and B cell count.

In further investigations the abundance of used V-genes within the TIL-B libraries observed in NGS was analysed. In order to outline a potentially altered V-gene usage, all TIL-B libraries can be compared to the V-gene distribution described for naïve phage display libraries (Kügler et al. 2015) and the *in vivo* repertoire (Tiller et al. 2013). YUHAN007 and YUHAN009, which had the lowest B cell infiltration and the lowest diversity estimated by NGS, differed in many characteristics compared to both, the published data and the other TIL-B libraries. Thus, the IGHV1 subfamily was observed less frequently whereas a higher abundance of IGHV3, IGHV5 and IGHV7 was observed. Interestingly, such an overrepresentation of IGHV5 has also been described for the repertoire of TIL-Bs and germinal center B cells derived from ductal breast carcinoma patients (Nzula et al. 2003) and patients suffering from systemic lupus erythematosus (Fraser et al. 2003). Consistent with the observation for YUHAN007 and YUHAN009, Fraser and colleagues additionally described a reduction of IGHV1 genes (Fraser et al. 2003). Excluding YUHAN007 and YUHAN009, the remaining TIL-B libraries showed a similar V-gene distribution among each other. However, the abundance of some subfamilies was altered compared to the published data. Within the light chain genes, IGLV3 was increased compared to both the naïve libraries and the *in vivo* repertoire (Kügler et al. 2015; Tiller et al. 2013). Although it has been described to be rare, subfamily IGHV2 was increased in most libraries similar to the observations published for the repertoire of TIL-Bs derived from breast carcinoma patients (Nzula et al. 2003). Additionally, the IGHV4 subfamily was more abundant than expected regarding the naïve libraries, whereas the normally frequent subfamily IGHV3 was considerably reduced. This also has been described for TIL-Bs in breast and cervical cancer (Nzula et al. 2003; P. O'Brien et al. 2001). Although comparable data is scarce and patient numbers considered in the present study are low, this data indicates an altered V-gene distribution within the TIL-B repertoire, which correlates with the reported suspicion of a preferential usage of specific subfamilies within a disease context. However, in the current stage of our and published research, the underlying mechanism, why and how V-gene subfamilies are preferred in TIL-B cells from head and neck tumors is not understood.

4.2 Selection of TIL-B-antibodies on cancer-related targets

The previous paragraph described that TIL-B libraries from head and neck tumor patients show some distinctive characteristics, which make them peculiar compared to the normal antibody repertoire in the peripheral blood. To further investigate the presence of cancer-related antibodies within the TIL-B libraries, selection on a known cancer target was conducted. The matrix metalloproteinase 9 (MMP-9) is a zinc-dependent endopeptidase, which is further categorised into the gelatinase subgroup of the MMP-family (Huang 2018). Parallel investigations in this research group analysing the antibody response of the same patients to

tumor cell material, identified MMP-9 as potential target of antibodies from TIL-B cells (Kilian Zilkens, personal communication). This finding was underpinned by literature describing MMP-9 as prognostic marker for different types of cancer, since its expression and activity was upregulated in tumor cells and correlated with tumor stage, vessel invasion, increased frequency of metastases and poor survival rates (Shao et al. 2011; Cho et al. 2003). These pro-tumorigenic effects of MMP-9 are believed to be mainly caused by its ability to degrade the extracellular matrix (ECM), which leads to increased tumor invasion and facilitates metastasis formation (Zeng et al. 1999; Kurahara et al. 1999).

In the present study, 19 unique anti-MMP-9 antibodies were isolated from patient-based TIL-B libraries. Analysing the NGS data, it was observed that these antibodies originated from four different libraries revealing, that antibodies targeting MMP-9 were present in >50% of seven head and neck cancer patients. Interestingly, MMP-9 has been described to be important in different head and neck cancers including laryngeal carcinoma (Bogusiewicz et al. 2003) and oral carcinoma, in which it was only active within the tumor but not in the surrounding stroma (Kato et al. 2005). Furthermore, Ruokolainen and colleagues reported, that MMP-9 is expressed in >80% of HNSCC and correlates with more aggressive relapse and shortened survival (Ruokolainen 2004). These findings outline the important role of MMP-9 in head and neck cancer and may explain the presence of anti-MMP-9 antibodies in the majority of patients in this study. In the past, therapeutic inhibition of MMPs was studied but long suffered from dose-limiting side-effects caused by unspecific targeting of various members of the MMP-family. However, more recently it experiences a revival with novel, more specific MMP-inhibitors undergoing clinical trials (Fields 2019). Among them is a humanised antibody, which has been shown to reduce primary tumor growth in a mouse model of colorectal carcinoma (Marshall et al. 2015). Consistently, Juric and colleagues reported the development of a monoclonal anti-MMP-9 antibody, which reduced tumor growth in breast cancer in combination with an anti-PD-L1 antibody (Juric et al. 2018). These findings outline the vast potential of MMP-9-specific antibodies in cancer therapy and the crucial need of highly specific MMP-9-inhibitors. The best three candidates out of the 19 MMP-9-binding antibodies isolated from TIL-Bs were further characterised and showed different binding characteristics depending on the applications. Whereas the performance of clone Mep040.2_A_H5 in flow cytometry and immunoprecipitation was poor, this clone was highly reactive in ELISA and immunoblotting. This data suggests a linear, consecutive epitope, which probably was not well accessible on soluble, natively folded MMP-9. Furthermore, this clone showed cross-reactivity to additional proteins of the cell lysates probably making it inappropriate for therapeutic application. In contrast to Mep040.2_A_H5, the other two clones successfully bound to MMP-9 in ELISA and on cells but not or weakly in immunoblotting indicating a conformational epitope. Affinities of Mep040.2_A_D2 and Mep040.2_D_A8 to soluble MMP-9 in BLI were in a nanomolar range

and cross-reactivity to other cell lysate components was negligible. This indicates MMP-9-selective binding and makes them suitable candidates for further investigations. In future experiments, these antibodies should be tested in immunohistochemistry to exclude binding to non-tumoral human tissue. Furthermore, it should be investigated if binding of the antibodies affects the enzymatic activity of MMP-9 to estimate their applicability in therapeutic strategies.

In summary, the selection of TIL-B libraries on MMP-9 provided highly affine anti-MMP-9 antibodies. This finding demonstrated the presence of cancer-related antibodies within the TIL-B libraries and created the link between the TIL-B repertoire and the corresponding antibody response to tumor antigens, which is investigated in parallel in our research group (Kilian Zilkens, personal communication). Moreover, the isolation of anti-MMP-9 antibodies from four different patient-derived libraries underlines the relevance of MMP-9 as tumor target in head and neck cancer.

4.3 Selection of TIL-B-antibodies on cancer cells

The successful isolation of anti-MMP-9 antibodies demonstrated that TIL-B-derived libraries contain cancer-related antibodies. Although the discovery of antibodies targeting well-defined proteins provides insights into potential anti-tumor reactions, selection against large target panels is time consuming and fails to deliver novel non-described target candidates. To overcome this limitation, the discovery of antibodies was refocused on cancer cells followed by subsequent identification of their unknown targets. The suggestion to use patient-derived libraries as source of tumor-specific antibodies has been described before using different approaches. Thus, selections have been performed on autologous target panels and cancer cell lines (Pavoni et al. 2007; Punt et al. 1994) or on tumor cell lysates (Novinger et al. 2015; Campa et al. 2016; Imahayashi et al. 2000) obtaining the B cells either from peripheral blood, draining lymph nodes or tumor tissue. Currently, various studies are available concerning different types of cancer such as breast cancer, colorectal carcinoma and lung cancer (Reuschenbach et al. 2009). However, for head and neck cancer published investigations are still rare. Cancers of the head and neck often exhibit immunosuppressive characteristics comprising tumor cell modulation as part of immune escape and the recruitment of tumor-promoting cells, which raises the suspicion that infiltrated immune cells may have a tumor-supportive function rather than acting anti-tumorigenic (Tong et al. 2012). Recently, Lechner and colleagues reported a comprehensive analysis of different B cell subsets in head and neck cancer, which revealed an increased number of plasma cells and serum reactivity to tumor-associated antigens indicating that a humoral anti-tumor response may be initiated in head and neck cancer patients (Lechner et al. 2019). In the present study, patient-based antibody libraries were selected on cancer cells, which is to our knowledge for the first time described for antibody repertoires of TIL-B cells derived from head and neck cancer. A total of 22 unique

antibodies were isolated, which bound to the pharyngeal carcinoma cell line FaDu but not to the non-cancerous HEK293 or CHO-K1 control cells. For nine antibodies, immunoprecipitation and mass spectrometry identified integrin-α3β1, CD9 and CD71 as their respective targets, which all are well-described cancer-related proteins.

Integrins are a large family of heterodimeric surface receptors, which interact with proteins of the ECM to mediate adhesion (Hynes 1987; Humphries 2000). In total, there are 19 alpha and 8 beta subunits known to assemble into 24 different heterodimers, which are further grouped according to their ligands (Barczyk et al. 2010). Integrin-α3β1 herein belongs to the laminin-binding subgroup. In addition to their role in cell adhesion, integrins function as bidirectional signalling molecules mediating proliferation, apoptosis, polarity, motility and differentiation by transducing extracellular signals (outside-in). On the other hand, they are sensitive to intracellular signalling, which promotes their activation resulting in a conformational change of both extracellular domains and an altered reaction to agonists and antagonists (inside-out) (Hynes 2002; Tolomelli et al. 2017). Additionally, their interaction with different proteins of the ECM such as other integrins, cadherins, growth factor receptors and MMPs has been described to influence tumorigenesis and metastasis formation in cancer (Tolomelli et al. 2017; Roggiani et al. 2016). This may be caused by integrin-dependent adhesion mediating the arrest of invading tumor cells at distant organs within the metastatic cascade (Sökeland and Schumacher 2019). Due to these pivotal characteristics, most integrins (19 out of 24) have been already traded as potential therapeutic targets (Raab-Westphal et al. 2017). However, the laminin-binding integrins such as integrin-α3β1 have not been of particular interest so far, as their role in tumor progression is controversial and depends on the individual tumor type and stage (Raab-Westphal et al. 2017; Ramovs et al. 2017). Nevertheless, there are studies, which outline the beneficial aspects of integrin-α3β1 targeting. Kurokawa and colleagues for instance suggested integrin-α3 as reliable biomarker for cervical lymph node metastases in tongue squamous cell carcinoma (Kurokawa et al. 2008). Furthermore it has been found, that expression levels of integrin-α3 are correlates with poor overall survival in head and neck squamous cell carcinoma (HNSSC) and that integrin-α3-knockdown leads to reduced cell migration and invasion of a HNSCC cell line (Koshizuka et al. 2017). Consistently, Lusche and colleagues described that blocking of integrin-α3β1 inhibits aggregation within tumor spheroid formation *in vitro* (Lusche et al. 2019). Consequently, the isolation of anti-integrin-α3β1 antibodies form patient-derived TIL-B libraries was an interesting finding, which supported the assumption that the isolated antibodies may be part of an anti-tumor immune response. The selected antibodies bound to integrin-α3β1 in ELISA, flow cytometry and immunoprecipitation. Cross-reactivity to other components of the tested whole cell lysates was low indicating specific binding. BLI measurement revealed a high on-rate but also a high off-rate. In consequence, the calculated affinities were low with K_d values in a three-digit nM range, which was

unexpected regarding the good performance of the antibodies in the other assays. In ELISA, the observed binding is usually affected by avidity effects due to dense immobilisation of the antigen, which leads to apparently stronger binding, whereas in the used BLI measurement setting the antibody is captured first leading to a 1:1 interaction. However, even considering a particularly strong avidity effect, in this case the K_d was 1000-times higher than the calculated EC50 in ELISA, which was unusual. In SEC, 95-97% monomers were observed for the considered antibodies indicating that protein multimer formation or aggregation did not affect the BLI assays. Interestingly, integrins have been described to exist in different conformations depending on their state of activation (Figure 28). The resting conformation is referred to as "bent" since the extracellular domains of both α- and β-chain are folded over, whereas in the extended state both chains are straight and either bound to a ligand (extended-open) or free (extended-closed) (Tolomelli et al. 2017; Campbell and Humphries 2011). Humphries proposed that clustering of integrins and conformational changes upon excitation creates novel binding sites for antibodies, which consequently distinguish between integrins according to their activation and ligand binding state (Humphries 2004).

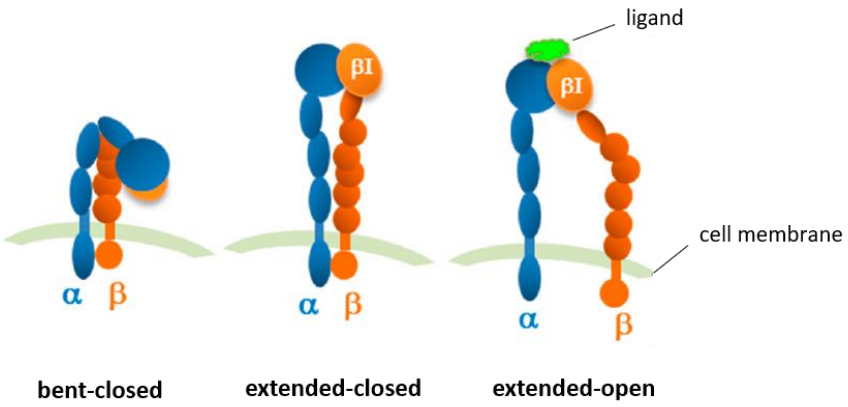

Figure 28: Three conformational states of integrins (Tolomelli et al. 2017)

The epitope of the integrin-α3β1-binding antibodies in this study is still unknown but since the antibodies did not bind in immunoblotting (data not shown) a conformational, potentially non-consecutive epitope is likely. Regarding the good performance of the antibodies on cells in flow cytometry and on cell lysates in immunoprecipitation, it is possible that the appropriate antibody binding site may only be accessible in the extended conformation, which may be only present in a cellular context. In ELISA in turn, partial denaturation of the antigen during immobilisation may have led to unfolding of "bent" integrin, thus revealing the epitope of the antibodies. In BLI in contrast, the recombinant integrin was in solution and thus the epitope was maybe not accessible or conformationally different due to the "bent" state. The different

states of the same antigen and the bivalent avidity effect can explain, why the same antibodies are binding to cell-associated and immobilised integrin, whereas binding to soluble recombinant protein was poor in BLI. Further investigations including inversion of the assay setup (immobilised antigen) and the implementation of different technologies such as surface plasmon resonance (SPR) (Homola et al. 1999) or kinetic exclusion assay (KinExA) (Darling and Brault 2004) for affinity determination on cells might be helpful to reliably estimate the actual affinity. Identification of the minimal epitope for instance by using peptide arrays (Lawson et al. 2019) or the ORFeome phage display technology (Fühner et al. 2018) may also be useful to further access and assign the antibody binding site and to investigate if it is indeed covered within the “bent” conformation. Furthermore, the antibodies should be tested in bioassays to investigate their functional effects, for instance by analysing their abilities to block integrin-α3β1 signalling or ligand binding, which may lead to the inhibition of cancer cell aggregation or motility (Lusche et al. 2019).

In addition to the anti-integrin-α3β1 antibodies, CD9-binding antibodies were identified upon selection on cancer cells. As a member of the tetraspanin superfamily, CD9 is a widely expressed transmembrane protein consisting of four transmembrane domains, two extracellular loops and an intracellular terminus (Boucheix and Rubinstein 2001; Brosseau et al. 2018; Maecker et al. 1997). Besides the interaction with other membrane proteins, tetraspanins are known to associate with each other to form so-called tetraspanin-enriched microdomains (TEMs), which influence various cellular processes such as cell adhesion, motility, growth, differentiation and signal transduction (Brosseau et al. 2018; Hemler 2014; Charrin et al. 2014; Hemler 2003). The role of CD9 in cancer is controversial because correlations with both tumor suppression (Higashiyama et al. 1995; Copeland et al. 2013) and poor prognosis for the patients (Rappa et al. 2015) have been reported. These contrasting effects are believed to be dependent on the different interaction partners of CD9, which vary according to the given cellular context (Hemler 2014). Association with the prostaglandin F2 receptor negative regulator (PTGFRN) for instance, has been described to correlate with a tumor-promoting effect in glioblastoma, whereas association with EWI-2 in contrast inhibited tumor growth (Kolesnikova et al. 2009). Interestingly, in the present study PTGFRN was identified as a co-precipitate of CD9 in immunoprecipitation from FaDu cell lysate (faint band at ~130 kDa) demonstrating their interaction in the considered cell line. In addition, association of tetraspanins with laminin-binding integrins such as integrin-α3β1 has been reported and suggestions were made, that this interaction may be the reason why their signalling pathways differ from those mediated by other integrins (Stipp 2010). Within the tetraspanin complex, the integrin-α3 subunit is directly connected to CD151, which links it to CD9 and CD81 (Yauch et al. 1998; Stipp 2010). Association with the TEM-complex in turn regulates integrin-dependent cell behaviour outlining its significant impact (Gustafson-Wagner and Stipp 2013). The high

complexity of their interactions with different proteins and their functional role in diverse biological processes seem to cause the controversial effects of both CD9 and integrin-α3β1 in a disease context, which makes them interesting targets for therapy and diagnostics (Vences-Catalán and Levy 2018; Rappa et al. 2015; Gustafson-Wagner and Stipp 2013).

In the present study, five CD9-binding antibodies were isolated from TIL-B libraries. Although no binding to immobilised CD9 in ELISA could be observed, the antibodies were shown to bind to CD9-expressing cells confirming the results obtained from immunoprecipitation and mass spectrometry. We assume, that denaturation of the multi-pass transmembrane protein CD9 during immobilisation in ELISA or recombinant production lead to the destruction of the epitopes. Furthermore, since CD9 is strongly associated with other membrane proteins, it is possible that conformational epitopes are only formed upon interaction with certain partners (e.g. PTGFRN, which was co-precipitated) and hence, are present on CD9-expressing cells but not on purified CD9. Consequently, affinity measurement by BLI was not possible, but immunoprecipitation of CD9 from cell lysate indicates highly affine binding of the antibodies isolated from the TIL-B libraries. Interestingly, the sequences of the five isolated CD9-binding antibodies were all based on the same V-gene recombination and shared most of the CDRs but were still unique due to various point mutations. Many of these mutations were identical in all clones, whereas some of them differed in one or the other position indicating the same clonal origin. For Mep038.1_MPA_A7 and Mep038.1_MPB_F1 the most amino acid exchanges were found compared to germline. Interestingly, for these two clones also the highest signal intensities in flow cytometry were observed indicating, that the number of point mutations correlated with stronger binding. This observation raises the suspicion, that the isolated antibodies may be affinity matured as consequence of an anti-tumor immune response within the patient and may represent different stages of maturation. Similar observations referring to increased mutation rates within the CDRs and a decreased germline identity (GI) have been reported previously for patient-derived antibodies in different types of cancer (DeFalco et al. 2018; Novinger et al. 2015). The overall GI of the isolated CD9-antibodies ranged between 90% and 98%, which is similar to affinity-matured antibodies (Hansen et al. 2002; Gellrich et al. 1999; O'Brien et al. 2001) and consistent with the observation, that these antibodies originated from IgG (at least the HC).

The five anti-CD9 antibodies among each other as well as the two anti-integrin-α3β1 antibodies showed the same VDJ and VJ recombination and a CDR3-identity of >85% as reported for clonally related antibodies (Rajewsky 1996; Tipton et al. 2015). Somatic hypermutations have been described to be characterised by increased rates of non-silent mutations (amino acid exchanges) in CDRs compared to framework regions (FR) (Rajewsky 1996; Nzula et al. 2003; Hansen et al. 2002). Indeed, high rates of non-silent mutations were also observed in the

FaDu-binding antibodies, even if mutations within the first 8 amino acids were excluded, because they may be artificially generated by the degenerated PCR primer. For the anti-CD9 antibodies, mutation rates in general were lower within the heavy chain (1 – 4% in CDR versus 0.42% in FR), whereas the light chain was more frequently mutated (10-13% in CDRs versus 1-6% in FR). The observed mutation rates are comparable to somatically hypermutated antibodies observed in ductal breast carcinoma patients (Hansen et al. 2002) and in germinal center B cells upon antigen stimulation (Kuraoka et al. 2016). Analysing the utilised V-genes, it was found that all FaDu-binding antibodies comprised gene subfamilies, which have been previously described in an antigen-dependent context. Thus, IGHV3-30, IGHV1-18, IGHV3-21, IGHV6-57 and IGHV1-51 have been reported to be either enriched upon target selection of naïve antibody phage display libraries (Kügler et al. 2015) or even within tumors and draining lymph nodes of breast cancer patients (Novinger et al. 2015). Moreover, subfamily IGHV4-34 has been described to play an important role in autoimmune activity and has been predominantly found in autoreactive systemic lupus erythematosus (Tipton et al. 2015). Although, it remains to be proven if the FaDu-binding antibodies really contributed to anti-tumor immunity or if they are just expressed from bystander TIL-B cells attracted by cytokines in the tumor microenvironment (Reuschenbach et al. 2009; Yuen et al. 2016), these findings strongly indicate clonal relation and somatic hypermutation of the isolated antibodies. Targeting CD9 with the TIL-B-derived antibodies consequently may be a promising strategy in cancer therapy. Thus, it already has been shown, that silencing of CD9 and its interaction partner CD81 strongly impaired integrin-α3β1-dependent directed motility of breast cancer cells (Gustafson-Wagner and Stipp 2013). Additionally, Rappa and colleagues reported, that a monoclonal anti-CD9 antibody inhibited the metastatic capacity of breast cancer cells and decreased tumor growth in mice (Rappa et al. 2015). Interestingly, CD9 is not only expressed on cells but also present on the surface of most cancer-associated exosomes, which are extracellular vesicles mediating cell-to-cell communication and metastasis formation (Yoshioka et al. 2013). Targeting CD9 with antibodies in turn lead to the elimination of cancer-associated exosomes by macrophages, which efficiently reduced metastasis formation (Nishida-Aoki et al. 2017). In summary, these findings provide evidence, that the anti-CD9 antibodies isolated from TIL-B libraries could have play an important role within the tumor microenvironment and therefore, may find broad application in cancer therapy. Consequently, CD9 as target and antibodies targeting this tetraspanin and its pathways should be further investigated.

In addition to integrin-α3β1 and CD9, the transferrin receptor 1 (CD71) was identified as target of the remaining considered FaDu-binding antibodies. CD71 is a type II transmembrane glycoprotein, which prevails as homodimer consisting of two monomers connected by two disulfide bonds (Jing and Trowbridge 1987). Through internalisation upon binding of iron-loaded transferrin (Tf), CD71 mediates the uptake of iron, which is essential for cellular

metabolism, respiration and as co-factor for DNA synthesis (Daniels et al. 2006; Neckers and Trepel 1986). Since it is crucial for cell survival and growth, CD71 is ubiquitously expressed in low levels on most normal cells, whereas its expression is massively increased in rapidly proliferating cells such as epidermal cells and activated PBMCs (Daniels et al. 2006; Shindelman et al. 1981). This is consistent with the observations made while characterising the two anti-CD71 antibodies isolated from the TIL-B libraries. In immunoprecipitation, CD71-corresponding bands were also visible in the control lysate but in notably lower concentration compared to the FaDu lysate. Consistently, weak binding to all control cell lines was observed in flow cytometry, which was also present using the commercial anti-CD71 control antibody. Additionally, expression of low levels of CD71 has been described for HEK293, which was used for transfection and as control cell line (Thul et al. 2017). This indicated, that the observed binding of the antibodies to the control cells and lysates was caused by ubiquitous expression of CD71 rather than by cross-reactivity to other antigens. Since CD71 has been reported to be upregulated in various types of cancer such as esophageal squamous cell carcinoma (Chan et al. 2014), pancreatic cancer (Ryschich et al. 2004) and breast cancer (Shindelman et al. 1981; Habashy et al. 2010), CD71 has been already traded as potential target for cancer therapy. In the past decade, various strategies have been reported to affect CD71 function for instance through direct blocking of Tf-binding, inhibition of receptor internalisation or recycling and by using the internalising CD71 for the delivery of therapeutic agents (Daniels-Wells and Penichet 2016; Luria-Pérez et al. 2016). Although targeting a ubiquitously expressed protein is challenging due to undesired side-effects, a number of publications reported promising results with one therapeutic agent currently undergoing clinical trials (Luria-Pérez et al. 2016). The CD71-binding antibodies selected in this study showed reactivity to both the immobilised recombinant CD71 in ELISA as well as to CD71-expressing cells in flow cytometry. In both assays, clone Mep038.1_MPA_B3 delivered higher signal intensities compared to Mep038.1_MPB_F3. In kinetic measurement, very low K_d values of 0.37 nM and 5.35 nM were obtained, which indicated high affinities and correlated with the good performance in immunoprecipitation and immunostaining in flow cytometry. Compared to the EC50 determined in ELISA, the obtained K_d values were even lower than expected. In our research group, it has been observed previously, that antibodies binding to immobilised CD71 in ELISA may not always bind to soluble CD71 and vice versa, which indicates, that CD71 conformationally changes upon immobilisation and potentially explains the observed weaker binding in ELISA (Thomas Schirrmann, personal communication). Nevertheless, both tested antibodies showed high affinities to soluble CD71 and negligible cross-reactivity to other components of the tested cell lysates, which makes them interesting candidates for future investigations estimating their applicability in cancer therapy.

In summary, the present study describes the selection of affine antibodies against the four cancer-related proteins MMP-9, integrin-α3β1, CD9 and CD71. To our knowledge this is the first identification of potential target proteins using the TIL-B antibody repertoire of head and neck cancer patients. The isolated antibodies bound their respective targets with high affinities in different assays comprising ELISA, flow cytometry, immunoprecipitation and BLI. The identification of clonally related, somatically hypermutated antibodies against well-described cancer-associated proteins and the predominant isolation of selection-associated V-gene subfamilies strongly outline the important role of TIL-B cells in anti-tumor immunity as suggested by many other studies. This approach may also lead to the identification of novel target and antibody candidates contributing to the development of therapeutic strategies.

5. Outlook

Up to now the development of novel therapeutic or diagnostic antibodies for cancer is crucially restricted by the discovery of druggable targets especially in solid tumors, which in turn is complicated by the wide range of different cancer types, variable characteristics of the tumor cells and their microenvironment and the need of a tumor-selective expression.

The present study describes the selection of cancer-cell-binding antibodies from the TIL-B antibody repertoire and the identification of the respective targets by immunoprecipitation and mass spectrometry to overcome the limitation to known tumor markers. Antibodies against well-described cancer-related proteins were isolated, demonstrating the great potential of this approach, which can be further improved in future investigations even for novel targets, target complexes and pathways. In this study, seven TIL-B libraries were constructed and analysed. Increasing the patient number for future experiments would diversify the considered antibody and target pools and greatly improve reliability of the NGS output, thus allowing a deeper insight into the V-gene usage and the clonality of TIL-Bs. Additionally, more cancer cell lines could be considered in the selection process to isolate antibodies against targets, which are shared on different cancer cells. This may increase the chance to discover universal cancer-selective antibodies, which do not bind to normal cells. Considering, that in the present study nine out of 22 FaDu-binding antibodies were suitable for immunoprecipitation and further examined, several clones remained unidentified, which may deliver novel target proteins. Future investigations should focus on different strategies for target identification to overcome the limitation of immunoprecipitation, which usually requires high affinities. Analysis of peptide or protein arrays (Lawson et al. 2019) and the ORFeome phage display technology (Fühner et al. 2018) may contribute to successfully identify the targets of a broader range of antibodies. Regarding library construction, a differentiation of more defined B cell subpopulations may be beneficial to exclude bias caused by tumor-promoting Bregs or chemokine-attracted bystander B cells in future studies, for instance by implementing a more comprehensive immunostaining for flow cytometry. Fluorescence-activated cell sorting (FACS) would additionally allow construction of libraries based on single B cells in order to retain the natural antibody pairing (Tiller et al. 2008) further reducing potential bias within the libraries. Regarding the isolated antibodies against MMP-9, integrin-α3β1, CD9 and CD71, future experiments also need to include the identification of their individual epitopes and the characterisation of their effects on tumor cells by investigating their potential blocking, internalisation and cytotoxic abilities in cellular assays. Furthermore, tumor-selectivity should be analysed by immunohistochemistry to exclude cross-reactivity with non-tumoral tissue and to estimate if they may be applicable in molecular biology, diagnostics or cancer therapy.

6. Summary

Tumor-infiltrating lymphocytes (TIL) have been shown to contribute to an anti-tumor immunity correlating with improved survival of patients suffering from different types of cancer. Due to the close proximity to lymphatic tissue and the high frequency of related viral infections, cancers of the head and neck belong to the most highly infiltrated tumor types. Patients greatly benefit from immunotherapy, which aims to redirect or enhance their own anti-tumor immune response, but further development of efficient strategies is limited by the discovery of novel antibodies and targets. Tumor-infiltrating B cells (TIL-B) have been described as promising source of novel antigen-experienced and somatically hypermutated anti-tumor antibodies for many cancer types but published investigations considering head and neck cancers are rare.

In the present study, novel antibodies against cancer-related proteins were isolated for the first time using the antibody repertoire of B cells infiltrating head and neck cancers. Human antibody gene libraries were constructed based on TIL-Bs isolated from fresh tumor specimens, analysed in next generation sequencing (NGS) and used for phage display selection. NGS analysis revealed an altered V-gene distribution within the TIL-B libraries compared to published naïve scFv-libraries and the *in vivo* repertoire. In some characteristics the TIL-B libraries were more similar to libraries, which were constructed from antigen-experienced B cells indicating a preferential V-gene usage in a disease context. Antibodies against the well-known cancer target matrix metalloproteinase 9 (MMP-9) were isolated and characterised proving the presence of cancer-relevant antibodies within the TIL-B repertoire. To overcome the limitation to known antigens, TIL-B libraries were panned against the pharyngeal carcinoma cell line FaDu. Targets of the respective cell-binding antibodies were identified by immunoprecipitation and mass spectrometry revealing that nine of them bound to the cancer-associated proteins integrin-α3β1, CD9 and CD71. Sequence analysis of the isolated anti-integrin-α3β1 and anti-CD9 antibodies indicated clonal relation due to an identical V-gene recombination and frequent point mutations. The isolated antibodies were characterised and shown to be negligibly cross-reactive and affine to their respective target in various applications including ELISA, immunoprecipitation, flow cytometry and biolayer interferometry (BLI).

In conclusion, this study describes the isolation of antibodies from TIL-B libraries against the well-known cancer-related targets MMP-9, integrin-α3β1, CD9 and CD71. The observed altered V-gene distribution within the libraries and the isolation of probably clonally related, highly mutated antibodies strongly indicate that they may have contributed to an anti-tumor immune response within the respective head and neck cancer patients. The identification of well-described cancer-related proteins as their targets demonstrates the vast potential of the TIL-B repertoire in the discovery of novel anti-tumor antibodies and may lead to the discovery of novel tumor targets for the development of novel therapeutic strategies.

7. Acknowledgements

Submitting a thesis is a special moment, which releases overwhelming thoughts, feelings and memories of the past few years full of experiences. At this point I want to thank all people who were part of this journey and thus contributed to this work.

First of all, I would like to express my gratitude to my mentor and first examiner **Prof. Dr. Stefan Dübel** for his great support throughout the years and for giving me the chance to work on this project. A big thank also goes to my third examiner **Prof. Dr. Michael Hust** who was always open for questions and prepared to give advices.

I would like to sincerely thank **Prof. Dr. Andreas Gerstner** not only for being my second examiner but more important for being an outstanding and enthusiastic cooperation partner paving the way for a great and efficient collaboration.

My gratitude goes to **Dr. Thomas Schirrmann** for providing valuable input and for his continuous effort to enable and drive this project. A big thank also goes to **Dr. Lars Toleikis** for facilitating a great collaboration leading this project to success.

A special thank goes to **Dr. Jonas Kügler** and **Dr. Carolin Sellmann** for their sustaining support and their great commitment. Thanks also to **Dr. Roland Kellner**, not only for the mass spectrometric analysis but also for the excellent scientific discussions. A big thank goes to **Dr. Thomas Clarke** for implementing the NGS analysis.

I would like to thank **Dr. André Frenzel** and **Dr. Philipp Kuhn** for generously sharing their expertise and giving valuable scientific advices at any time!

I want to thank all my colleagues of the **Yumab Team** for creating a unique and cordial atmosphere and for providing constant motivation – it was a pleasure to work with you. Thanks to all members of the **Department of Biotechnology** for their support and an enjoyable time.

A very special thank goes to **Kilian** who was the best PhD partner I could imagine and who became a close friend over the years. Thanks for all the joint experiences, the deep conversations and the funniest lab days. We divided demotivated days in half but instead doubled the feelings of success and for this I am very grateful.

Last but not least, I would like to express my deepest gratitude to my parents **Erika and Waldemar Philippi** and my sister **Adelina** who encouraged me my whole life and never stopped believing in me. Thanks also to my godson **Elias** for letting the sun rise with every single smile. A special thank goes to **Torben** for being my home and for grounding, supporting and motivating me in every situation. Thank you all very much – without you, this work would not have been possible.

8. References

Aderem, Alan, and David M. Underhill. 1999. “Mechanisms of Phagocytosis in Macrophages.” *Annual Review of Immunology* 17 (1): 593–623. https://doi.org/10.1146/annurev.immunol.17.1.593.

Affara, Nesrine I., Brian Ruffell, Terry R. Medler, Andrew J. Gunderson, Magnus Johansson, Sophia Bornstein, Emily Bergsland, et al. 2014. “B Cells Regulate Macrophage Phenotype and Response to Chemotherapy in Squamous Carcinomas.” *Cancer Cell* 25 (6): 809–21. https://doi.org/10.1016/j.ccr.2014.04.026.

Ahmad, Zuhaida Asra, Swee Keong Yeap, Abdul Manaf Ali, Wan Yong Ho, Noorjahan Banu Mohamed Alitheen, and Muhajir Hamid. 2012. “scFv Antibody: Principles and Clinical Application.” *Clinical and Developmental Immunology* 2012: 1–15. https://doi.org/10.1155/2012/980250.

Almand, B., J. R. Resser, B. Lindman, S. Nadaf, J. I. Clark, E. D. Kwon, D. P. Carbone, and D. I. Gabrilovich. 2000. “Clinical Significance of Defective Dendritic Cell Differentiation in Cancer.” *Clinical Cancer Research: An Official Journal of the American Association for Cancer Research* 6 (5): 1755–66.

Almeida, Maria, Andres C. García-Montero, and Alberto Orfao. 2015. “Cell Purification: A New Challenge for Biobanks.” *Pathobiology* 81 (5–6): 261–75. https://doi.org/10.1159/000358306.

Alsibai, Kinan Drak, and Didier Meseure. 2018. “Significance of Tumor Microenvironment Scoring and Immune Biomarkers in Patient Stratification and Cancer Outcomes.” In *Histopathology - An Update*, edited by Supriya Srivastava. InTech. http://www.intechopen.com/books/histopathology-an-update/significance-of-tumor-microenvironment-scoring-and-immune-biomarkers-in-patient-stratification-and-c.

Andreu, Pauline, Magnus Johansson, Nesrine I. Affara, Ferdinando Pucci, Tingting Tan, Simon Junankar, Lidiya Korets, et al. 2010. “FcRgamma Activation Regulates Inflammation-Associated Squamous Carcinogenesis.” *Cancer Cell* 17 (2): 121–34. https://doi.org/10.1016/j.ccr.2009.12.019.

Ang, K. Kian, Jonathan Harris, Richard Wheeler, Randal Weber, David I. Rosenthal, Phuc Felix Nguyen-Tân, William H. Westra, et al. 2010. “Human Papillomavirus and Survival of Patients with Oropharyngeal Cancer.” *New England Journal of Medicine* 363 (1): 24–35. https://doi.org/10.1056/NEJMoa0912217.

Arabpour, Mohsen, Reza Rasolmali, Abdoul-Rasoul Talei, Fereshteh Mehdipour, and Abbas Ghaderi. 2019. “Granzyme B Production by Activated B Cells Derived from Breast Cancer-Draining Lymph Nodes.” *Molecular Immunology* 114 (October): 172–78. https://doi.org/10.1016/j.molimm.2019.07.019.

Balermpas, P, Y Michel, J Wagenblast, O Seitz, C Weiss, F Rödel, C Rödel, and E Fokas. 2014. “Tumour-Infiltrating Lymphocytes Predict Response to Definitive Chemoradiotherapy in Head and Neck Cancer.” *British Journal of Cancer* 110 (2): 501–9. https://doi.org/10.1038/bjc.2013.640.

Barbas, C. F., A. S. Kang, R. A. Lerner, and S. J. Benkovic. 1991. “Assembly of Combinatorial Antibody Libraries on Phage Surfaces: The Gene III Site.” *Proceedings of the National Academy of Sciences* 88 (18): 7978–82. https://doi.org/10.1073/pnas.88.18.7978.

Barczyk, Malgorzata, Sergio Carracedo, and Donald Gullberg. 2010. “Integrins.” *Cell and Tissue Research* 339 (1): 269–80. https://doi.org/10.1007/s00441-009-0834-6.

Barrett, David M., Nathan Singh, David L. Porter, Stephan A. Grupp, and Carl H. June. 2014. “Chimeric Antigen Receptor Therapy for Cancer.” *Annual Review of Medicine* 65 (1): 333–47. https://doi.org/10.1146/annurev-med-060512-150254.

Blank, Christian, Thomas F. Gajewski, and Andreas Mackensen. 2005. “Interaction of PD-L1 on Tumor Cells with PD-1 on Tumor-Specific T Cells as a Mechanism of Immune Evasion: Implications for Tumor Immunotherapy.” *Cancer Immunology, Immunotherapy* 54 (4): 307–14. https://doi.org/10.1007/s00262-004-0593-x.

Boder, Eric T., Maryam Raeeszadeh-Sarmazdeh, and J. Vincent Price. 2012. “Engineering Antibodies by Yeast Display.” *Archives of Biochemistry and Biophysics* 526 (2): 99–106. https://doi.org/10.1016/j.abb.2012.03.009.

Bogusiewicz, Michal, Marta Stryjecka-Zimmer, Marcin Szymanski, Tomasz Rechberger, and Wieslaw Golabek. 2003. “Activity of Matrix Metalloproteinases-2 and -9 in Advanced Laryngeal Cancer.” *Otolaryngology–Head and Neck Surgery* 128 (1): 132–36. https://doi.org/10.1067/mhn.2003.8.

Bonner, James A., Paul M. Harari, Jordi Giralt, Nozar Azarnia, Dong M. Shin, Roger B. Cohen, Christopher U. Jones, et al. 2006. “Radiotherapy plus Cetuximab for Squamous-Cell Carcinoma of the Head and Neck.” *New England Journal of Medicine* 354 (6): 567–78. https://doi.org/10.1056/NEJMoa053422.

Bouaziz, Jean-David, Sebastien Calbo, Maud Maho-Vaillant, Anne Saussine, Martine Bagot, Armand Bensussan, and Philippe Musette. 2010. “IL-10 Produced by Activated Human B Cells Regulates CD4+ T-Cell Activation in Vitro.” *European Journal of Immunology* 40 (10): 2686–91. https://doi.org/10.1002/eji.201040673.

Boucheix, C., and E. Rubinstein. 2001. “Tetraspanins:” *Cellular and Molecular Life Sciences* 58 (9): 1189–1205. https://doi.org/10.1007/PL00000933.

Boyer, S. N., D. E. Wazer, and V. Band. 1996. “E7 Protein of Human Papilloma Virus-16 Induces Degradation of Retinoblastoma Protein through the Ubiquitin-Proteasome Pathway.” *Cancer Research* 56 (20): 4620–24.

Bray, Freddie, Jacques Ferlay, Isabelle Soerjomataram, Rebecca L. Siegel, Lindsey A. Torre, and Ahmedin Jemal. 2018. “Global Cancer Statistics 2018: GLOBOCAN Estimates of Incidence and Mortality Worldwide for 36 Cancers in 185 Countries.” *CA: A Cancer Journal for Clinicians* 68 (6): 394–424. https://doi.org/10.3322/caac.21492.

Breitling, Frank, Stefan Dübel, Thomas Seehaus, Iris Klewinghaus, and Melvyn Little. 1991. “A Surface Expression Vector for Antibody Screening.” *Gene* 104 (2): 147–53. https://doi.org/10.1016/0378-1119(91)90244-6.

Brennan, Joseph A., Jay O. Boyle, Wayne M. Koch, Steven N. Goodman, Ralph H. Hruban, Yolanda J. Eby, Marion J. Couch, Arlene A. Forastiere, and David Sidransky. 1995. “Association between Cigarette Smoking and Mutation of the p53 Gene in Squamous-Cell Carcinoma of the Head and Neck.” *New England Journal of Medicine* 332 (11): 712–17. https://doi.org/10.1056/NEJM199503163321104.

Brosseau, Carole, Luc Colas, Antoine Magnan, and Sophie Brouard. 2018. “CD9 Tetraspanin: A New Pathway for the Regulation of Inflammation?” *Frontiers in Immunology* 9 (October). https://doi.org/10.3389/fimmu.2018.02316.

Bruun, Tim-Henrik, Veronika Grassmann, Benjamin Zimmer, Benedikt Asbach, David Peterhoff, Alexander Kliche, and Ralf Wagner. 2017. “Mammalian Cell Surface Display for Monoclonal Antibody-Based FACS Selection of Viral Envelope Proteins.” *mAbs* 9 (7): 1052–64. https://doi.org/10.1080/19420862.2017.1364824.

Burnet, F. M. 1970. “The Concept of Immunological Surveillance.” In *Progress in Tumor Research*, edited by R.S. Schwartz, 13:1–27. S. Karger AG. https://www.karger.com/Article/FullText/386035.

Campa, Michael J., M. Anthony Moody, Ruijun Zhang, Hua-Xin Liao, Elizabeth B. Gottlin, and Edward F. Patz. 2016. “Interrogation of Individual Intratumoral B Lymphocytes from Lung Cancer Patients for Molecular Target Discovery.” *Cancer Immunology, Immunotherapy* 65 (2): 171–80. https://doi.org/10.1007/s00262-015-1787-0.

Campbell, I. D., and M. J. Humphries. 2011. “Integrin Structure, Activation, and Interactions.” *Cold Spring Harbor Perspectives in Biology* 3 (3): a004994–a004994. https://doi.org/10.1101/cshperspect.a004994.

Carter, Laura L., Lynette A. Fouser, Jason Jussif, Lori Fitz, Bija Deng, Clive R. Wood, Mary Collins, Tasuku Honjo, Gordon J. Freeman, and Beatriz M. Carreno. 2002. “PD-1:PD-L Inhibitory Pathway Affects Both CD4+ and CD8+ T Cells and Is Overcome by IL-2.” *European Journal of Immunology* 32 (3): 634. https://doi.org/10.1002/1521-4141(200203)32:3<634::AID-IMMU634>3.0.CO;2-9.

Chan, Kin Tak, Mei Yuk Choi, Kenneth K.Y. Lai, Winnie Tan, Lai Nar Tung, Ho Yu Lam, Daniel K.H. Tong, Nikki P. Lee, and Simon Law. 2014. “Overexpression of Transferrin Receptor CD71 and Its Tumorigenic Properties in Esophageal Squamous Cell Carcinoma.” *Oncology Reports* 31 (3): 1296–1304. https://doi.org/10.3892/or.2014.2981.

Charrin, S., S. Jouannet, C. Boucheix, and E. Rubinstein. 2014. “Tetraspanins at a Glance.” *Journal of Cell Science* 127 (17): 3641–48. https://doi.org/10.1242/jcs.154906.

Chikamatsu, Kazuaki, Koichi Sakakura, Minoru Toyoda, Katsumasa Takahashi, Takanori Yamamoto, and Keisuke Masuyama. 2012. “Immunosuppressive Activity of CD14+ HLA-DR− Cells in Squamous Cell Carcinoma of the Head and Neck.” *Cancer Science* 103 (6): 976–83. https://doi.org/10.1111/j.1349-7006.2012.02248.x.

Chimal-Ramírez, G. K., N. A. Espinoza-Sánchez, and E. M. Fuentes-Pananá. 2013. “Protumor Activities of the Immune Response: Insights in the Mechanisms of Immunological Shift, Oncotraining, and Oncopromotion.” *Journal of Oncology* 2013: 1–16. https://doi.org/10.1155/2013/835956.

Cho, Nam Hoon, Hyo Sub Shim, Sun Young Rha, Suki Hee Kang, Sung Hui Hong, Young Deuk Choi, Sung Jun Hong, and Sang Ho Cho. 2003. “Increased Expression of Matrix Metalloproteinase 9 Correlates with Poor Prognostic Variables in Renal Cell Carcinoma.” *European Urology* 44 (5): 560–66. https://doi.org/10.1016/S0302-2838(03)00362-2.

Cobrinik, David, Steven F. Dowdy, Philip W. Hinds, Sibylle Mittnacht, and Robert A. Weinberg. 1992. “The Retinoblastoma Protein and the Regulation of Cell Cycling.” *Trends in Biochemical Sciences* 17 (8): 312–15. https://doi.org/10.1016/0968-0004(92)90443-D.

Cohen, Jacob T., Ziv Gil, Yoav Binenbaum, Shorook Na’ara, and Moran Amit. 2015. “An Orthotopic Mouse Model of Laryngeal Squamous Cell Carcinoma.” *Annals of Otology, Rhinology & Laryngology* 124 (2): 143–47. https://doi.org/10.1177/0003489414549575.

Cohen, Martin H., Huanyu Chen, Stacy Shord, Chana Fuchs, Kun He, Hong Zhao, Sharon Sickafuse, Patricia Keegan, and Richard Pazdur. 2013. “Approval Summary: Cetuximab in Combination with Cisplatin or Carboplatin and 5-Fluorouracil for the First-Line Treatment of Patients with Recurrent Locoregional or Metastatic Squamous Cell Head and Neck Cancer.” *The Oncologist* 18 (4): 460–66. https://doi.org/10.1634/theoncologist.2012-0458.

Colbeck, Emily Jayne, Ann Ager, Awen Gallimore, and Gareth Wyn Jones. 2017. “Tertiary Lymphoid Structures in Cancer: Drivers of Antitumor Immunity, Immunosuppression, or Bystander Sentinels in Disease?” *Frontiers in Immunology* 8 (December). https://doi.org/10.3389/fimmu.2017.01830.

Copeland, Ben T., Matthew J. Bowman, Claude Boucheix, and Leonie K. Ashman. 2013. “Knockout of the Tetraspanin *Cd9* in the TRAMP Model of *de Novo* Prostate Cancer Increases Spontaneous Metastases in an Organ-Specific Manner: Suppressor of de Novo Prostate Cancer Development.” *International Journal of Cancer* 133 (8): 1803–12. https://doi.org/10.1002/ijc.28204.

Coronella, Julia A., Catherine Spier, Matthew Welch, Katrina T. Trevor, Alison T. Stopeck, Hugo Villar, and Evan M. Hersh. 2002. “Antigen-Driven Oligoclonal Expansion of Tumor-Infiltrating B Cells in Infiltrating Ductal Carcinoma of the Breast.” *The Journal of Immunology* 169 (4): 1829–36. https://doi.org/10.4049/jimmunol.169.4.1829.

Daniels, Tracy R., Tracie Delgado, Jose A. Rodriguez, Gustavo Helguera, and Manuel L. Penichet. 2006. “The Transferrin Receptor Part I: Biology and Targeting with Cytotoxic Antibodies for the Treatment of Cancer.” *Clinical Immunology* 121 (2): 144–58. https://doi.org/10.1016/j.clim.2006.06.010.

Daniels-Wells, Tracy R, and Manuel L Penichet. 2016. “Transferrin Receptor 1: A Target for Antibody-Mediated Cancer Therapy.” *Immunotherapy* 8 (9): 991–94. https://doi.org/10.2217/imt-2016-0050.

Darling, Ryan J., and Pierre-Alexandre Brault. 2004. “Kinetic Exclusion Assay Technology: Characterization of Molecular Interactions.” *ASSAY and Drug Development Technologies* 2 (6): 647–57. https://doi.org/10.1089/adt.2004.2.647.

DeFalco, Jeff, Michael Harbell, Amy Manning-Bog, Gilson Baia, Alexander Scholz, Beatriz Millare, May Sumi, et al. 2018. “Non-Progressing Cancer Patients Have Persistent B Cell Responses Expressing Shared Antibody Paratopes That Target Public Tumor Antigens.” *Clinical Immunology* 187 (February): 37–45. https://doi.org/10.1016/j.clim.2017.10.002.

Desiderio, Angiola, Rosella Franconi, Marian Lopez, Maria Elena Villani, Francesca Viti, Roberta Chiaraluce, Valerio Consalvi, Dario Neri, and Eugenio Benvenuto. 2001. “A Semi-Synthetic Repertoire of Intrinsically Stable Antibody Fragments Derived from a Single-Framework Scaffold 1 1Edited by J. Kahn.” *Journal of Molecular Biology* 310 (3): 603–15. https://doi.org/10.1006/jmbi.2001.4756.

Dieu-Nosjean, Marie-Caroline, Martine Antoine, Claire Danel, Didier Heudes, Marie Wislez, Virginie Poulot, Nathalie Rabbe, et al. 2008. “Long-Term Survival for Patients With Non–Small-Cell Lung Cancer With Intratumoral Lymphoid Structures.” *Journal of Clinical Oncology* 26 (27): 4410–17. https://doi.org/10.1200/JCO.2007.15.0284.

Dunn, Gavin P., Lloyd J. Old, and Robert D. Schreiber. 2004. “The Three Es of Cancer Immunoediting.” *Annual Review of Immunology* 22 (1): 329–60. https://doi.org/10.1146/annurev.immunol.22.012703.104803.

Espina, Virginia, Michael Heiby, Mariaelena Pierobon, and Lance A Liotta. 2007. “Laser Capture Microdissection Technology.” *Expert Review of Molecular Diagnostics* 7 (5): 647–57. https://doi.org/10.1586/14737159.7.5.647.

Fagin, J A, K Matsuo, A Karmakar, D L Chen, S H Tang, and H P Koeffler. 1993. “High Prevalence of Mutations of the p53 Gene in Poorly Differentiated Human Thyroid Carcinomas.” *Journal of Clinical Investigation* 91 (1): 179–84. https://doi.org/10.1172/JCI116168.

Fahr, Wieland, and André Frenzel. 2018. “Phage Display and Selections on Cells.” In *Phage Display*, edited by Michael Hust and Theam Soon Lim, 1701:321–30. New York, NY: Springer New York. http://link.springer.com/10.1007/978-1-4939-7447-4_17.

Fakhry, C., W. H. Westra, S. Li, A. Cmelak, J. A. Ridge, H. Pinto, A. Forastiere, and M. L. Gillison. 2008. “Improved Survival of Patients With Human Papillomavirus-Positive Head and Neck Squamous Cell Carcinoma in a Prospective Clinical Trial.” *JNCI Journal of the National Cancer Institute* 100 (4): 261–69. https://doi.org/10.1093/jnci/djn011.

Ferrone, Soldano, and Francesco M. Marincola. 1995. “Loss of HLA Class I Antigens by Melanoma Cells: Molecular Mechanisms, Functional Significance and Clinial Relevance.” *Immunology Today* 16 (10): 487–94. https://doi.org/10.1016/0167-5699(95)80033-6.

Fields, Gregg B. 2019. “The Rebirth of Matrix Metalloproteinase Inhibitors: Moving Beyond the Dogma.” *Cells* 8 (9): 984. https://doi.org/10.3390/cells8090984.

Fraser, Nicola L. W., Gary Rowley, Max Field, and David I. Stott. 2003. “The VH Gene Repertoire of Splenic B Cells and Somatic Hypermutation in Systemic Lupus Erythematosus.” *Arthritis Research & Therapy* 5 (2): R114-121.

Fridman, W. H., R. Remark, J. Goc, N. A. Giraldo, E. Becht, Scott A. Hammond, D. Damotte, M.-C. Dieu-Nosjean, and Catherine Sautès-Fridman. 2014. “The Immune Microenvironment: A Major Player in Human Cancers.” *International Archives of Allergy and Immunology* 164 (1): 13–26. https://doi.org/10.1159/000362332.

Fühner, Viola, Philip Alexander Heine, Saskia Helmsing, Sebastian Goy, Jasmin Heidepriem, Felix F. Loeffler, Stefan Dübel, Ralf Gerhard, and Michael Hust. 2018. “Development of Neutralizing and Non-Neutralizing Antibodies Targeting Known and Novel Epitopes of TcdB of Clostridioides Difficile.” *Frontiers in Microbiology* 9 (December). https://doi.org/10.3389/fmicb.2018.02908.

Garon, Edward B., Naiyer A. Rizvi, Rina Hui, Natasha Leighl, Ani S. Balmanoukian, Joseph Paul Eder, Amita Patnaik, et al. 2015. “Pembrolizumab for the Treatment of Non–Small-Cell Lung Cancer.” *New England Journal of Medicine* 372 (21): 2018–28. https://doi.org/10.1056/NEJMoa1501824.

Gastman, B. R., Y. Atarshi, T. E. Reichert, T. Saito, L. Balkir, H. Rabinowich, and T. L. Whiteside. 1999. “Fas Ligand Is Expressed on Human Squamous Cell Carcinomas of the Head and Neck, and It Promotes Apoptosis of T Lymphocytes.” *Cancer Research* 59 (20): 5356–64.

Gatti, Richard A., and Robert A. Good. 1971. “Occurrence of Malignancy in Immunodeficiency Diseases: A Literature Review.” *Cancer* 28 (1): 89–98. https://doi.org/10.1002/1097-0142(197107)28:1<89::AID-CNCR2820280117>3.0.CO;2-Q.

Gatto, Dominique, and Robert Brink. 2010. “The Germinal Center Reaction.” *Journal of Allergy and Clinical Immunology* 126 (5): 898–907. https://doi.org/10.1016/j.jaci.2010.09.007.

Gellrich, Sylke, Sascha Rutz, Astrid Borkowski, Sven Golembowski, Erika Gromnica-Ihle, Wolfram Sterry, and Sigbert Jahn. 1999. “Analysis of VH-D-JH Gene Transcripts in B Cells Infiltrating the Salivary Glands and Lymph Node Tissues of Patients with Sjögren’s Syndrome.” *Arthritis & Rheumatism* 42 (2): 240–47. https://doi.org/10.1002/1529-0131(199902)42:2<240::AID-ANR5>3.0.CO;2-I.

Gentles, Andrew J, Aaron M Newman, Chih Long Liu, Scott V Bratman, Weiguo Feng, Dongkyoon Kim, Viswam S Nair, et al. 2015. “The Prognostic Landscape of Genes and Infiltrating Immune Cells across Human Cancers.” *Nature Medicine* 21 (8): 938–45. https://doi.org/10.1038/nm.3909.

Germain, Claire, Sacha Gnjatic, and Marie-Caroline Dieu-Nosjean. 2015. “Tertiary Lymphoid Structure-Associated B Cells Are Key Players in Anti-Tumor Immunity.” *Frontiers in Immunology* 6: 67. https://doi.org/10.3389/fimmu.2015.00067.

Germain, Claire, Sacha Gnjatic, Fella Tamzalit, Samantha Knockaert, Romain Remark, Jérémy Goc, Alice Lepelley, et al. 2014. “Presence of B Cells in Tertiary Lymphoid Structures Is Associated with a Protective Immunity in Patients with Lung Cancer.” *American Journal of Respiratory and Critical Care Medicine* 189 (7): 832–44. https://doi.org/10.1164/rccm.201309-1611OC.

Ghiringhelli, François, Pierre E. Puig, Stephan Roux, Arnaud Parcellier, Elise Schmitt, Eric Solary, Guido Kroemer, François Martin, Bruno Chauffert, and Laurence Zitvogel. 2005. “Tumor Cells Convert Immature Myeloid Dendritic Cells into TGF-B–secreting Cells Inducing CD4 $^{+}$ CD25 $^{+}$ Regulatory T Cell Proliferation.” *The Journal of Experimental Medicine* 202 (7): 919–29. https://doi.org/10.1084/jem.20050463.

Glanville, J, S D’Angelo, Ta Khan, St Reddy, L Naranjo, F Ferrara, and Arm Bradbury. 2015. “Deep Sequencing in Library Selection Projects: What Insight Does It Bring?” *Current Opinion in Structural Biology* 33 (August): 146–60. https://doi.org/10.1016/j.sbi.2015.09.001.

Goc, Jérémy, Wolf-Herman Fridman, Catherine Sautès-Fridman, and Marie-Caroline Dieu-Nosjean. 2013. “Characteristics of Tertiary Lymphoid Structures in Primary Cancers.” *OncoImmunology* 2 (12): e26836. https://doi.org/10.4161/onci.26836.

Goldsmith, Merrill E., and William H. Konigsberg. 1977. “Adsorption Protein of the Bacteriophage Fd: Isolation, Molecular Properties, and Location in the Virus.” *Biochemistry* 16 (12): 2686–94. https://doi.org/10.1021/bi00631a016.

Graus, F, J Dalmou, R Reñé, M Tora, N Malats, J J Verschuuren, F Cardenal, et al. 1997. “Anti-Hu Antibodies in Patients with Small-Cell Lung Cancer: Association with Complete Response to Therapy and Improved Survival.” *Journal of Clinical Oncology* 15 (8): 2866–72. https://doi.org/10.1200/JCO.1997.15.8.2866.

Gunderson, A. J., M. M. Kaneda, T. Tsujikawa, A. V. Nguyen, N. I. Affara, B. Ruffell, S. Gorjestani, et al. 2016. “Bruton Tyrosine Kinase-Dependent Immune Cell Cross-Talk Drives Pancreas Cancer.” *Cancer Discovery* 6 (3): 270–85. https://doi.org/10.1158/2159-8290.CD-15-0827.

Gustafson-Wagner, Elisabeth, and Christopher S. Stipp. 2013. “The CD9/CD81 Tetraspanin Complex and Tetraspanin CD151 Regulate α3β1 Integrin-Dependent Tumor Cell Behaviors by Overlapping but Distinct Mechanisms.” Edited by Maddy Parsons. *PLoS ONE* 8 (4): e61834. https://doi.org/10.1371/journal.pone.0061834.

Habashy, Hany Onsy, Desmond G. Powe, Cindy M. Staka, Emad A. Rakha, Graham Ball, Andrew R. Green, Mohammed Aleskandarany, et al. 2010. “Transferrin Receptor (CD71) Is a Marker of Poor Prognosis in Breast Cancer and Can Predict Response to Tamoxifen.” *Breast Cancer Research and Treatment* 119 (2): 283–93. https://doi.org/10.1007/s10549-009-0345-x.

Hagn, Magdalena, Elisabeth Schwesinger, Verena Ebel, Kai Sontheimer, Julia Maier, Thamara Beyer, Tatiana Syrovets, et al. 2009. “Human B Cells Secrete Granzyme B When Recognizing Viral Antigens in the Context of the Acute Phase Cytokine IL-21.” *The Journal of Immunology* 183 (3): 1838–45. https://doi.org/10.4049/jimmunol.0901066.

Hanahan, Douglas, and Lisa M. Coussens. 2012. “Accessories to the Crime: Functions of Cells Recruited to the Tumor Microenvironment.” *Cancer Cell* 21 (3): 309–22. https://doi.org/10.1016/j.ccr.2012.02.022.

Hanahan, Douglas, and Robert A. Weinberg. 2011. “Hallmarks of Cancer: The next Generation.” *Cell* 144 (5): 646–74. https://doi.org/10.1016/j.cell.2011.02.013.

Hansen, Margit H., Heidi V. Nielsen, and Henrik J. Ditzel. 2002. “Translocation of an Intracellular Antigen to the Surface of Medullary Breast Cancer Cells Early in Apoptosis Allows for an Antigen-Driven Antibody Response Elicited by Tumor-Infiltrating B Cells.” *The Journal of Immunology* 169 (5): 2701–11. https://doi.org/10.4049/jimmunol.169.5.2701.

Hemler, Martin E. 2003. “Tetraspanin Proteins Mediate Cellular Penetration, Invasion, and Fusion Events and Define a Novel Type of Membrane Microdomain.” *Annual Review of Cell and Developmental Biology* 19 (1): 397–422. https://doi.org/10.1146/annurev.cellbio.19.111301.153609.

Hemler, Martin E. 2014. “Tetraspanin Proteins Promote Multiple Cancer Stages.” *Nature Reviews Cancer* 14 (1): 49–60. https://doi.org/10.1038/nrc3640.

Higashiyama, M., T. Taki, Y. Ieki, M. Adachi, C. L. Huang, T. Koh, K. Kodama, O. Doi, and M. Miyake. 1995. “Reduced Motility Related Protein-1 (MRP-1/CD9) Gene Expression as a Factor of Poor Prognosis in Non-Small Cell Lung Cancer.” *Cancer Research* 55 (24): 6040–44.

Hino, Ryosuke, Kenji Kabashima, Yu Kato, Hiroaki Yagi, Motonobu Nakamura, Tasuku Honjo, Taku Okazaki, and Yoshiki Tokura. 2010. “Tumor Cell Expression of Programmed Cell Death-1 Ligand 1 Is a Prognostic Factor for Malignant Melanoma.” *Cancer* 116 (7): 1757–66. https://doi.org/10.1002/cncr.24899.

Ho, William Y, Joseph N Blattman, Michelle L Dossett, Cassian Yee, and Philip D Greenberg. 2003. “Adoptive Immunotherapy: Engineering T Cell Responses as Biologic Weapons for Tumor Mass Destruction.” *Cancer Cell* 3 (5): 431–37. https://doi.org/10.1016/S1535-6108(03)00113-2.

Homola, Jiří, Sinclair S. Yee, and Günter Gauglitz. 1999. “Surface Plasmon Resonance Sensors: Review.” *Sensors and Actuators B: Chemical* 54 (1–2): 3–15. https://doi.org/10.1016/S0925-4005(98)00321-9.

Horwitz, A. H., C. P. Chang, M. Better, K. E. Hellstrom, and R. R. Robinson. 1988. “Secretion of Functional Antibody and Fab Fragment from Yeast Cells.” *Proceedings of the National Academy of Sciences* 85 (22): 8678–82. https://doi.org/10.1073/pnas.85.22.8678.

Houtkamp, Mischa A., Onno J. de Boer, Chris M. van der Loos, Allard C. van der Wal, and Anton E. Becker. 2001. “Adventitial Infiltrates Associated with Advanced Atherosclerotic Plaques: Structural Organization Suggests Generation of Local Humoral Immune Responses.” *The Journal of Pathology* 193 (2): 263–69. https://doi.org/10.1002/1096-9896(2000)9999:9999<::AID-PATH774>3.0.CO;2-N.

Hu, Ping, Wenhua Zhang, Hongbo Xin, and Glenn Deng. 2016. “Single Cell Isolation and Analysis.” *Frontiers in Cell and Developmental Biology* 4 (October). https://doi.org/10.3389/fcell.2016.00116.

Huang, Hao. 2018. “Matrix Metalloproteinase-9 (MMP-9) as a Cancer Biomarker and MMP-9 Biosensors: Recent Advances.” *Sensors* 18 (10): 3249. https://doi.org/10.3390/s18103249.

Humby, Frances, Michele Bombardieri, Antonio Manzo, Stephen Kelly, Mark C Blades, Bruce Kirkham, Jo Spencer, and Costantino Pitzalis. 2009. “Ectopic Lymphoid Structures Support Ongoing Production of Class-Switched Autoantibodies in Rheumatoid Synovium.” Edited by Tom Huizinga. *PLoS Medicine* 6 (1): e1. https://doi.org/10.1371/journal.pmed.0060001.

Humphries, M. J. 2000. “Integrin Structure.” *Biochemical Society Transactions* 28 (4): 311–39.

Humphries, M.J. 2004. “Monoclonal Antibodies as Probes of Integrin Priming and Activation.” *Biochemical Society Transactions* 32 (3): 407–11. https://doi.org/10.1042/bst0320407.

Hust, Michael, André Frenzel, Thomas Schirrmann, and Stefan Dübel. 2014. “Selection of Recombinant Antibodies from Antibody Gene Libraries.” In *Gene Function Analysis*,

edited by Michael F. Ochs, 1101:305–20. Totowa, NJ: Humana Press. http://link.springer.com/10.1007/978-1-62703-721-1_14.

Huston, J. S., D. Levinson, M. Mudgett-Hunter, M. S. Tai, J. Novotny, M. N. Margolies, R. J. Ridge, R. E. Bruccoleri, E. Haber, and R. Crea. 1988. “Protein Engineering of Antibody Binding Sites: Recovery of Specific Activity in an Anti-Digoxin Single-Chain Fv Analogue Produced in Escherichia Coli.” *Proceedings of the National Academy of Sciences* 85 (16): 5879–83. https://doi.org/10.1073/pnas.85.16.5879.

Hutchins, A. P., D. Diez, and D. Miranda-Saavedra. 2013. “The IL-10/STAT3-Mediated Anti-Inflammatory Response: Recent Developments and Future Challenges.” *Briefings in Functional Genomics* 12 (6): 489–98. https://doi.org/10.1093/bfgp/elt028.

Hynes, R. 1987. “Integrins: A Family of Cell Surface Receptors.” *Cell* 48 (4): 549–54. https://doi.org/10.1016/0092-8674(87)90233-9.

Hynes, Richard O. 2002. “Integrins: Bidirectional, Allosteric Signaling Machines.” *Cell* 110 (6): 673–87. https://doi.org/10.1016/s0092-8674(02)00971-6.

Imahayashi, Satoru, Yuji Ichiyoshi, Ichiro Yoshino, Ryozo Eifuku, Mitsuhiro Takenoyama, and Kosei Yasumoto. 2000. “Tumor-Infiltrating B-Cell-Derived IgG Recognizes Tumor Components in Human Lung Cancer.” *Cancer Investigation* 18 (6): 530–36. https://doi.org/10.3109/07357900009012192.

Jäger, Volker, Konrad Büssow, Andreas Wagner, Susanne Weber, Michael Hust, André Frenzel, and Thomas Schirrmann. 2013. “High Level Transient Production of Recombinant Antibodies and Antibody Fusion Proteins in HEK293 Cells.” *BMC Biotechnology* 13 (1): 52. https://doi.org/10.1186/1472-6750-13-52.

Jie, H-B, N Gildener-Leapman, J Li, R M Srivastava, S P Gibson, T L Whiteside, and R L Ferris. 2013. “Intratumoral Regulatory T Cells Upregulate Immunosuppressive Molecules in Head and Neck Cancer Patients.” *British Journal of Cancer* 109 (10): 2629–35. https://doi.org/10.1038/bjc.2013.645.

Jing, S. Q., and I. S. Trowbridge. 1987. “Identification of the Intermolecular Disulfide Bonds of the Human Transferrin Receptor and Its Lipid-Attachment Site.” *The EMBO Journal* 6 (2): 327–31.

Juric, Vladi, Chris O’Sullivan, Erin Stefanutti, Maria Kovalenko, Andrew Greenstein, Vivian Barry-Hamilton, Igor Mikaelian, et al. 2018. “MMP-9 Inhibition Promotes Anti-Tumor Immunity through Disruption of Biochemical and Physical Barriers to T-Cell Trafficking to Tumors.” Edited by Yves St-Pierre. *PLOS ONE* 13 (11): e0207255. https://doi.org/10.1371/journal.pone.0207255.

Kato, Keizo, Akira Hara, Toshiya Kuno, Nami Kitaori, Zhi Huilan, Hideki Mori, Makoto Toida, and Toshiyuki Shibata. 2005. “Matrix Metalloproteinases 2 and 9 in Oral Squamous Cell Carcinomas: Manifestation and Localization of Their Activity.” *Journal of Cancer Research and Clinical Oncology* 131 (6): 340–46. https://doi.org/10.1007/s00432-004-0654-8.

Keir, Mary E., Yvette E. Latchman, Gordon J. Freeman, and Arlene H. Sharpe. 2005. “Programmed Death-1 (PD-1):PD-Ligand 1 Interactions Inhibit TCR-Mediated Positive Selection of Thymocytes.” *Journal of Immunology (Baltimore, Md.: 1950)* 175 (11): 7372–79. https://doi.org/10.4049/jimmunol.175.11.7372.

Kemp, Troy J., Jill M. Moore, and Thomas S. Griffith. 2004. “Human B Cells Express Functional TRAIL/Apo-2 Ligand after CpG-Containing Oligodeoxynucleotide Stimulation.” *The Journal of Immunology* 173 (2): 892–99. https://doi.org/10.4049/jimmunol.173.2.892.

Khan, Adnan R., Emily Hams, Achilleas Floudas, Tim Sparwasser, Casey T. Weaver, and Padraic G. Fallon. 2015. “PD-L1hi B Cells Are Critical Regulators of Humoral Immunity.” *Nature Communications* 6 (1). https://doi.org/10.1038/ncomms6997.

Kim, Chang H. 2006. “Regulation of Humoral Immunity by FoxP3+ Regulatory T Cells.” *Expert Review of Clinical Immunology* 2 (6): 859–68. https://doi.org/10.1586/1744666X.2.6.859.

Klussmann, Jens P., Elif Gültekin, Soenke J. Weissenborn, Ulrike Wieland, Volker Dries, Hans P. Dienes, Hans E. Eckel, Herbert J. Pfister, and Pawel G. Fuchs. 2003. “Expression of p16 Protein Identifies a Distinct Entity of Tonsillar Carcinomas Associated with

Human Papillomavirus." *The American Journal of Pathology* 162 (3): 747–53. https://doi.org/10.1016/S0002-9440(10)63871-0.
Koenig, Alice, and Olivier Thaunat. 2016. "Lymphoid Neogenesis and Tertiary Lymphoid Organs in Transplanted Organs." *Frontiers in Immunology* 7 (December). https://doi.org/10.3389/fimmu.2016.00646.
Köhler, G., and C. Milstein. 1975. "Continuous Cultures of Fused Cells Secreting Antibody of Predefined Specificity." *Nature* 256 (5517): 495–97. https://doi.org/10.1038/256495a0.
Kolesnikova, Tatiana V., Alexander R. Kazarov, Madeleine E. Lemieux, Marc A. Lafleur, Santosh Kesari, Andrew L. Kung, and Martin E. Hemler. 2009. "Glioblastoma Inhibition by Cell Surface Immunoglobulin Protein EWI-2, In Vitro and In Vivo." *Neoplasia* 11 (1): 77–IN10. https://doi.org/10.1593/neo.81180.
Koshizuka, Keiichi, Toyoyuki Hanazawa, Naoko Kikkawa, Takayuki Arai, Atsushi Okato, Akira Kurozumi, Mayuko Kato, Koji Katada, Yoshitaka Okamoto, and Naohiko Seki. 2017. "Regulation of ITGA3 by the Anti-Tumor miR-199 Family Inhibits Cancer Cell Migration and Invasion in Head and Neck Cancer." *Cancer Science* 108 (8): 1681–92. https://doi.org/10.1111/cas.13298.
Kramer, R. Arjen, Wilfred E. Marissen, Jaap Goudsmit, Therese J. Visser, Marieke Clijsters-Van der Horst, Arjen Q. Bakker, Maureen de Jong, et al. 2005. "The Human Antibody Repertoire Specific for Rabies Virus Glycoprotein as Selected from Immune Libraries." *European Journal of Immunology* 35 (7): 2131–45. https://doi.org/10.1002/eji.200526134.
Kreimer, A. R. 2005. "Human Papillomavirus Types in Head and Neck Squamous Cell Carcinomas Worldwide: A Systematic Review." *Cancer Epidemiology Biomarkers & Prevention* 14 (2): 467–75. https://doi.org/10.1158/1055-9965.EPI-04-0551.
Kügler, Jonas, Florian Tomszak, André Frenzel, and Michael Hust. 2018. "Construction of Human Immune and Naive scFv Libraries." In *Phage Display*, edited by Michael Hust and Theam Soon Lim, 1701:3–24. New York, NY: Springer New York. http://link.springer.com/10.1007/978-1-4939-7447-4_1.
Kügler, Jonas, Sonja Wilke, Doris Meier, Florian Tomszak, André Frenzel, Thomas Schirrmann, Stefan Dübel, et al. 2015. "Generation and Analysis of the Improved Human HAL9/10 Antibody Phage Display Libraries." *BMC Biotechnology* 15 (1): 10. https://doi.org/10.1186/s12896-015-0125-0.
Kurahara, Shin-ichi, Masanori Shinohara, Tetsuro Ikebe, Seiji Nakamura, Mahiro Beppu, Akimitsu Hiraki, Hiroshi Takeuchi, and Kanemitsu Shirasuna. 1999. "Expression of MMPS, MT-MMP, and TIMPs in Squamous Cell Carcinoma of the Oral Cavity: Correlations with Tumor Invasion and Metastasis." *Head & Neck* 21 (7): 627–38. https://doi.org/10.1002/(SICI)1097-0347(199910)21:7<627::AID-HED7>3.0.CO;2-2.
Kuraoka, Masayuki, Aaron G. Schmidt, Takuya Nojima, Feng Feng, Akiko Watanabe, Daisuke Kitamura, Stephen C. Harrison, Thomas B. Kepler, and Garnett Kelsoe. 2016. "Complex Antigens Drive Permissive Clonal Selection in Germinal Centers." *Immunity* 44 (3): 542–52. https://doi.org/10.1016/j.immuni.2016.02.010.
Kurokawa, Akira, Masaki Nagata, Nobutaka Kitamura, Arhab A. Noman, Makoto Ohnishi, Tokio Ohyama, Takanori Kobayashi, Susumu Shingaki, Ritsuo Takagi, and for the Oral, Maxillofacial Pathology, and Surgery Group. 2008. "Diagnostic Value of Integrin α3, β4, and β5 Gene Expression Levels for the Clinical Outcome of Tongue Squamous Cell Carcinoma." *Cancer* 112 (6): 1272–81. https://doi.org/10.1002/cncr.23295.
Kuss, I. 2004. "Decreased Absolute Counts of T Lymphocyte Subsets and Their Relation to Disease in Squamous Cell Carcinoma of the Head and Neck." *Clinical Cancer Research* 10 (11): 3755–62. https://doi.org/10.1158/1078-0432.CCR-04-0054.
Largeot, Anne, Giulia Pagano, Susanne Gonder, Etienne Moussay, and Jerome Paggetti. 2019. "The B-Side of Cancer Immunity: The Underrated Tune." *Cells* 8 (5): 449. https://doi.org/10.3390/cells8050449.
Larkin, James, Vanna Chiarion-Sileni, Rene Gonzalez, Jean Jacques Grob, C. Lance Cowey, Christopher D. Lao, Dirk Schadendorf, et al. 2015. "Combined Nivolumab and Ipilimumab or Monotherapy in Untreated Melanoma." *New England Journal of Medicine* 373 (1): 23–34. https://doi.org/10.1056/NEJMoa1504030.

Lassen, Pernille, Jesper G. Eriksen, Annelise Krogdahl, Marianne Hamilton Therkildsen, Benedicte P. Ulhøi, Marie Overgaard, Lena Specht, et al. 2011. “The Influence of HPV-Associated p16-Expression on Accelerated Fractionated Radiotherapy in Head and Neck Cancer: Evaluation of the Randomised DAHANCA 6&7 Trial.” *Radiotherapy and Oncology* 100 (1): 49–55. https://doi.org/10.1016/j.radonc.2011.02.010.

Lawson, Nicola L., Carly I. Dix, Paul W. Scorer, Christopher J. Stubbs, Edmond Wong, Liam Hutchinson, Eileen J. McCall, et al. 2019. “Mapping the Binding Sites of Antibodies Utilized in Programmed Cell Death Ligand-1 Predictive Immunohistochemical Assays for Use with Immuno-Oncology Therapies.” *Modern Pathology*, September. https://doi.org/10.1038/s41379-019-0372-z.

Lechner, Axel, Hans A. Schlößer, Martin Thelen, Kerstin Wennhold, Sacha I. Rothschild, Ramona Gilles, Alexander Quaas, et al. 2019. “Tumor-Associated B Cells and Humoral Immune Response in Head and Neck Squamous Cell Carcinoma.” *OncoImmunology* 8 (3): 1535293. https://doi.org/10.1080/2162402X.2018.1535293.

Lei, Yu, Yuying Xie, Yee Sun Tan, Mark E. Prince, Jeffrey S. Moyer, Jacques Nör, and Gregory T. Wolf. 2016. “Telltale Tumor Infiltrating Lymphocytes (TIL) in Oral, Head & Neck Cancer.” *Oral Oncology* 61 (October): 159–65. https://doi.org/10.1016/j.oraloncology.2016.08.003.

Li, Y., M. A. Nichols, J. W. Shay, and Y. Xiong. 1994. “Transcriptional Repression of the D-Type Cyclin-Dependent Kinase Inhibitor p16 by the Retinoblastoma Susceptibility Gene Product pRb.” *Cancer Research* 54 (23): 6078–82.

Lukas, J., N. Niu, and M. F. Press. 2000. “p53 Mutations and Expression in Breast Carcinoma in Situ.” *The American Journal of Pathology* 156 (1): 183–91. https://doi.org/10.1016/S0002-9440(10)64718-9.

Luria-Pérez, Rosendo, Gustavo Helguera, and José A. Rodríguez. 2016. “Antibody-Mediated Targeting of the Transferrin Receptor in Cancer Cells.” *Boletín Médico Del Hospital Infantil de México* 73 (6): 372–79. https://doi.org/10.1016/j.bmhimx.2016.11.004.

Lusche, Daniel F., Michael R. Klemme, Benjamin A. Soll, Ryan J. Reis, Cristopher C. Forrest, Tiffany S. Nop, Deborah J. Wessels, Brian Berger, Rebecca Glover, and David R. Soll. 2019. “Integrin α-3 ß-1’s Central Role in Breast Cancer, Melanoma and Glioblastoma Cell Aggregation Revealed by Antibodies with Blocking Activity.” *mAbs* 11 (4): 691–708. https://doi.org/10.1080/19420862.2019.1583987.

Maecker, H. T., S. C. Todd, and S. Levy. 1997. “The Tetraspanin Superfamily: Molecular Facilitators.” *FASEB Journal: Official Publication of the Federation of American Societies for Experimental Biology* 11 (6): 428–42.

Maglioco, Andrea, Damián G. Machuca, María Noel Badano, Paula Nannini, Gabriela V. Camerano, Héctor Costa, Roberto Meiss, Raúl A. Ruggiero, Mirta Giordano, and Graciela I. Dran. 2017. “B Cells Inhibit the Antitumor Immunity against an Established Murine Fibrosarcoma.” *Oncology Letters* 13 (5): 3225–32. https://doi.org/10.3892/ol.2017.5810.

Mandal, Rajarsi, Yasin Şenbabaoğlu, Alexis Desrichard, Jonathan J. Havel, Martin G. Dalin, Nadeem Riaz, Ken-Wing Lee, et al. 2016. “The Head and Neck Cancer Immune Landscape and Its Immunotherapeutic Implications.” *JCI Insight* 1 (17). https://doi.org/10.1172/jci.insight.89829.

Marin-Acevedo, Julian A., Bhagirathbhai Dholaria, Aixa E. Soyano, Keith L. Knutson, Saranya Chumsri, and Yanyan Lou. 2018. “Next Generation of Immune Checkpoint Therapy in Cancer: New Developments and Challenges.” *Journal of Hematology & Oncology* 11 (1). https://doi.org/10.1186/s13045-018-0582-8.

Markowitz, Lauri E., Eileen F. Dunne, Mona Saraiya, Harrell W. Chesson, C. Robinette Curtis, Julianne Gee, Joseph A. Bocchini, Elizabeth R. Unger, and Centers for Disease Control and Prevention (CDC). 2014. “Human Papillomavirus Vaccination: Recommendations of the Advisory Committee on Immunization Practices (ACIP).” *MMWR. Recommendations and Reports: Morbidity and Mortality Weekly Report. Recommendations and Reports* 63 (RR-05): 1–30.

Marshall, Derek C., Susan K. Lyman, Scott McCauley, Maria Kovalenko, Rhyannon Spangler, Chian Liu, Michael Lee, et al. 2015. “Selective Allosteric Inhibition of MMP9 Is

Efficacious in Preclinical Models of Ulcerative Colitis and Colorectal Cancer." Edited by Fabio Cominelli. *PLOS ONE* 10 (5): e0127063. https://doi.org/10.1371/journal.pone.0127063.

Massarelli, Erminia, William William, Faye Johnson, Merrill Kies, Renata Ferrarotto, Ming Guo, Lei Feng, et al. 2019. "Combining Immune Checkpoint Blockade and Tumor-Specific Vaccine for Patients With Incurable Human Papillomavirus 16–Related Cancer: A Phase 2 Clinical Trial." *JAMA Oncology* 5 (1): 67. https://doi.org/10.1001/jamaoncol.2018.4051.

Mauri, Claudia, and Anneleen Bosma. 2012. "Immune Regulatory Function of B Cells." *Annual Review of Immunology* 30 (1): 221–41. https://doi.org/10.1146/annurev-immunol-020711-074934.

McCafferty, John, Andrew D. Griffiths, Greg Winter, and David J. Chiswell. 1990. "Phage Antibodies: Filamentous Phage Displaying Antibody Variable Domains." *Nature* 348 (6301): 552–54. https://doi.org/10.1038/348552a0.

Miethe, Sebastian, Christine Rasetti-Escargueil, Yvonne Liu, Siham Chahboun, Thibaut Pelat, Arnaud Avril, Andrè Frenzel, et al. 2014. "Development of Neutralizing scFv-Fc against Botulinum Neurotoxin A Light Chain from a Macaque Immune Library." *mAbs* 6 (2): 446–59. https://doi.org/10.4161/mabs.27773.

Mizoguchi, Atsushi, Emiko Mizoguchi, Hidetoshi Takedatsu, Richard S Blumberg, and Atul K Bhan. 2002. "Chronic Intestinal Inflammatory Condition Generates IL-10-Producing Regulatory B Cell Subset Characterized by CD1d Upregulation." *Immunity* 16 (2): 219–30. https://doi.org/10.1016/S1074-7613(02)00274-1.

Mu, Chuan-Yong, Jian-An Huang, Ying Chen, Cheng Chen, and Xue-Guang Zhang. 2011. "High Expression of PD-L1 in Lung Cancer May Contribute to Poor Prognosis and Tumor Cells Immune Escape through Suppressing Tumor Infiltrating Dendritic Cells Maturation." *Medical Oncology* 28 (3): 682–88. https://doi.org/10.1007/s12032-010-9515-2.

Münger, Karl, and Peter M Howley. 2002. "Human Papillomavirus Immortalization and Transformation Functions." *Virus Research* 89 (2): 213–28. https://doi.org/10.1016/S0168-1702(02)00190-9.

Murdoch, Craig, Munitta Muthana, Seth B. Coffelt, and Claire E. Lewis. 2008. "The Role of Myeloid Cells in the Promotion of Tumour Angiogenesis." *Nature Reviews Cancer* 8 (8): 618–31. https://doi.org/10.1038/nrc2444.

Namazie, Ali, Sassan Alavi, Olufunmilayo I. Olopade, Giovanni Pauletti, Neema Aghamohammadi, M. Aghamohammadi, Jeffrey A. Gornbein, et al. 2002. "Cyclin D1 Amplification and p16(MTS1/CDK4I) Deletion Correlate With Poor Prognosis in Head and Neck Tumors:" *The Laryngoscope* 112 (3): 472–81. https://doi.org/10.1097/00005537-200203000-00013.

Nazemalhosseini-Mojarad, Ehsan, Somayeh Mohammadpour, Amir Torshizi Esafahani, Ehsan Gharib, Pegah Larki, Afshin Moradi, Mohammad Amin Porhoseingholi, Hamid Asadzade Aghdaei, Peter J. K. Kuppen, and Mohammad Reza Zali. 2019. "Intratumoral Infiltrating Lymphocytes Correlate with Improved Survival in Colorectal Cancer Patients: Independent of Oncogenetic Features: NAZEMALHOSSEINI-MOJARAD et Al.." *Journal of Cellular Physiology* 234 (4): 4768–77. https://doi.org/10.1002/jcp.27273.

Neckers, Leonard M., and J. B. Trepel. 1986. "Transferrin Receptor Expression and the Control of Cell Growth." *Cancer Investigation* 4 (5): 461–70. https://doi.org/10.3109/07357908609017524.

Nelson, Brad H. 2010. "CD20+ B Cells: The Other Tumor-Infiltrating Lymphocytes." *Journal of Immunology (Baltimore, Md.: 1950)* 185 (9): 4977–82. https://doi.org/10.4049/jimmunol.1001323.

Nimmerjahn, Falk, and Jeffrey V. Ravetch. 2008. "Fcγ Receptors as Regulators of Immune Responses." *Nature Reviews Immunology* 8 (1): 34–47. https://doi.org/10.1038/nri2206.

Nishida-Aoki, Nao, Naoomi Tominaga, Fumitaka Takeshita, Hikaru Sonoda, Yusuke Yoshioka, and Takahiro Ochiya. 2017. "Disruption of Circulating Extracellular Vesicles as a Novel

Therapeutic Strategy against Cancer Metastasis." *Molecular Therapy* 25 (1): 181–91. https://doi.org/10.1016/j.ymthe.2016.10.009.

Novinger, Leah J., Takamaru Ashikaga, and David N. Krag. 2015. "Identification of Tumor-Binding scFv Derived from Clonally Related B Cells in Tumor and Lymph Node of a Patient with Breast Cancer." *Cancer Immunology, Immunotherapy: CII* 64 (1): 29–39. https://doi.org/10.1007/s00262-014-1612-1.

Nzula, Sazini, James J. Going, and David I. Stott. 2003. "Antigen-Driven Clonal Proliferation, Somatic Hypermutation, and Selection of B Lymphocytes Infiltrating Human Ductal Breast Carcinomas." *Cancer Research* 63 (12): 3275–80.

O'Brien, Philippa M., David W. M. Millan, Jonathon A. Davis, and M. Saveria Campo. 2005. "In Situ Isolation of Immunoglobulin Sequences Expressed by Single Tumor-Infiltrating B Cells Using Laser-Assisted Microdissection." *Molecular Biotechnology* 29 (2): 101–9.

O'Brien, Philippa, Emmanouella Tsirimonaki, David Coomber, David Millan, Jonathon Davis, and Saveria Campo. 2001. "Immunoglobulin Genes Expressed by B-Lymphocytes Infiltrating Cervical Carcinomas Show Evidence of Antigen-Driven Selection." *Cancer Immunology, Immunotherapy* 50 (10): 523–32. https://doi.org/10.1007/s00262-001-0234-6.

Olkhanud, Purevdorj B., Bazarragchaa Damdinsuren, Monica Bodogai, Ronald E. Gress, Ranjan Sen, Katarzyna Wejksza, Enkhzol Malchinkhuu, Robert P. Wersto, and Arya Biragyn. 2011. "Tumor-Evoked Regulatory B Cells Promote Breast Cancer Metastasis by Converting Resting $CD4^+$ T Cells to T-Regulatory Cells." *Cancer Research* 71 (10): 3505–15. https://doi.org/10.1158/0008-5472.CAN-10-4316.

Pagès, Franck, Amos Kirilovsky, Bernhard Mlecnik, Martin Asslaber, Marie Tosolini, Gabriela Bindea, Christine Lagorce, et al. 2009. "In Situ Cytotoxic and Memory T Cells Predict Outcome in Patients With Early-Stage Colorectal Cancer." *Journal of Clinical Oncology* 27 (35): 5944–51. https://doi.org/10.1200/JCO.2008.19.6147.

Pagès, Franck, Bernhard Mlecnik, Florence Marliot, Gabriela Bindea, Fang-Shu Ou, Carlo Bifulco, Alessandro Lugli, et al. 2018. "International Validation of the Consensus Immunoscore for the Classification of Colon Cancer: A Prognostic and Accuracy Study." *The Lancet* 391 (10135): 2128–39. https://doi.org/10.1016/S0140-6736(18)30789-X.

Pai, Sara I., and William H. Westra. 2009. "Molecular Pathology of Head and Neck Cancer: Implications for Diagnosis, Prognosis, and Treatment." *Annual Review of Pathology: Mechanisms of Disease* 4 (1): 49–70. https://doi.org/10.1146/annurev.pathol.4.110807.092158.

Pardoll, Drew M. 2012. "The Blockade of Immune Checkpoints in Cancer Immunotherapy." *Nature Reviews Cancer* 12 (4): 252–64. https://doi.org/10.1038/nrc3239.

Pavoni, Emiliano, Giorgia Monteriù, Daniela Santapaola, Fiorella Petronzelli, Anna Maria Anastasi, Angela Pelliccia, Valeria D'Alessio, Rita De Santis, and Olga Minenkova. 2007. "Tumor-Infiltrating B Lymphocytes as an Efficient Source of Highly Specific Immunoglobulins Recognizing Tumor Cells." *BMC Biotechnology* 7 (October): 70. https://doi.org/10.1186/1472-6750-7-70.

Pelucchi, Claudio, Silvano Gallus, Werner Garavello, Cristina Bosetti, and Carlo La Vecchia. 2008. "Alcohol and Tobacco Use, and Cancer Risk for Upper Aerodigestive Tract and Liver:" *European Journal of Cancer Prevention* 17 (4): 340–44. https://doi.org/10.1097/CEJ.0b013e3282f75e91.

Penn, Israel. 1978. "Tumors Arising in Organ Transplant Recipients." In *Advances in Cancer Research*, 28:31–61. Elsevier. https://linkinghub.elsevier.com/retrieve/pii/S0065230X08606454.

Peterson, W. D., C. S. Stulberg, and W. F. Simpson. 1971. "A Permanent Heteroploid Human Cell Line with Type B Glucose-6-Phosphate Dehydrogenase." *Proceedings of the Society for Experimental Biology and Medicine. Society for Experimental Biology and Medicine (New York, N.Y.)* 136 (4): 1187–91. https://doi.org/10.3181/00379727-136-35455.

Punt, C. J., J. A. Barbuto, H. Zhang, W. J. Grimes, K. D. Hatch, and E. M. Hersh. 1994. “Anti-Tumor Antibody Produced by Human Tumor-Infiltrating and Peripheral Blood B Lymphocytes.” *Cancer Immunology, Immunotherapy: CII* 38 (4): 225–32.

Pylayeva-Gupta, Y., S. Das, J. S. Handler, C. H. Hajdu, M. Coffre, S. B. Koralov, and D. Bar-Sagi. 2016. “IL35-Producing B Cells Promote the Development of Pancreatic Neoplasia.” *Cancer Discovery* 6 (3): 247–55. https://doi.org/10.1158/2159-8290.CD-15-0843.

Raab-Westphal, Sabine, John Marshall, and Simon Goodman. 2017. “Integrins as Therapeutic Targets: Successes and Cancers.” *Cancers* 9 (12): 110. https://doi.org/10.3390/cancers9090110.

Rajewsky, Klaus. 1996. “Clonal Selection and Learning in the Antibody System.” *Nature* 381 (6585): 751–58. https://doi.org/10.1038/381751a0.

Ramovs, Veronika, Lisa te Molder, and Arnoud Sonnenberg. 2017. “The Opposing Roles of Laminin-Binding Integrins in Cancer.” *Matrix Biology* 57–58 (January): 213–43. https://doi.org/10.1016/j.matbio.2016.08.007.

Rangan, S. R. S. 1972. “A New Human Cell Line (FaDu) from a Hypopharyngeal Carcinoma.” *Cancer* 29 (1): 117–21. https://doi.org/10.1002/1097-0142(197201)29:1<117::AID-CNCR2820290119>3.0.CO;2-R.

Rappa, Germana, Toni M. Green, Jana Karbanová, Denis Corbeil, and Aurelio Lorico. 2015. “Tetraspanin CD9 Determines Invasiveness and Tumorigenicity of Human Breast Cancer Cells.” *Oncotarget* 6 (10). https://doi.org/10.18632/oncotarget.3419.

Reck, Martin, Delvys Rodríguez-Abreu, Andrew G. Robinson, Rina Hui, Tibor Csőszi, Andrea Fülöp, Maya Gottfried, et al. 2016. “Pembrolizumab versus Chemotherapy for PD-L1–Positive Non–Small-Cell Lung Cancer.” *New England Journal of Medicine* 375 (19): 1823–33. https://doi.org/10.1056/NEJMoa1606774.

Reed, A. L., J. Califano, P. Cairns, W. H. Westra, R. M. Jones, W. Koch, S. Ahrendt, et al. 1996. “High Frequency of p16 (CDKN2/MTS-1/INK4A) Inactivation in Head and Neck Squamous Cell Carcinoma.” *Cancer Research* 56 (16): 3630–33.

Reichert, Torsten E., Laura Strauss, Eva M. Wagner, William Gooding, and Theresa L. Whiteside. 2002. “Signaling Abnormalities, Apoptosis, and Reduced Proliferation of Circulating and Tumor-Infiltrating Lymphocytes in Patients with Oral Carcinoma.” *Clinical Cancer Research: An Official Journal of the American Association for Cancer Research* 8 (10): 3137–45.

Reuschenbach, Miriam, Magnus von Knebel Doeberitz, and Nicolas Wentzensen. 2009. “A Systematic Review of Humoral Immune Responses against Tumor Antigens.” *Cancer Immunology, Immunotherapy* 58 (10): 1535–44. https://doi.org/10.1007/s00262-009-0733-4.

Ricklin, Daniel, George Hajishengallis, Kun Yang, and John D Lambris. 2010. “Complement: A Key System for Immune Surveillance and Homeostasis.” *Nature Immunology* 11 (9): 785–97. https://doi.org/10.1038/ni.1923.

Roggiani, Francesca, Delia Mezzanzanica, Katia Rea, and Antonella Tomassetti. 2016. “Guidance of Signaling Activations by Cadherins and Integrins in Epithelial Ovarian Cancer Cells.” *International Journal of Molecular Sciences* 17 (9): 1387. https://doi.org/10.3390/ijms17091387.

Rondot, Susanne, Joachim Koch, Frank Breitling, and Stefan Dübel. 2001. “A Helper Phage to Improve Single-Chain Antibody Presentation in Phage Display.” *Nature Biotechnology* 19 (1): 75–78. https://doi.org/10.1038/83567.

Rubtsov, Anatoly V., Kira Rubtsova, John W. Kappler, Jordan Jacobelli, Rachel S. Friedman, and Philippa Marrack. 2015. “CD11c-Expressing B Cells Are Located at the T Cell/B Cell Border in Spleen and Are Potent APCs.” *The Journal of Immunology* 195 (1): 71–79. https://doi.org/10.4049/jimmunol.1500055.

Ruokolainen, H. 2004. “Expression of Matrix Metalloproteinase-9 in Head and Neck Squamous Cell Carcinoma: A Potential Marker for Prognosis.” *Clinical Cancer Research* 10 (9): 3110–16. https://doi.org/10.1158/1078-0432.CCR-03-0530.

Russo, Giulio, Doris Meier, Saskia Helmsing, Esther Wenzel, Fabian Oberle, André Frenzel, and Michael Hust. 2018. “Parallelized Antibody Selection in Microtiter Plates.” In *Phage*

Display, edited by Michael Hust and Theam Soon Lim, 1701:273–84. New York, NY: Springer New York. http://link.springer.com/10.1007/978-1-4939-7447-4_14.

Ryschich, E., G. Huszty, H.P. Knaebel, M. Hartel, M.W. Büchler, and J. Schmidt. 2004. "Transferrin Receptor Is a Marker of Malignant Phenotype in Human Pancreatic Cancer and in Neuroendocrine Carcinoma of the Pancreas." *European Journal of Cancer* 40 (9): 1418–22. https://doi.org/10.1016/j.ejca.2004.01.036.

Sadreddini, Sanam, Mehrnosh Seifi-Najmi, Babollah Ghasemi, Hossein Samadi Kafil, Vahideh Alinejad, Sevil Sadreddini, Vahid Younesi, Farhad Jadidi-Niaragh, and Mehdi Yousefi. 2015. "Design and Construction of Immune Phage Antibody Library against Tetanus Neurotoxin: Production of Single Chain Antibody Fragments." Edited by Andrew Hiatt. *Human Antibodies* 23 (3–4): 73–79. https://doi.org/10.3233/HAB-150287.

Sarvaria, Anushruti, J Alejandro Madrigal, and Aurore Saudemont. 2017. "B Cell Regulation in Cancer and Anti-Tumor Immunity." *Cellular & Molecular Immunology* 14 (8): 662–74. https://doi.org/10.1038/cmi.2017.35.

Sautès-Fridman, Catherine, Myriam Lawand, Nicolas A. Giraldo, Hélène Kaplon, Claire Germain, Wolf Herman Fridman, and Marie-Caroline Dieu-Nosjean. 2016. "Tertiary Lymphoid Structures in Cancers: Prognostic Value, Regulation, and Manipulation for Therapeutic Intervention." *Frontiers in Immunology* 7 (October). https://doi.org/10.3389/fimmu.2016.00407.

Scheffner, Martin, Bruce A. Werness, Jon M. Huibregtse, Arnold J. Levine, and Peter M. Howley. 1990. "The E6 Oncoprotein Encoded by Human Papillomavirus Types 16 and 18 Promotes the Degradation of p53." *Cell* 63 (6): 1129–36. https://doi.org/10.1016/0092-8674(90)90409-8.

Schmidt, Marianne, Claus-Juergen Scholz, Christine Polednik, and Jeanette Roller. 2016. "Spheroid-Based 3-Dimensional Culture Models: Gene Expression and Functionality in Head and Neck Cancer." *Oncology Reports* 35 (4): 2431–40. https://doi.org/10.3892/or.2016.4581.

Schroeder, Harry W., and Lisa Cavacini. 2010. "Structure and Function of Immunoglobulins." *Journal of Allergy and Clinical Immunology* 125 (2): S41–52. https://doi.org/10.1016/j.jaci.2009.09.046.

Schroff, R. W., K. A. Foon, S. M. Beatty, R. K. Oldham, and A. C. Morgan. 1985. "Human Anti-Murine Immunoglobulin Responses in Patients Receiving Monoclonal Antibody Therapy." *Cancer Research* 45 (2): 879–85.

Schwab, Katjana S., Glenn Kristiansen, Hans H. Schild, Stefanie E.A. Held, Annkristin Heine, and Peter Brossart. 2018. "Successful Treatment of Refractory Squamous Cell Cancer of the Head and Neck with Nivolumab and Ipilimumab." *Case Reports in Oncology* 11 (1): 17–20. https://doi.org/10.1159/000485562.

Schwartz, Marc, Yu Zhang, and Joseph D. Rosenblatt. 2016. "B Cell Regulation of the Anti-Tumor Response and Role in Carcinogenesis." *Journal for ImmunoTherapy of Cancer* 4 (1). https://doi.org/10.1186/s40425-016-0145-x.

Seidel, Ursula J. E., Patrick Schlegel, and Peter Lang. 2013. "Natural Killer Cell Mediated Antibody-Dependent Cellular Cytotoxicity in Tumor Immunotherapy with Therapeutic Antibodies." *Frontiers in Immunology* 4. https://doi.org/10.3389/fimmu.2013.00076.

Shalapour, Shabnam, Joan Font-Burgada, Giuseppe Di Caro, Zhenyu Zhong, Elsa Sanchez-Lopez, Debanjan Dhar, Gerald Willimsky, et al. 2015. "Immunosuppressive Plasma Cells Impede T-Cell-Dependent Immunogenic Chemotherapy." *Nature* 521 (7550): 94–98. https://doi.org/10.1038/nature14395.

Shao, Keke, Weifeng Ding, Feng Wang, Haiquan Li, Da Ma, and Huimin Wang. 2011. "Emulsion PCR: A High Efficient Way of PCR Amplification of Random DNA Libraries in Aptamer Selection." *PloS One* 6 (9): e24910. https://doi.org/10.1371/journal.pone.0024910.

Shindelman, Jeffrey E., Ann E. Ortmeyer, and Howard H. Sussman. 1981. "Demonstration of the Transferrin Receptor in Human Breast Cancer Tissue. Potential Marker for Identifying Dividing Cells." *International Journal of Cancer* 27 (3): 329–34. https://doi.org/10.1002/ijc.2910270311.

Simsa, Peter, Jean-Luc Teillaud, David I. Stott, József Tóth, and Beatrix Kotlan. 2005. “Tumor-Infiltrating B Cell Immunoglobulin Variable Region Gene Usage in Invasive Ductal Breast Carcinoma.” *Pathology Oncology Research: POR* 11 (2): 92–97. https://doi.org/PAOR.2005.11.2.0092.

Skerra, A, and A Plückthun. 1988. “Assembly of a Functional Immunoglobulin Fv Fragment in Escherichia Coli.” *Science* 240 (4855): 1038–41. https://doi.org/10.1126/science.3285470.

Smeby, Jørgen, Anita Sveen, Christian H Bergsland, Ina A Eilertsen, Stine A Danielsen, Peter W Eide, Merete Hektoen, et al. 2019. “Exploratory Analyses of Consensus Molecular Subtype-Dependent Associations of *TP53* Mutations with Immunomodulation and Prognosis in Colorectal Cancer.” *ESMO Open* 4 (3): e000523. https://doi.org/10.1136/esmoopen-2019-000523.

Smeets, Serge J., Albertus T. Hesselink, Ernst-Jan M. Speel, Annick Haesevoets, Peter J.F. Snijders, Michael Pawlita, Chris J.L.M. Meijer, Boudewijn J.M. Braakhuis, C. René Leemans, and Ruud H. Brakenhoff. 2007. “A Novel Algorithm for Reliable Detection of Human Papillomavirus in Paraffin Embedded Head and Neck Cancer Specimen.” *International Journal of Cancer* 121 (11): 2465–72. https://doi.org/10.1002/ijc.22980.

Sökeland, Greta, and Udo Schumacher. 2019. “The Functional Role of Integrins during Intra- and Extravasation within the Metastatic Cascade.” *Molecular Cancer* 18 (1). https://doi.org/10.1186/s12943-018-0937-3.

Stipp, Christopher S. 2010. “Laminin-Binding Integrins and Their Tetraspanin Partners as Potential Antimetastatic Targets.” *Expert Reviews in Molecular Medicine* 12 (January). https://doi.org/10.1017/S1462399409001355.

Swann, Jeremy B., and Mark J. Smyth. 2007. “Immune Surveillance of Tumors.” *Journal of Clinical Investigation* 117 (5): 1137–46. https://doi.org/10.1172/JCI31405.

Talamini, R., C. Bosetti, C. La Vecchia, L. Dal Maso, F. Levi, E. Bidoli, E. Negri, et al. 2002. “Combined Effect of Tobacco and Alcohol on Laryngeal Cancer Risk: A Case-Control Study.” *Cancer Causes & Control: CCC* 13 (10): 957–64.

Thul, Peter J., Lovisa Åkesson, Mikaela Wiking, Diana Mahdessian, Aikaterini Geladaki, Hammou Ait Blal, Tove Alm, et al. 2017. “A Subcellular Map of the Human Proteome.” *Science* 356 (6340): eaal3321. https://doi.org/10.1126/science.aal3321.

Tiller, Thomas, Eric Meffre, Sergey Yurasov, Makoto Tsuiji, Michel C. Nussenzweig, and Hedda Wardemann. 2008. “Efficient Generation of Monoclonal Antibodies from Single Human B Cells by Single Cell RT-PCR and Expression Vector Cloning.” *Journal of Immunological Methods* 329 (1–2): 112–24. https://doi.org/10.1016/j.jim.2007.09.017.

Tiller, Thomas, Ingrid Schuster, Dorothée Deppe, Katja Siegers, Ralf Strohner, Tanja Herrmann, Marion Berenguer, et al. 2013. “A Fully Synthetic Human Fab Antibody Library Based on Fixed VH/VL Framework Pairings with Favorable Biophysical Properties.” *mAbs* 5 (3): 445–70. https://doi.org/10.4161/mabs.24218.

Tipton, Christopher M, Christopher F Fucile, Jaime Darce, Asiya Chida, Travis Ichikawa, Ivan Gregoretti, Sandra Schieferl, et al. 2015. “Diversity, Cellular Origin and Autoreactivity of Antibody-Secreting Cell Population Expansions in Acute Systemic Lupus Erythematosus.” *Nature Immunology* 16 (7): 755–65. https://doi.org/10.1038/ni.3175.

Tolomelli, Alessandra, Paola Galletti, Monica Baiula, and Daria Giacomini. 2017. “Can Integrin Agonists Have Cards to Play against Cancer? A Literature Survey of Small Molecules Integrin Activators.” *Cancers* 9 (12): 78. https://doi.org/10.3390/cancers9070078.

Tonegawa, Susumu. 1983. “Somatic Generation of Antibody Diversity.” *Nature* 302 (5909): 575–81. https://doi.org/10.1038/302575a0.

Tong, Charles C. L., Johnny Kao, and Andrew G. Sikora. 2012. “Recognizing and Reversing the Immunosuppressive Tumor Microenvironment of Head and Neck Cancer.” *Immunologic Research* 54 (1–3): 266–74. https://doi.org/10.1007/s12026-012-8306-6.

Trott, Maria, Svenja Weiß, Sascha Antoni, Joachim Koch, Hagen von Briesen, Michael Hust, and Ursula Dietrich. 2014. “Functional Characterization of Two scFv-Fc Antibodies from an HIV Controller Selected on Soluble HIV-1 Env Complexes: A Neutralizing V3- and a Trimer-Specific gp41 Antibody.” Edited by Stefan Pöhlmann. *PLoS ONE* 9 (5): e97478. https://doi.org/10.1371/journal.pone.0097478.

Tsou, Peiling, Hiroyuki Katayama, Edwin J. Ostrin, and Samir M. Hanash. 2016. “The Emerging Role of B Cells in Tumor Immunity.” *Cancer Research* 76 (19): 5597–5601. https://doi.org/10.1158/0008-5472.CAN-16-0431.

Velcheti, Vamsidhar, and Kurt Schalper. 2016. “Basic Overview of Current Immunotherapy Approaches in Cancer.” *American Society of Clinical Oncology Educational Book*, no. 36(May): 298–308. https://doi.org/10.1200/EDBK_156572.

Vences-Catalán, Felipe, and Shoshana Levy. 2018. “Immune Targeting of Tetraspanins Involved in Cell Invasion and Metastasis.” *Frontiers in Immunology* 9 (June). https://doi.org/10.3389/fimmu.2018.01277.

Vieira, Jeffrey, and Joachim Messing. 1987. “[1] Production of Single-Stranded Plasmid DNA.” In *Methods in Enzymology*, 153:3–11. Elsevier. https://linkinghub.elsevier.com/retrieve/pii/0076687987530440.

von Behring, and Kitasato. 1890. “Ueber das zustandekommen der diphtherie-immunität und der tetanus-immunität bei thieren.” *Dtsch Med Wochenschr* 16: 1113–14.

Walunas, Theresa L., Deborah J. Lenschow, Christina Y. Bakker, Peter S. Linsley, Gordon J. Freeman, Jonathan M. Green, Craig B. Thompson, and Jeffrey A. Bluestone. 1994. “CTLA-4 Can Function as a Negative Regulator of T Cell Activation.” *Immunity* 1 (5): 405–13. https://doi.org/10.1016/1074-7613(94)90071-X.

Wang, Shulin, and Wafik S. El-Deiry. 2007. “P53, Cell Cycle Arrest and Apoptosis.” In *25 Years of p53 Research*, edited by Pierre Hainaut and Klas G. Wiman, 141–63. Dordrecht: Springer Netherlands. http://link.springer.com/10.1007/978-1-4020-2922-6_6.

Weinberger, P. M. 2004. “Prognostic Significance of p16 Protein Levels in Oropharyngeal Squamous Cell Cancer.” *Clinical Cancer Research* 10 (17): 5684–91. https://doi.org/10.1158/1078-0432.CCR-04-0448.

Wennhold, Kerstin, Tanja M. Weber, Nela Klein-Gonzalez, Martin Thelen, Maria Garcia-Marquez, Geothy Chakupurakal, Anne Fiedler, et al. 2017. “CD40-Activated B Cells Induce Anti-Tumor Immunity <i>in Vivo</i>” *Oncotarget* 8 (17). https://doi.org/10.18632/oncotarget.7720.

Werness, B., A. Levine, and P. Howley. 1990. “Association of Human Papillomavirus Types 16 and 18 E6 Proteins with p53.” *Science* 248 (4951): 76–79. https://doi.org/10.1126/science.2157286.

Yang, Andrew, Emily Farmer, John Lin, T.-C. Wu, and Chien-Fu Hung. 2017. “The Current State of Therapeutic and T Cell-Based Vaccines against Human Papillomaviruses.” *Virus Research* 231: 148–65. https://doi.org/10.1016/j.virusres.2016.12.002.

Yauch, Robert L., Fedor Berditchevski, Mary Beth Harler, Jonathan Reichner, and Martin E. Hemler. 1998. “Highly Stoichiometric, Stable, and Specific Association of Integrin α3β1 with CD151 Provides a Major Link to Phosphatidylinositol 4-Kinase, and May Regulate Cell Migration.” Edited by Mark Ginsberg. *Molecular Biology of the Cell* 9 (10): 2751–65. https://doi.org/10.1091/mbc.9.10.2751.

Yoshioka, Yusuke, Yuki Konishi, Nobuyoshi Kosaka, Takeshi Katsuda, Takashi Kato, and Takahiro Ochiya. 2013. “Comparative Marker Analysis of Extracellular Vesicles in Different Human Cancer Types.” *Journal of Extracellular Vesicles* 2 (1): 20424. https://doi.org/10.3402/jev.v2i0.20424.

Young, Miki, Darren Rodenhizer, Teresa Dean, Elisa D’Arcangelo, Bin Xu, Laurie Ailles, and Alison P. McGuigan. 2018. “A TRACER 3D Co-Culture Tumour Model for Head and Neck Cancer.” *Biomaterials* 164 (May): 54–69. https://doi.org/10.1016/j.biomaterials.2018.01.038.

Yu, Xin, Kristin Harden, Lino C Gonzalez, Michelle Francesco, Eugene Chiang, Bryan Irving, Irene Tom, et al. 2009. “The Surface Protein TIGIT Suppresses T Cell Activation by Promoting the Generation of Mature Immunoregulatory Dendritic Cells.” *Nature Immunology* 10 (1): 48–57. https://doi.org/10.1038/ni.1674.

Yuen, Grace J., Ezana Demissie, and Shiv Pillai. 2016. “B Lymphocytes and Cancer: A Love–Hate Relationship.” *Trends in Cancer* 2 (12): 747–57. https://doi.org/10.1016/j.trecan.2016.10.010.

Zeng, Dong-Qiang, Yun-Fang Yu, Qi-Yun Ou, Xiao-Yin Li, Ru-Zhi Zhong, Chuan-Miao Xie, and Qiu-Gen Hu. 2016. “Prognostic and Predictive Value of Tumor-Infiltrating

Lymphocytes for Clinical Therapeutic Research in Patients with Non-Small Cell Lung Cancer." *Oncotarget* 7 (12). https://doi.org/10.18632/oncotarget.7282.

Zeng, Zhao-Shi, Alfred M. Cohen, and José G. Guillem. 1999. "Loss of Basement Membrane Type IV Collagen Is Associated with Increased Expression of Metalloproteinases 2 and 9 (MMP-2 and MMP-9) during Human Colorectal Tumorigenesis." *Carcinogenesis* 20 (5): 749–55. https://doi.org/10.1093/carcin/20.5.749.

Zhao, Dong-Mei, Angela M. Thornton, Richard J. DiPaolo, and Ethan M. Shevach. 2006. "Activated CD4+CD25+ T Cells Selectively Kill B Lymphocytes." *Blood* 107 (10): 3925–32. https://doi.org/10.1182/blood-2005-11-4502.

Zhu, Chen, Ana C Anderson, Anna Schubart, Huabao Xiong, Jaime Imitola, Samia J Khoury, Xin Xiao Zheng, Terry B Strom, and Vijay K Kuchroo. 2005. "The Tim-3 Ligand Galectin-9 Negatively Regulates T Helper Type 1 Immunity." *Nature Immunology* 6 (12): 1245–52. https://doi.org/10.1038/ni1271.

9. Supplemental information

Suppl. Table 1: Overview of the NGS output considering read depth and unique sequences

Library	B cells*	Read depth**		Unique reads	
		Vκ/Vλ	VH	Vκ/Vλ	VH
YUHAN007-κ	2.4 $x10^4$	3 $x10^4$	3 $x10^4$	9 $x10^2$	1 $x10^3$
YUHAN007-λ		1 $x10^4$	1 $x10^4$	4 $x10^2$	7 $x10^2$
YUHAN008-κ	3.2 $x10^5$	7 $x10^4$	7 $x10^4$	6 $x10^3$	8 $x10^3$
YUHAN008-λ		2 $x10^4$	2 $x10^4$	2 $x10^3$	3 $x10^3$
YUHAN009-κ	6.6 $x10^3$	2 $x10^4$	3 $x10^4$	4 $x10^2$	4 $x10^2$
YUHAN009-λ		1 $x10^4$	2 $x10^4$	4 $x10^2$	3 $x10^2$
YUHAN011-κ	5.6 $x10^4$	3 $x10^4$	3 $x10^4$	3 $x10^3$	4 $x10^3$
YUHAN011-λ		3 $x10^4$	4 $x10^4$	3 $x10^3$	4 $x10^3$
YUHAN012-κ	1.8 $x10^5$	2 $x10^4$	2 $x10^4$	3 $x10^3$	4 $x10^3$
YUHAN012-λ		3 $x10^4$	3 $x10^4$	3 $x10^3$	4 $x10^3$
YUHAN022-κ	4.9 $x10^5$	4 $x10^4$	4 $x10^4$	7 $x10^3$	8 $x10^3$
YUHAN022-λ		2 $x10^4$	2 $x10^4$	4 $x10^3$	5 $x10^3$
YUHAN028-κ	2.5 $x10^6$	9 $x10^4$	7 $x10^3$	2 $x10^4$	3 $x10^3$
YUHAN028-λ		7 $x10^4$	2 $x10^4$	1 $x10^4$	7 $x10^3$

*theoretical B cell count **overlapping, functional and appropriately sized